RATES OF DRYING IN DEEP BEDS OF AGGLOMERATED IRON ORES

A THESIS

Presented for the Degree of

Doctor of Philosophy

in the

University of London

by

KHAWAJA NAYYAR IQBAL

JUNE 1974

John Percy Research Group
Department of Metallurgy
Imperial College of Science
and Technology
London, S.W.7.

ABSTRACT

Rates of drying were studied in deep beds of green iron ore pellets, sinter feed and other materials by passing pre-heated air upwards through the bed. An apparatus has been developed to continuously measure the changes in both weight loss and pressure drop across the bed during drying. The material to be dried was contained in a glass column suspended from a counter-balanced beam. A load cell was used to determine the pressure drop. A mercury trough was used to seal the lower end of the column.

For both sinter feed and green pellets, the drying rate was found to be constant over a large proportion of the total drying time and was independent of the material to be dried but varied approximately linearly with flow rate and temperature of the inlet air in the range 0.4 $m^3/s\ m^2$ to 1.4 $m^3/s\ m^2$ and 50°C to 200°C respectively.

A model of the drying process was proposed in which a drying zone of constant height moves up the bed at a uniform velocity, giving rise to a constant drying rate. The drying rate could not be predicted from the model but a relationship based on both the model and the data from the drying experiments was used to predict the drying rates. This relationship was fitted to the experimental data of other workers and was found to provide reasonable agreement with their results. The relationship was applied to typical data for a pellet firing machine in order to

calculate the length of the grate required for drying which was found to be in reasonable agreement with the length used. Similarly the relationship was used to investigate the probability of pre-drying sinter feed on the strand upstream of the ignition hood.

CONTENTS

LIST OF FIGURES

LIST OF TABLES

LIST OF PLATES

CHAPTER 1

INTRODUCTION

CHAPTER I INTRODUCTION

In both the iron ore sintering process and iron ore pellet hardening process, rates of drying should be investigated. These processes are described below and improvements are outlined which require a knowledge of drying rates at some stage in the process.

a) Iron Ore Sintering Process

This process is used to prepare iron ores for the blast furnace in order to achieve a burden with uniform and desirable physical and chemical properties. A typical sinter strand is shown in Fig.1.1. The feed usually consists of iron ore fines, coke breeze, return fines from the screens at the output end of the strand and finely ground limestone. These materials should be less than about 4mm in size. They are mixed with water in order to improve the permeability of the bed. The wet mixture is then fed onto one end of a continuous travelling grate. A cut off blade controls the height of the bed, and the raw feed then passes under an ignition hood. The coke on the surface layer of the bed is ignited. Air is drawn down-wards through the bed and the coke is combusted below the surface as the bed travels towards the output end of the strand. This results in an ignition zone travelling downwards through the bed as shown in Fig.1.1. All the material above the ignition zone is sintered, provided the temperature of the solid reaches the sintering temperature, and all the material below the zone will remain as raw feed. The hot sinter heats the incoming air. This hot air then transfers its heat to the material below the sinter and ignites the coke just below the sintered region. This gas-solid heat transfer

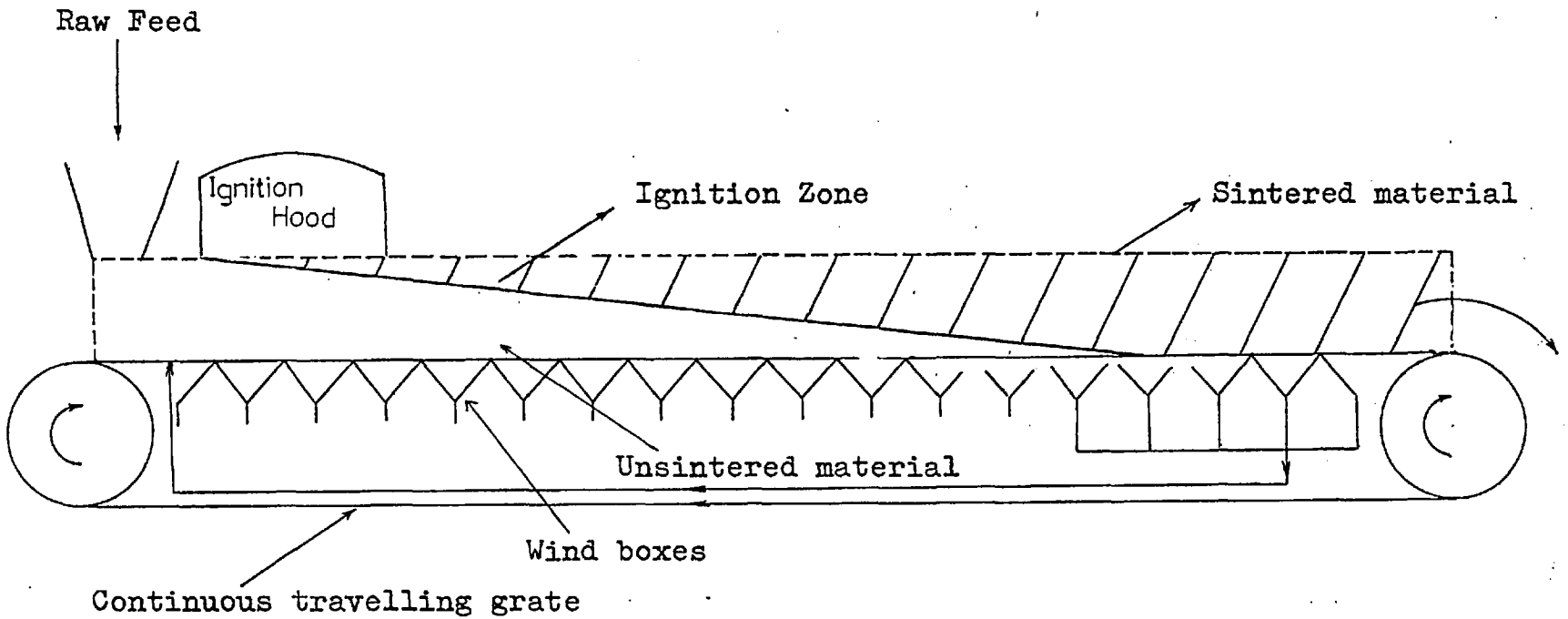

FIGURE 1.1 - Sinter Strand

mechanism results in a heat wave which passes downwards through the bed. The heat wave is shown as gas and solid temperature distributions in Fig.1.2. for a partly sintered bed. The various regimes in the heat wave are also shown in Fig.1.2.

Drying of the wet zone occurs below the ignition zone. The drying process is likely to result in the transfer of water from this part of the bed in the region of the bed close to the grate. This problem has been found to occur in practice and the accumulation of water severely reduces the permeability of the bed due to the formation of mud. The pressure drop across the bed is increased and the air flow is therefore reduced. The speed of the strand has to be decreased to ensure that sintering is completed before the material reaches the end of the strand. The output of the sinter is therefore reduced.

This problem could be solved by pre-drying the raw feed prior to the ignition, using hot air obtained from the last few wind-boxes on the strand or from the sinter cooler. In order to accomplish this, a relationship between drying rate, and the temperature and flow rate of the drying air is required for any given strand. This information would then allow the length of the strand that is required for drying to be calculated.

b) Pellet Hardening Processes

Pellet hardening processes, like the sintering process, are used to prepare iron ores for the blast furnace. Iron ore fines are pelletized (a) to achieve a uniform composition of mixtures of solids and to prevent segregation of these mixtures, e.g. self fluxing pellets containing lime,

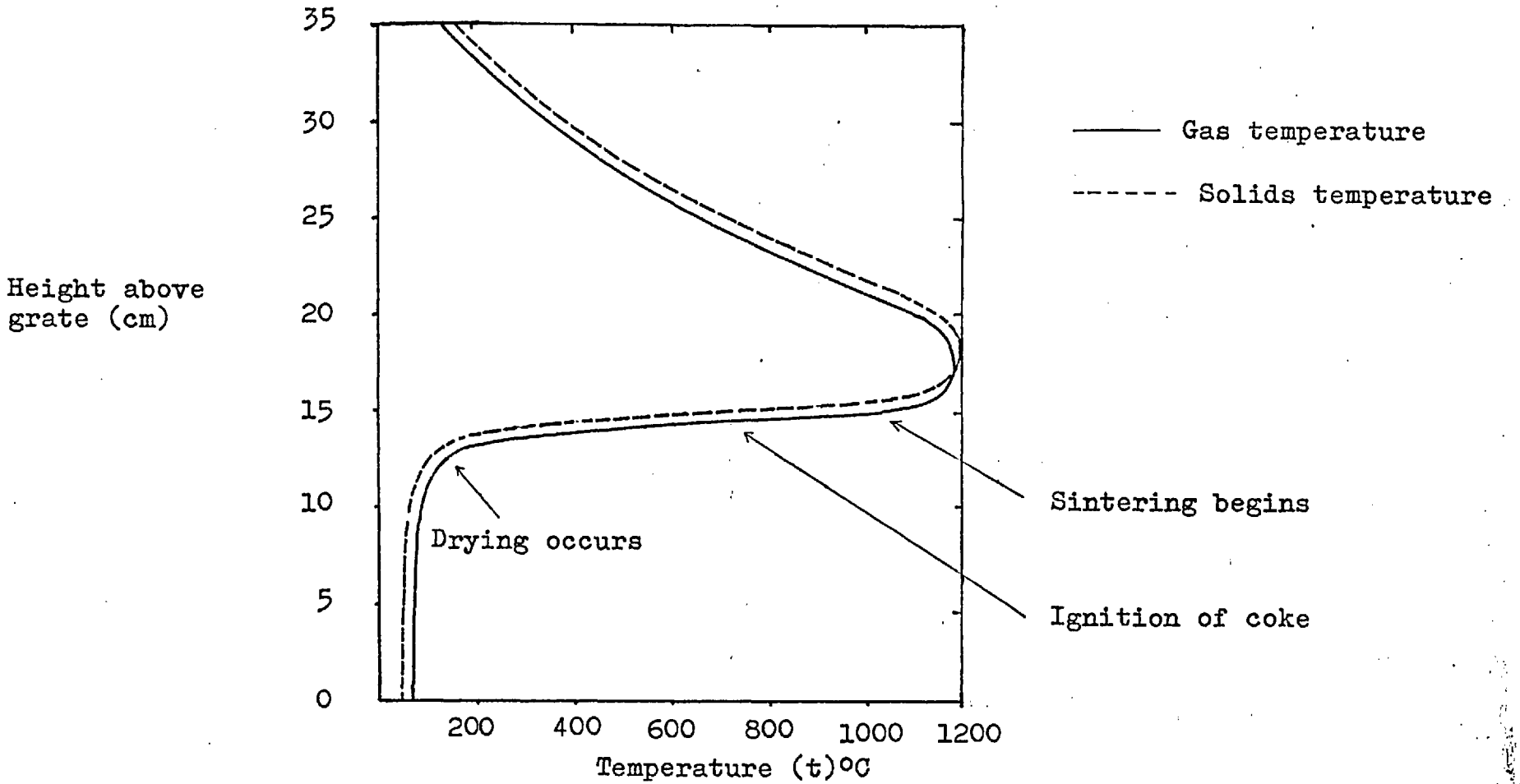

FIGURE 1.2 - Typical gas and solids temperature distributions in a partly sintered bed.

(b) pellets are easier to handle than finely ground materials, (c) pellets form a permeable burden in the blast furnace. Finely ground iron ore is mixed with water and a binder, and rolled into pellets usually 10-15mm in diameter in a drum or disc pelletizer. These pellets are then coated with coal before being fed to the pellet hardening machine. A pellet firing machine is shown in Fig.1.3. This is similar to a sinter strand, except that most of the heat for hardening the pellets is provided by a furnace instead of coke in the bed. The machine consists of three sections, i.e. a drying section, followed by the hardening furnace, and a cooling section. The pellets are distributed uniformly onto the travelling grate and are first dried using up-draught hot air obtained from the recuperation zone. Hardening of the pellets begins when the dried pellets pass under the furnace and air is drawn down-draught through the bed at about 1300°C.

There are three main types of pellet hardening processes in commercial use[1]. The one described above is called the travelling grate process. The other two are:-

i) Shaft furnace process;

ii) Grate-kiln process.

In the shaft furnace process, green pellets are charged to the furnace by a belt feeder travelling back and forth across the top of the furnace. The stock is kept at a constant level by continuously removing hardened pellets from the bottom of the shaft at a controlled rate. Material descends through the shaft counter-current to rising gases. The product is screened and the under-size is ground, pelletized and recirculated.

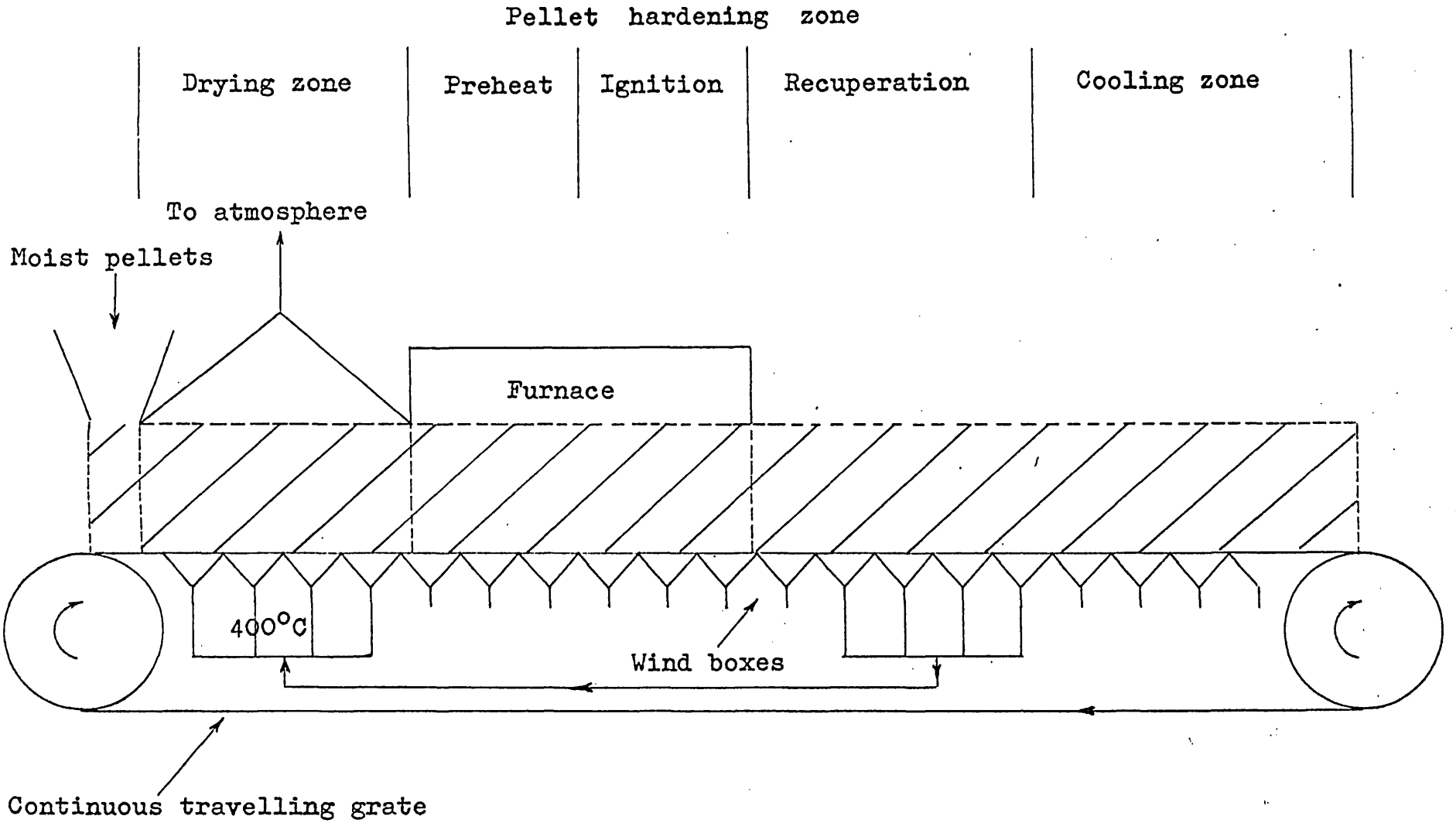

FIGURE 1.3 - Pelletizing Machine

In the grate-kiln process, the material is laid on a grate and pre-heated by down-draught air. The pellets then pass into a rotary kiln, with fuel oil and hot air passing counter-current and finally cooled in a rotary cooler. The combustion products from the kiln are used for pre-heating, and the air from the rotary cooler is re-used in the combustion zone.

The drying section of the pellet hardening process is very similar to the pre-drying of sinter feed mentioned above.

c) Proposed Investigation

The object of the proposed research is to investigate the rates of drying of green iron ore pellets and iron ore sinter feed under the conditions experienced in the pellet hardening and sintering processes.

In the investigation that follows, the drying rates of a typical iron ore sinter feed and of green pellets were obtained from experiments carried out in a packed bed using air flow rates and temperatures typical of sintering and pellet hardening processes. The air flow rates used in these processes are up to 1.8 m^3/s per m^2 of bed area and the air temperatures used for drying are up to 450°C.

A theoretical model is proposed for predicting drying rates of materials in deep packed beds when the following process variables are known:-

Inlet air temperatures,

Inlet air flow rate,

Inlet air humidity,

Height of the bed,

And thermal properties of air and solids.

CHAPTER 2

PREVIOUS WORK

CHAPTER 2 PREVIOUS WORK

This chapter has been divided into five sections, dealing with the mechanisms of drying and the heat, mass and momentum transfer associated with this work.

2.1 - Evaporation from a free surface

The initial stages of drying sinter feed and green pellets involve evaporation from a free surface, so it is necessary to understand the mechanism of evaporation. Before discussing evaporation, it is important to explain the following terms:-

i) Wet bulb temperature.

ii) Adiabatic saturation temperature.

iii) Humid heat.

(i) If a stream of unsaturated gas is passed over the surface of a liquid, evaporation takes place and the humidity of the gas is increased. The temperature of the liquid falls below that of the gas, so that heat then flows from the gas to the liquid and, at equilibrium, the heat supplied by the gas is just sufficient to vaporize the liquid. The temperature finally attained by the liquid is the wet bulb temperature.

(ii) If a gas is passed over the surface of a liquid at such a rate that the time of contact is sufficient for equilibrium to be established, the gas will become saturated and both phases will be brought to the same temperature. In a thermally insulated system, the total sensible heat falls by an amount equal to the latent heat of the liquid evaporated. As a result of continued passage of the gas, the temperature of the liquid gradually approaches an equilibrium value which is known as the adiabatic saturation temperature.

(iii) Under the conditions mentioned in (ii), the whole of the heat of vaporization of the liquid must come from the sensible heat of the gas. The temperature of the gas falls from a value t_g to the adiabatic saturation temperature $t_{g_{a.s.}}$ and its humidity increases from $\times$ to $\times_{a.s}$.

A heat balance gives

$$(t_g - t_{g_{a.s}})\, \mathcal{S} = (\times_{a.s} - \times)\, \lambda \qquad 2.1$$

$$\text{i.e.} \quad \mathcal{S} = \frac{(\times_{a.s} - \times)\, \lambda}{t_g - t_{g_{a.s}}} \qquad 2.2$$

where $\mathcal{S}$ is known as the humid heat of gas. For small changes of $\times$, $\mathcal{S}$ will be almost constant.

Evaporation in general refers to the vaporization of a liquid. A liquid will vaporize when its vapour pressure is greater than the partial pressure of its vapour at the wet bulb temperature of the air in contact with it.

$$\text{Therefore} \quad E \propto P_L - P_A \qquad 2.3$$

$$= h_D\, (P_L - P_A) \qquad 2.4$$

When the two pressures become equal, i.e. when the phase equilibrium state is reached, vaporization will stop. Difficulties arise in the evaluation of mass transfer coefficients since the composition of the gas-vapour mixture varies with distance from the surface of the liquid. The physical properties therefore are not constant and some mean values must be used. If Prandtl and Schmidt numbers for a mixture of gas and vapour are approximately equal, then the Lewis relation applies:-

$$\frac{h}{h_D} = c_p\, \rho \qquad 2.5$$

where c_p and ρ are the mean specific heat and density of the vapour phase respectively,

Therefore $$\frac{h}{h_D \rho_A} = c_p \frac{\rho}{\rho_A} \qquad 2.6$$

where ρ_A is the mean density of gas at partial pressure P_A.

This relation can be used to calculate mass transfer co-efficients approximately even when the diffusivity of the mixture is not known. The Lewis relation is not generally accurate. However it applies very closely to the air-water vapour system.

Unless the humidity is very high, the specific heat and the humid heat are of the same order, and the density of the gas-vapour mixture approximates to that of the gas alone. Under these conditions, therefore

$$\delta = \frac{h}{h_D \rho_A} \qquad 2.7$$

This is approximately true generally for water vapour systems, and accurately so when the humidity is equal to 0.047.

2.1.1 - Effect of evaporation on heat transfer co-efficient.

The modification of h including the influence of evaporation on the heat transfer mechanism has been derived by Bennet and Myers [2] as follows. Fig.2.1 shows the situation at the vapour-liquid interface on the surface of the liquid.

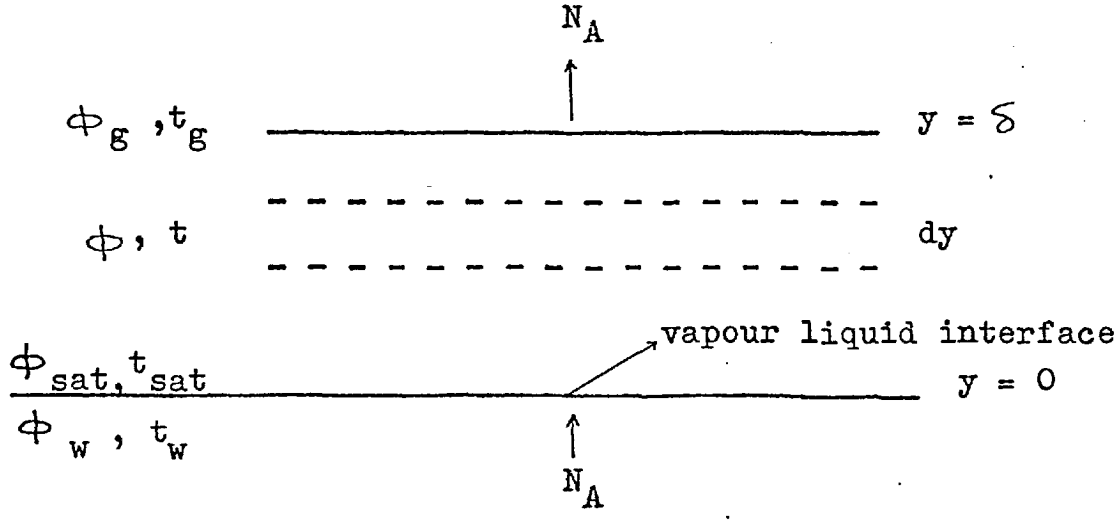

Fig.2.1 - Situation at the vapour liquid interface.

A stationary film of thickness δ is assumed to exist above the vapour-liquid interface. At $y = 0$, the air is saturated with water vapour at temperature t_{sat}. At $y = \delta$, an unsaturated air-water vapour mixture exists. The composition of this mixture is approximately equal to the composition of the bulk gas in the free stream. Evaporation results in a constant flux N_A of water vapour from the surface. There is no net flux of air. The flux of water vapour modifies the heat transfer co-efficient as shown below.

In the element dy, a heat balance gives

$$N_A \lambda + N_A(\phi - \phi_{sat}) = K \frac{dt}{dy} \qquad 2.8$$

where $\lambda = \phi_{sat} - \phi_w$

Integrating from $y = 0$ to $y = \delta$ and from $t = t_{sat}$ to $t = t_g$ gives

$$N_A \int_0^{\delta} dy = K \int_{t_{sat}}^{t_g} \frac{dt}{\lambda + (\phi - \phi_{sat})} \qquad 2.9$$

But $\phi - \phi_{sat} = c_{p_w}(t - t_{sat})$, where c_{p_w} is the specific heat of water vapour; and the above equation can be written as

$$N_A \int_0^{\delta} dy = K \int_0^{t_g - t_{sat}} \frac{d(t-t_{sat})}{\lambda + c_{p_w}(t-t_{sat})} \qquad 2.10$$

$$N_A = \frac{K}{\delta \cdot c_{p_w}} \ln \left[1 + \frac{c_{p_w}}{\lambda} (t_g - t_{sat}) \right] \qquad 2.11$$

At the interface

$$N_A \lambda = h^o (t_g - t_{sat}) \qquad 2.12$$

$$\text{giving } h^o = \frac{K\lambda}{\delta c_{p_w}} \frac{\ln\left[1 + \frac{c_{p_w}}{\lambda}(t_g - t_{sat})\right]}{(t_g - t_{sat})} \qquad 2.13$$

$$\text{But } h = \frac{K}{\delta} \qquad 2.14$$

substituting h in the above equation

$$h^o = h \frac{\lambda}{c_{p_w}} \frac{\ln\left[1 + \frac{c_{p_w}}{\lambda}(t_g - t_{sat})\right]}{(t_g - t_{sat})} \qquad 2.15$$

where h^o is the new heat transfer co-efficient including the effect of evaporation.

2.2 - Mechanism of drying.

The drying of solids is usually taken to mean the removal of a liquid (most often water) from the solid by evaporation. There are various reasons for drying, e.g. to provide definite properties to the material and to make it more suitable for handling.

Various stages usually occur during the drying of solids. As the moisture content decreases, a period of constant drying rate ends at a definite moisture content, known as the critical moisture content. This stage is reached when free evaporation of water from the surface stops, as explained in Section 2.1 of this chapter, and there is insufficient water left on the surface to maintain a continuous film covering the entire drying area. One or two falling rate periods then occur.

The various stages of drying will now be dealt with in detail.

2.2.1.1 - Constant rate period.

In this period, the rate of drying/unit surface area depends entirely on parameters external to the solid being dried, such as velocity, temperature and humidity of the drying air. If the external conditions are maintained constant, then the drying rate in this period is constant. In this period it is also known that if all the heat for vaporization of water is supplied in the drying air (known as convective drying), the temperature of the solid will equilibrate at or close to the wet bulb temperature of the outlet air as explained on page 20. Hence the material temperature and the rate of drying are relatively easily calculated for this period if the flow conditions are known.

Once the critical moisture content is reached, the material enters into one or more falling rate periods. The critical moisture content depends not only on the nature of the solid being dried, but also on its size and shape and of the previous rate of drying.

2.2.1.2 - First falling rate period.

During the last part of the constant rate period, the area of wetted surface begins to diminish until, eventually, evaporation from the residual wet area is insufficient to maintain saturation in the air film, and the drying rate consequently falls. The factors which control this period are the rate of supply of water to the surface, by mechanisms to be discussed later, and the rate of diffusion of vapour across the air film above the surface.

2.2.1.3 - Second falling rate period.

When the surface is completely dry, evaporation takes place entirely from within the solid, the vapour reaching the surface by molecular diffusion. This is the start of the falling rate period. At this stage the water level has gone deep down into the solid and is not there in sufficient quantities to be able to reach the surface through capillaries, therefore the controlling factor for drying is vapour diffusion. Hence this period is not likely to be affected by external conditions.

2.2.2 - Forces affecting the movement of moisture in a bed of solids.

Duration of the constant and first falling rate periods, and the characteristics of the two falling rate periods are largely dependent upon the structure of the solid. There are two main theories put forward to explain the movement of liquids during drying.

2.2.2.1 - The diffusion theory.

Diffusion of liquid moisture may occur because of concentration gradients between the depths of the solids where the concentration is high, and the surface where it is low. This method of moisture transfer is probably limited to such materials as glue, gelatin, soap, flour, textile, paper and wood[3]. During the constant rate period of such solids, the surface moisture concentration is reduced, but the concentration in the depths of the solids remains high. The resulting high diffusivity permits movement of the moisture to the surface as fast as it can be evaporated, and the rate remains constant. When

dry spots appear owing to the projection of portions of the solid into the gas film, the falling rate period or periods start. Further drying occurs at rates, which are entirely controlled by the diffusion rates within the solid.

2.2.2.2 - Capillary theory.[3,4,5,6]

Moisture in granular and porous solids such as sand, paint pigments, ground iron ore and iron ore sinter feed moves through the capillaries and the interstices of the solids by surface tension. The capillaries extend from small reservoirs of moisture in the solid to the drying surface. As drying proceeds, the water at the surface is replaced by air entering the solid through the pores. The moisture is eventually drawn to spaces between the granules of the surface. This is the start of the falling rate periods. The sub-surface reservoirs eventually dry up, the liquid surface recedes into the capillaries, evaporation occurs below the surface in a zone which gradually recedes deeper into the solid, and a second falling rate period results. During this period, diffusion of vapour within the solid will occur from the place of vaporization to the surface.

2.3 - Flow of Fluids through packed beds.

Packed beds are used in order to bring about intimate contact between two fluids or between a fluid and a solid. The work under discussion deals with drying of packed beds of moist porous materials with pre-heated air.

A distinctive feature of a packed bed of granular particles is the extreme irregularity of the intersticial channels or passages. Several mechanisms of fluid flow through porous materials [7] are known to exist. The

primary mechanism is of a purely mechanical nature, namely flow as a result of a pressure differential. However flow may also occur as a result of thermal gradients.

Reynold's classical work showed that two flow regimes occur in a pipe depending on the fluid velocity, i.e. laminar and turbulent flow. A packed bed may be considered to be a series of pipes and so both these regimes can occur in a packed bed as well and will be described below.

Darcy examined the rate of flow of water through sand beds of various thicknesses under laminar flow conditions. He showed that the average velocity, as measured over the whole area of the bed, was directly proportional to the driving pressure, and inversely proportional to the thickness of the bed.

$$\text{i.e.} \quad V = a' \frac{\Delta P}{L} \qquad 2.16$$

It is possible to formulate an equation which will be applicable when either laminar or turbulent flow exists in the bed. The following factors must be considered when fluids flow through packed beds[8]:

i) Rate of fluid flow.

ii) Viscosity and density of fluid.

iii) Closeness and orientation of packing.

iv) Size, shape and surface of particles.

The first two variables concern the fluid, while the last two concern the solids. These variables will now be dealt with in turn.

(i) Rate of fluid flow

It is known that the pressure drop through a granular bed is proportional to the fluid velocity at low flow rates (see Eqn. 2.16), and is approximately proportional to the square root of the velocity at high flow rates. Reynolds formulated the following equation for flow of fluids through pipes :-

$$\frac{\Delta P}{L} = a' V + b \rho V^2 \qquad 2.17$$

A transformation of equation (2.17) yields a linear expression, i.e.

$$\frac{\Delta P}{L V} = a' + b \rho V \qquad 2.18$$

where a' and b are factors which are functions of the system. Equation (2.18) was found to be satisfactory for packed beds by Ergun[8].

(ii) Viscosity and density of the fluid

From Equation (2.18) it can be seen that in the limit as the velocity approaches zero, the ratio of pressure gradient to velocity will become constant.

$$V \xrightarrow{\text{limit}} o \quad \frac{\Delta P}{LV} = a' \qquad 2.19$$

This is a condition for viscous flow. According to Darcy's law given by Eqn.(2.16), the factor a' is proportional to the viscosity of the fluid. The other limiting condition is reached at high flow rates when the constant a' is negligible compared to the term $b \rho V$ in Eqn.(2.18). The term $b \rho V^2$ is the kinetic energy loss due to turbulence.

(iii) Closeness and orientation of packing

Carman[9] noted the works of Blake [10], Kozeny[11] and Burke and Plummer[12], and found that at low flow rates, i.e. laminar flow,

$$\frac{\Delta P g}{L} = k_1 \frac{(1-\epsilon)^2}{\epsilon^3} \frac{\mu V}{D_p^2} \qquad 2.20$$

and for high flow rates, i.e. turbulent flow,

$$\frac{\Delta P g}{L} = k_2 \frac{1-\epsilon}{\epsilon^3} \frac{\rho V^2}{D_p^2} \qquad 2.21$$

where k_1 and k_2 are coefficients of viscous and kinetic energies and ϵ is the voidage, i.e. unoccupied volume in the bed. A general equation which combines Equations (2.20) and (2.21), has been developed by Ergun and Orning[13] for pressure drop through fixed beds over a wide range of flow velocities.

$$\frac{\Delta P}{LV} \frac{\epsilon^3}{(1-\epsilon)^2} = a'' + b'' \frac{G}{1-\epsilon} \qquad 2.22$$

where a'' and b'' are factors of proportionality and G is the mass flow rate of drying air.

(iv) Size, shape and surface of particles

It is customary to use a characteristic dimension to represent the size of particles of any shape in pressure drop calculations. The characteristic dimension generally used is the diameter D_p of the equivalent sphere, i.e. a sphere which has the same volume as the particle. The specific surface of the particle is S, which is defined by :

$$S = \frac{6}{D_p} \qquad 2.23$$

Ergun and Orning on the basis of Kozeny and Burke's theoretical equations developed the following equation

$$\frac{\Delta P\, g_c}{L} = 2 \propto \mu \quad S^2 \; V_m \frac{(1-\epsilon)^2}{\epsilon^3} + \frac{\beta}{8} \; G \; V_m \; S \frac{(1-\epsilon)}{\epsilon^3} \qquad 2.24$$

where $\propto$ and β are statistical coefficients of viscous and kinetic energies respectively. Substituting Eqn.(2.23) in Eqn.(2.24),

$$\frac{\Delta P}{L} g_c = k_1 \frac{(1-\epsilon)^2}{\epsilon^3} \frac{\mu \; V_m}{D_p^2} + k_2 \frac{1-\epsilon}{\epsilon^3} \frac{\rho \; V_m^2}{D_p^2} \qquad 2.25$$

where $k_1 = 72 \propto$ and $k_2 = \frac{3}{4} \beta$

The coefficients k_1 and k_2 have been determined experimentally and have been found to be

$$k_1 = 150 , \quad k_2 = 1.75.$$

Equation (2.25) is known as the Ergun equation and its validity has been tested by Ergun with spheres, cylinders, tablets, nodules and crushed materials (e.g. glass, coke, etc.) and found to be satisfactory.

A linear form of Eqn.(2.25) is

$$\frac{\Delta P}{L} g_c \frac{D_p^2}{\mu \; V_m} \frac{\epsilon^3}{(1-\epsilon)^2} = k_1 + k_2 \frac{Re}{1-\epsilon} \qquad 2.26$$

where $Re = \frac{G \; D_p}{a \; \mu}$

The left hand side of Eqn.(2.26) is the ratio of the pressure gradient to the viscous energy term and will be designated by ψ , the friction factor.

$$\psi = k_1 + k_2 \frac{Re}{1-\epsilon} \qquad 2.27$$

According to Eqn.(2.26), a linear relationship exists between ψ and $\frac{Re}{1-\epsilon}$. A plot of log ψ against log $\frac{Re}{1-\epsilon}$ is shown in Fig. 2.2.

FIG. 2.2

Plot of Log ψ against Log $\frac{Re}{1-\epsilon}$

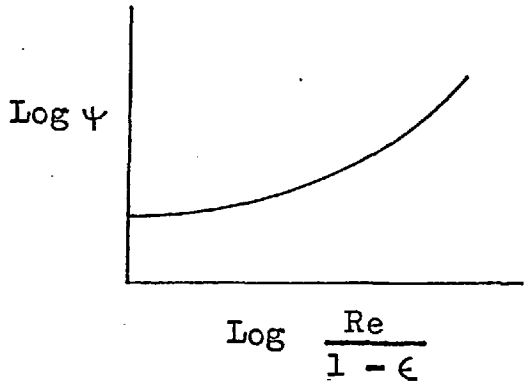

It should be noted that transition from laminar to turbulent flow is gradual in a packed bed as compared to pipes, and occurs between Re : 1 and 150 approximately [8].

Correction for wall effect

The influence of the walls of the column containing the bed is important, since the voidage is greater near the walls. Corrections for this should be made by measuring the average value of the voidage including the voidage next to the walls. Further correction should be made to account for the friction at the walls of the column.

Coulson[14] has shown that for stream-line flow, the wall effect can be taken into account by the use of an empirical factor. For a given pressure difference, the velocity through an infinite bed is less than that in a finite bed by a factor of $(1 + \frac{1}{2}\frac{S_c}{S})^2$, where S is the specific surface and S_c is the surface of the containing

vessel/unit volume of bed.

2.4 - Heat transfer in packed beds

In order to gain a deeper understanding of the process of heat transfer in packed beds related to this work, the research of some of the previous workers on the subject will be discussed.

(a) Schumann[15] derived mathematically the simple case of an incompressible fluid passing uniformly through a bed of perfectly conducting solid particles. He calculated the time variation of temperatures for both the fluid and the solid at any distance through the bed. He assumed that,

(i) solid particles are so small or have such high thermal conductivity that any particle may be considered as being at a uniform temperature at any time;

(ii) compared to the transfer of heat from fluid to solid, the transfer of heat by conduction in the fluid itself is negligible;

(iii) the rate of heat transfer from fluid to solid at any point is proportional to the average difference in temperature between fluid and solid at any point;

(iv) the change in volume of fluid and solid due to change in temperature may be neglected;

(v) the thermal constants are independent of temperature.

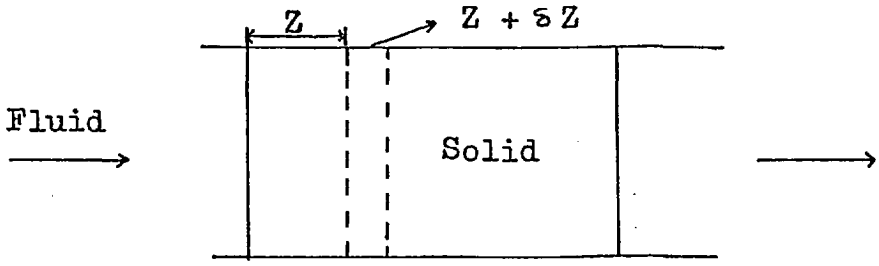

FIG.2.3 - Schumann's model of heat transfer.

The initial temperature of the solid was taken as zero.

Consider the transfer of heat to an element of fluid of unit cross-sectional area contained between Z and Z + δ Z. The heat imparted to this element by the solid in time δ T = - (constant x difference in temperature x width of the element) δ Z.

$$= - h (t_g - t_s) \delta Z . \delta T. \qquad 2.28$$

The heat carried in to the element by the fluid.

$$= \frac{- \partial t_g}{\partial Z} H_g \; V \epsilon \; dZ \; dT \qquad 2.29$$

The sum of these must be

= (rise in temperature in time dt) x (the heat capacity of the element)

$$= \frac{\partial t_g}{\partial T} H_g \; \epsilon \; dZ \; dT \qquad 2.30$$

The resulting equation is

$$\frac{\partial t_g}{\partial T} + V \frac{\partial t_g}{\partial Z} = - \frac{h}{H_g \epsilon} (t_g - t_s)$$

$$= - h_2 (t_g - t_s) \qquad 2.31$$

Similarly by considering an element of the solid, we find

$$\frac{\partial t_s}{\partial T} = h_1 (t_g - t_s) \qquad 2.32$$

where $h_1 = \frac{h}{H_s} (1 - \epsilon)$.

There are certain conditions which have to be satisfied in order to solve the problem, and they are :

At $Z = 0$,

$t_g = t_{g_o}$ for all time,

and $t_s = 0$ at $T = 0$.

By integrating Eqn.(2.32), it follows that at $Z = 0$,

$$t_s = t_{g_o}(1 - e^{-h_1 T}) \qquad 2.33$$

If we imagine the bed to extend to infinity in the positive Z direction, then we can find the temperatures at the farthest point reached by the fluid.

At $Z = VT$, $t_s = 0$.

$$t_g = t_{g_o} \; e^{-h_2 T} \qquad 2.34$$

Equation (2.34) is found by following the front-most element of fluid which is always in contact with a part of the solid still at zero temperature. If we therefore consider the heat transfer from this element to the solid, equation (2.31) becomes

$$\frac{dt_g}{dT} = - h_2 \, t_g \quad \text{at} \quad Z = VT \qquad 2.35$$

On integration, this equation leads to Eqn.(2.34). Schumann's solutions are given in graphical form in his paper.

(b) Furnas[16] passed hot combustion gases through cylinders filled in turn with iron ores, iron balls, and sinter, and on the basis of his experimental work, formulated an expression for the heat transfer coefficient,

$$h_v = A_s \frac{V^{0.7}\, t_{g_{av}}^{0.3}}{D_p^{0.9}} f'$$

Furnas plotted a graph between f' and voidage for obtaining the values of f'.

(c) Saunders and Ford[17] criticized Furnas's work saying that the heat capacity of his insulated container was several times that of the particles inside. This would influence the results, and would be different for different beds, making comparison between them unreliable. Also, owing to the small size of the hole through which the gases entered some of the beds, the flow was far from uniformly distributed across the bed. Also the ratio of particle diameter to container diameter was sufficiently large for extensive wall flow to occur, which may mean that Furnas's conclusion that the heat transfer is proportional to $D_p^{0.9}$ is not generally applicable. Furnas was surprised at the low index of 0.9 and suggested that for smaller sizes an increasing proportion of the open spaces in the bed becomes too small to permit the passage of a significant amount of gas, so that the relative area in contact with the gas stream in the smaller sizes becomes less. This explanation neglects the increase in velocity which must result from partial blocking of the bed if the total flow remains the same, although Furnas himself later says when explaining the increase in the heat transfer with decrease in the void fraction, that decreasing the voids also increases the linear velocity. It is therefore doubtful

whether Furnas's results are applicable except in the particular circumstances of his experiments.

Saunders and Ford carried out experiments with spheres of various diameters, placed in three geometrically similar cylinders. The spheres were of steel, lead and glass. Heating was by hot air, the temperature of which was 84°C. In a bed of spheres, each of diameter D_p, in a column of diameter D and height L, with the gas flowing parallel to the axis, the shape of the bed is determined by $\frac{D}{D_p}$ and $\frac{L}{D_p}$. For beds wide compared with the diameter of the spheres, $\frac{D}{D_p}$ need not be considered, and the shape is determined only by $\frac{L}{D_p}$. Therefore $\frac{t'_g - t_{s_o}}{t_{g_o} - t_{s_o}}$ depends upon the three groups.

$$\frac{V' T C'}{D_p C} \quad , \quad \frac{V' D C'}{K} \quad \text{and} \quad \frac{L}{D_p}$$

The dimensional analysis applied to heat transfer in the flow of gases through a bed of solid particles, carried out by Saunders and Ford, shows that the total heat transfer Q from the gas to the bed during time T is expressed in a relation between

$$\frac{4Q}{\pi D^2 L C(1-\epsilon)(t_{g_o} - t_{s_o})}$$

and the above three groups.

They came to the conclusion that if the particles are small enough, or if their thermal conductivity is high enough, the effects of temperature gradients inside them can be neglected, and

$\frac{t'_g - t_{s_o}}{t_{g_o} - t_{s_o}}$ and $\frac{4Q}{\pi D^2 L\, C(1-\epsilon)(t_{g_o} - t_{s_o})}$ depend only upon $\frac{V'\, T\, C'}{D_p\, C}$ and $\frac{h}{D_p}$.

Kitaev et al.[18] made the following comments on the work of Saunders and Ford.

i) The influence of thermal conducivity would have manifested itself except for the fact that Saunders and Ford used very small glass balls (6.35×10^{-3}m).

(ii) The low temperature range makes it difficult to extrapolate the authors data to high temperatures.

(d) Rowe and Claxton[19] measured heat and mass transfer from a single sphere in an assembly of similar spheres through which air or water was flowing. The results were described by the following set of equations :-

$$Nu \text{ (or } Sh) = A + B\, Pr^{1/3} (\text{or } Sc^{1/3})\, Re^n \qquad 2.36$$

where $A = \frac{2}{1-(1-\epsilon)^{1/3}}$

$B = \frac{2}{3\epsilon}$ (for air or water)

and $\frac{(2-3n)}{(3n-1)} = 4.65\, Re^{-0.28}$

The results apply to a regular rhombohedral arrangement of spheres, to a cubic arrangement, and to random packing, and can be applied to predict heat or mass to or from packed beds.

(e) Amundson[20] gave the differential equations describing the model of the heat transfer from a gas in plug flow to an adiabatically enclosed stationary bed of non-reacting spheres neglecting radiative effects. The equations allow for both turbulent axial thermal conductivity in the gas phase and resistance to heat transfer in the solid phase.

(f) Bradshaw et al.[21] passed heated nitrogen or air through randomly packed beds of steel balls, alumina balls and hematite pellets. They approximated Amundson's equations to the simpler equations of Schumann, given on page 33a, by the use of an effective heat transfer coefficient, which gave,

$$V_i H_g \frac{\partial t_g}{\partial L} + H_g \frac{\partial t_g}{\partial T} + h_E S (t_g - t_s) = 0 \qquad 2.37$$

$$H_s \frac{\partial t_s}{\partial T} + h_E S (t_s - t_g) = 0 \qquad 2.38$$

Equations (2.37) and (2.38) are similar to Schumann's equations (2.31) and (2.32) given on page 33a, the difference being a modified heat transfer coefficient

$$\frac{1}{h_E} = \frac{1}{h} + \frac{D_p}{10K_s} + \frac{K_{tr} S}{(V_i H_g)^2} \qquad 2.39$$

where

$\frac{1}{h_E}$ = effective resistance to heat transfer

$\frac{1}{h}$ = resistance to heat transfer in the boundary layer

$\frac{D_p}{10K_s}$ = resistance due to the properties of the solid

and $\frac{K_{tr}\, S}{(V_i\, H_g)^2}$ = resistance in the main gas stream.

From Eqn.(2.39) it is clear that the three terms on the right hand side represent three different resistances to heat transfer, which are in series.

(g) Acrivos[22] presented a numerical scheme known as the method of characteristics, for solving the equations of one dimensionel models.

The basic relations for a one dimensional isothermal model obtained by the application of three continuity equations, assuming plug flow and neglecting diffusion along the axis of the bed, are

$$V \frac{\partial \eta}{\partial Z} + \epsilon \frac{\partial \eta}{\partial T} = -(1 - \frac{\eta}{\rho_m}) R'(\eta, w, V) \qquad 2.40$$

$$\frac{\partial \eta}{\partial Z} = -\frac{1}{\rho_m} R'(\eta, w, V) \qquad 2.41$$

$$\frac{\partial w}{\partial T} = R'(\eta, w, V) \qquad 2.42$$

Acrivos used these equations for studying isothermal and adiabatic adsorption. Adsorption is the reverse of drying, and therefore the above equations and the method of characteristics could be applied to drying rate studies.

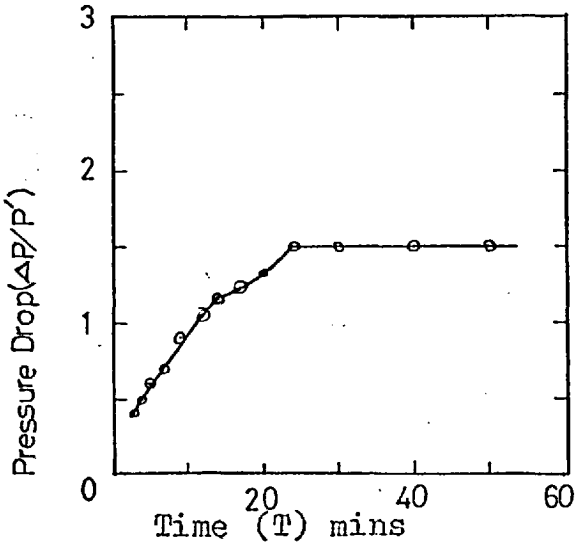

FIGURE 2.a-Shrinkage Curve.

2.5 - Drying of packed beds.

When a gas passes through a bed of wet granular materials, both a constant and one or two falling rate periods may result as in the case of slab or tray drying, discussed in section 2.2.

(a) Marshall and Hougen[23] carried out drying experiments on a number of different solid materials and showed that the drying time and drying rate curves for through circulation drying are analogous to those obtained for tray drying. They obtained a third curve unobtainable in tray drying, and called it a shrinkage curve. This shrinkage curve was obtained by the variation in pressure drop through the bed during drying, as shown in Fig. 2.a. Marshall and Hougen theoretically expressed their drying rates as

$$\text{Drying Rate} = \left\{ \left[\text{Re}, \text{Sc}, \frac{P}{p_{m\text{-}air}}, (p_s - p_a) \right] \right.$$

$$\propto \left(\frac{G}{a}\right)^n (p_s - p_a)$$

$$\propto \left(\frac{G}{a}\right)^n \Delta x \qquad 2.43$$

By experiments, they found the drying rates to be

$$Y' = A\left(\frac{G}{a}\right)^{0.8} \Delta x \qquad 2.44$$

where Y' is the drying rate in the constant rate period in Kg water evaporated/Kg dry solid.second. By assuming $\Delta x \propto \Delta t$

$$Y' = A' \left(\frac{G}{a}\right)^{0.8} \Delta t \qquad 2.45$$

With beds of pellets, the constant drying rate was shown to be approximately proportional to the reciprocal of the square root of the diameter of the pellets. From the correlation of extensive industrial data on through circulation drying, values of A for the constant rate period were determined for a wide range of materials. Under these various conditions of pelletizing, A was shown to be dependent upon the method of pelletizing used, and ranged from low values for heavy, dense materials, to high values for light fibrous materials.

(b) Gamson et al[24] extended Marshall and Hougen's work to give

$$Y' = A'' \left(\frac{G}{a}\right)^{0.8} D_p^{-0.44} \Delta x \qquad 2.46$$

where A'' is an experimental constant which depends on the material to be dried. They believed that the only resistance to mass transfer lay in the gaseous boundary layer because the constant rate period was associated with resistance occurring when free moisture existed at the surface. Hence the rate of mass transfer through the boundary layer can be expressed as

$$Y' = \frac{M' h_D' S (p_s - p_a)}{m} \qquad 2.47$$

where h_D' is the mass transfer coefficient in K moles/S m^2 atm and can be obtained from their j-factor correlation for mass transfer in a packed bed.

$$j_D = \frac{h_D' \; p_{m\,air} \; M'}{\frac{G}{a}} \left[\frac{\mu}{\rho D_v}\right]_f^{2/3}$$

$$= 0.989 \left(\frac{D_p \frac{G}{a}}{\mu}\right)^{-0.41} \quad \text{for turbulent flow} \qquad 2.48$$

substituting for h_D' in Eqn.(2.47) gives

$$Y' = A''' \frac{S}{m} \left(\frac{G}{a}\right)^{0.59} D_p^{-0.41} \Delta x \qquad 2.49$$

Equation (2.49) is in reasonable agreement with the empirical Eqn.(2.46).

Marshall and Hougen as well as Gamson et al in their equations have used over-all values of Δp, Δx and Δt. The use of Log mean values would be more accurate because the driving force varies with the position in the bed, as well as with time.

(c) Many other workers [25,26,27,28,29,30] have studied evaporation of water from packed beds, particularly to obtain mass transfer correlations of the form.

$$j_D = A \, Re^n \qquad 2.50$$

where $A = f(\epsilon)$

some of these correlations have taken into account the effect of axial mixing. Axial mixing[31] is important when the beds are shallow and when the ratio

$$R = \frac{\text{inlet driving force for mass transfer}}{\text{outlet driving force for mass transfer}}$$

is large. Epstein[31] obtained an axial mixing factor F, which is a multiplication factor used to correct the rate of mass transfer.

$$F = \frac{\ln R}{n(Re^{1/n} - 1)} \qquad 2.51$$

where n is the number of perfect mixers in series in the bed and is given by

$$n = \frac{L}{D_p} \quad \frac{Pe}{2} \qquad 2.52$$

The Peclet number $\left(\frac{D_p\ u}{E'}\right)$, where E' is axial dispersion coefficient, is given by Carberry[32] as $Pe \simeq 2$.

A general correlation for mass transfer in packed beds which includes the effect of axial mixing is given by Colquhoun - Lee and Stepanek[33] as

$$j_D = 1.24 \left(\frac{Re}{1 - \epsilon}\right)^{-0.39} \qquad 2.53$$

(d) Allerton[34] carried out experiments to study the mechanism of the drying of filter cakes. Glass balls were used to represent a filter cake and were placed in a rectangular test box, moistened, and hot air passed downwards through the bed. The sample was taken out at intervals, weighed and put back, taking care to avoid any moisture loss during the weighing operation. According to Allerton's model, and confirmed by his experiments, drying took place in a narrow zone of vaporization, shown in Fig.2.4.

FIG. 2.4

Allerton's model of drying.

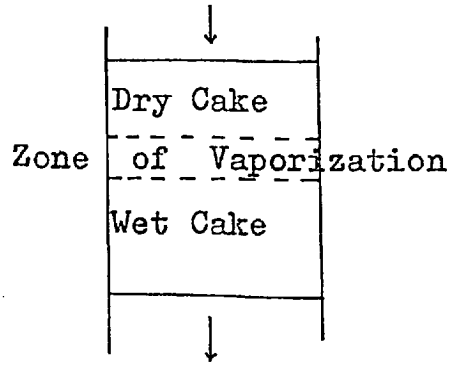

The area above the zone was assumed to be dry, and that

below the zone to be wet. The drying process was divided into a constant rate and decreasing rate periods. In the constant rate period, the drying air leaves the bed saturated at its adiabatic saturation temperature. The decreasing rate period starts, when the zone of vaporization reaches the bottom of the bed and air is no longer saturated. Allerton assumed that the vaporization zone moved down the bed at a constant rate during both of the drying periods, and suggested the following relation for calculating the thickness of the vaporization zone,

$$Z = \frac{\text{length of time of decreasing rate period}}{\text{total drying time}} L \qquad 2.54$$

The value of Z depends upon the conditions of drying, but is usually of the magnitude of 3.17×10^{-3}m to 6.35×10^{-3}m.

The following equation was given for obtaining the rates of drying during the constant rate period.

$$Y = \frac{G}{a} (x'_{as} - x'_o) \qquad 2.55$$

assuming that the air leaves the bed in a saturated condition. A material balance on an element in the bed gives

$$\delta Y = \frac{G}{a} \delta x$$

But $$\frac{a}{M'} \delta Y = h'_D (p_s - p_a) \delta S'$$

where S' is the area of the liquid surface. Expressing h'_D as a j-factor (see Eqn.2.50) and integrating over the drying zone between $S' = 0$ and $S' = S'$, and $p = p_1$ and $p = p_2$, he obtained

$$\frac{p_2 - p_1}{p_s - p_1} = 1 - e^{-\frac{j_D \, S'}{Sc_f^{2/3} \, A}} \qquad 2.56$$

where $\frac{j_D \, S'}{Sc_f^{2/3}}$ is called the drying factor and $(p_2 - p_1)$ is the actual change in partial pressure of water evaporated whereas $(p_s - p_1)$ is the change in partial pressure if equilibrium were obtained. The ratio $\frac{p_2 - p_1}{p_s - p_1}$ is therefore the efficiency of drying. The actual drying rate is 2.a therefore given by

$$Y'' = Y \frac{p_2 - p_1}{p_s - p_1} \qquad 2.57$$

Some of the flaws in Allerton's work are -

i) The apparatus had no arrangement for continuously weighing the test sample, which therefore had to be taken out at intervals for weighing. During the weighing some moisture loss must have occurred.

ii) The moisture content of the sample was so high that during the first few minutes of the run, moisture had to be wiped from the bottom of the test box when removed for weighing.

(e) Beveridge[35] studied the rates of drying of kieselguhr and zinc sulphide particles by passing air at upto 500°C through beds one foot deep. Steady gas conditions were attained before the bed containing particles of a known moisture content was placed in position. The movement of the drying zone through the bed was followed by measuring

the temperature variation with thermocouples inserted into the bed and in some of the large particles at different levels in the bed. The propagation of a heat wave in dry beds was also investigated for larger particles. This is the only work carried out at high temperatures, which is similar to the work under consideration.

Some of Beveridge's results have been plotted in Fig. 7 ** It can be seen from all the three curves that the velocity of the drying zone is proportional to the gas flow rate at a given temperature and moisture content. The large decrease in the velocity of the drying zone during the drying of wet particles is indicated in comparison of curves 1 which is drawn for dry particles, and curve 2 or 3 drawn for moist particles.

Beveridge's other results show that there is no significant effect of inlet air temperature on the velocity of the heat wave in dry beds. On the other hand, in the presence of water in the solids, the inlet air temperature does affect the drying zone velocity. An increase in inlet air temperature appears to increase the drying zone velocity in wet beds.

(f) Myklestad[36] in his theoretical analysis of packed bed drying says that in the drying of deep beds, there are four stages of drying, i.e. a constant rate period, one rising and two falling rate periods. He has given the following explanation for the rising rate period.

During the constant rate period, the temperature and humidity of the drying medium at any given point in the bed depend only on the height of the point from the bottom of

** in his paper [35] on page 101.

the bed. But after the bottom layer of the packed material has reached the critical moisture level, the psychometric condition of the drying medium becomes a function of time as well. Subsequently the rate of drying of the bottom layer gradually diminishes and the ascending drying medium becomes less cooled and less humidified; only where the drying medium enters at the bottom of the bed are its temperature and humidity constant at all times. This gradual improvement in the drying power of the drying medium is the reason for the increasing rate stage of drying of material at a point within the body of the bed.

Summary of previous work on drying in packed beds

Marshall and Hougen[23] as well as Gamson et al[24] have carried out drying experiments on very shallow beds. The ratio of particle diameter to bed height was approximately 1:4 and their empirical correlations should not be used to explain drying in deep packed beds. This is because the drying behaviour of such shallow beds can be expected to resemble closely that of slab or tray drying. Although many other workers[25-30,34] have studied the drying of deeper packed beds, all of these experiments were carried out with drying air below 100°C. Beveridge[35] is the only worker to have carried out drying experiments in packed beds at the high temperatures experienced in pellet firing processes, i.e. the temperatures were in the range 270°C to 410°C. He investigated empirically the velocity of a drying zone moving through deep beds but did not propose a method for predicting drying rates.

Therefore, in order to predict drying rates in deep beds at temperatures relevant to drying sinter feed and green pellets, a model of the drying process will be developed and this must be justified by appropriate experimental work. It is therefore proposed in this work that follows to weigh continuously a bed during drying and to compare the rates of drying obtained with rates predicted from the proposed model.

CHAPTER 3 MODEL OF DRYING IN DEEP BEDS

A theoretical model is presented for predicting the drying rates of materials in deep packed beds.

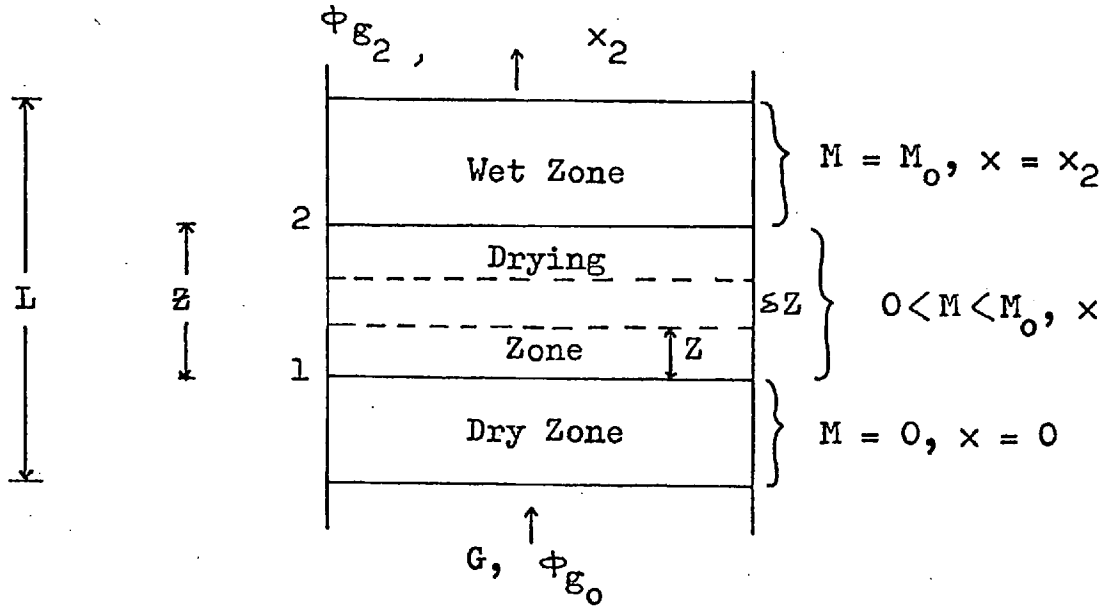

Fig. 3.1. Model of drying in deep beds.

The model assumes that at any time T after the start of drying, a drying zone of height Z is established in the bed, as shown in Fig. 3.1. The wet region which exists above the drying zone is assumed to have a uniform moisture content M_o, equal to the initial moisture content. A completely dry region exists below the drying zone.

The following assumptions will be made :-

i) The height of the drying zone Z is constant and is less than the total height of the bed.

ii) The drying zone moves up the bed with a constant speed u, and u is small compared to the air velocity in the bed.

iii) Air entering the drying zone is dry, whereas air leaving the drying zone is saturated.

iv) There are no heat losses from the walls of the bed.

v) No heat or mass transfer takes places in the wet zone

and no mass transfer occurs in the dry zone.

vi) All the heat transferred from the air to the drying zone is used in the evaporation of water, and the temperature of the solids in the drying zone therefore remains at the initial temperature of the solids.

vii) Resistance to heat and mass transfer lies in the gaseous phase only, i.e. the temperatures of liquid and solid are identical and there are no temperature gradients in either liquid or solid in the drying zone.

viii) There is no channelling of the drying air in the bed.

ix) Gas velocity is not influenced by pressure drop.

Assumptions (i) and (ii) imply that the overall drying rate is constant as long as the drying zone remains in the bed. This constant rate should not be confused with the constant rate obtained in slab or tray drying (section 2.2). In slab drying a constant rate is only obtained when there is free moisture on the surface of the solid. However, a constant rate could be obtained during the drying of packed beds when some or all of the solid in the drying zone has no free moisture on its surface. In the drying zone, M, ϕ_g, and x can therefore be considered to vary with Z only and to be independent of time, provided that $Z = 0$ at position 1.

Enthalpy and mass balances can now be formulated both for a differential element δZ in the drying zone, and for the entire drying zone.

Enthalpy Balances

For the element δZ in the drying zone,

$$G \frac{d \Phi_g}{dZ} \delta Z = m a u \lambda \frac{dM}{dZ} \delta Z \qquad 3.1$$

At $Z = 0$, $M = 0$, $\Phi_g = \Phi_{g_1}$

At $Z = Z$, $M = M_o$, $\Phi_g = \Phi_{g_2}$

Integrating Eqn.(3.1) between $Z = 0$ and $Z = Z$ gives the overall enthalpy balance

$$G (\Phi_{g_1} - \Phi_{g_2}) = m a u M_o \lambda \qquad 3.2$$

It should be noted that Φ_{g_2} is the sensible heat of the saturated air leaving the drying zone. The heat transferred from the air to the drying zone can also be expressed as :-

$$G (\Phi_{g_1} - \Phi_{g_2}) = h_V a (1 - \epsilon) Z t_m \qquad 3.3$$

where h_V is the volumetric heat transfer coefficient. The heat transfer coefficient h can be obtained from Eqn. 2.36 on page 37, assuming that the evaporation of water does not influence h. If mass transfer influences h, the equation 2.15 on page 24 must be used. In this equation, $(t_g - t_s)$ will be replaced by the log mean difference air temperature in the drying zone t_m, which is derived as follows :-

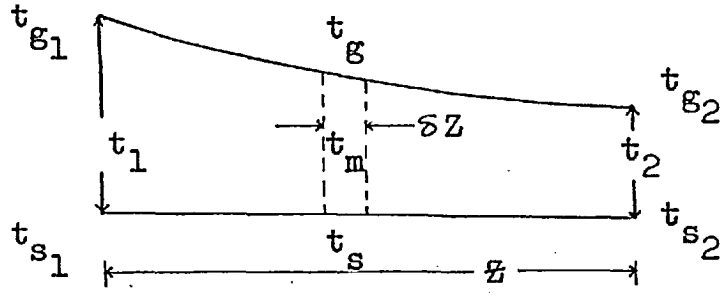

$$t_{s_1} = t_{s_2} = t_s$$

$$Q' = h_V Z t_m \quad , \quad \text{where} \quad t_m = t_g - t_s$$

Therefore $dt_m = dt_g - dt_s$, but $dt_s = 0$, (assumption IV, P. 51)

Therefore $dt_m = dt_g$

Heat lost by gas :-

$$dQ' = G \, \lambda_m \, dt_g$$

Therefore $$dt_m = \frac{dQ'}{G \, \lambda_m}$$

or $$t_1 - t_2 = \frac{Q'}{G \, \lambda_m}$$

Heat balance over an element δZ :-

$$h_v \, dZ \; t_m = dQ' = G \, \lambda_m \, dt_m$$

Integrating over Z,

$$h_v \frac{1}{G \, \lambda_m} \int_0^Z dZ = \int_{t_1}^{t_2} \frac{dt_m}{t_m}$$

or $$h_v \frac{1}{G \, \lambda_m} Z = \ln \frac{t_1}{t_2}$$

$$t_1 - t_2 = \frac{1}{G \, \lambda_m} Q' = \frac{1}{G \, \lambda_m} h_v \, Z \, t_m = \ln \frac{t_1}{t_2} \, t_m$$

or $$t_m = \frac{t_1 - t_2}{\ln \frac{t_1}{t_2}} = \frac{t_{g_1} - t_{g_2}}{\ln \frac{t_{g_1} - t_s}{t_{g_2} - t_s}} \qquad 3.4$$

Mass Balances

For the element δZ in the drying zone,

$$G \frac{dx}{dZ} \delta Z = m \, a \, u \frac{dM}{dZ} \delta Z \qquad 3.5$$

An overall balance can be obtained by integrating Eqn.(3.5) between $Z = 0$ and $Z = Z$.

At $Z = 0$, $x = 0$ by assumption (iii), and $M = 0$.

At $Z = Z$, $x = x_2$ and $M = M_o$.

Equation (3.5) becomes

$$G\ x_2 = m\ a\ u\ M_o \qquad 3.6$$

where $G\ x_2$ is the drying rate and x_2 is the saturation humidity of the air leaving the drying zone.

Combining Eqn.(3.2) and (3.3) ,

$$h_V\ a\ (1 - \epsilon)\ Z\ t_m = m\ a\ u\ M_o\ \lambda \qquad 3.7$$

From equations (3.6) and (3.7),

$$G\ x_2 = \frac{h_V\ a\ (1-\epsilon)\ Z\ t_m}{\lambda} \qquad 3.8$$

Equation (3.8) can be re-written as

$$\frac{G\ x_2}{a} = \frac{h_V\ (1-\epsilon)\ Z\ t_m}{\lambda} \qquad 3.9$$

where $\frac{G\ x_2}{a}$ is the specific drying rate.

$$\text{Or}\quad \frac{G\ x_2}{a} = \frac{h\ S\ (1-\epsilon)^2\ Z\ t_m}{\lambda} \qquad 3.10$$

The Lewis relationship gives

$$h_D = \frac{h}{\ell\ C_p} \quad \text{(Page 21)}$$

Hence Eqn.(3.10) becomes

$$\frac{G\,x_2}{a} = h_D\,S(1-\epsilon)^2\,Z\,\frac{\rho C_p\,t_m}{\lambda} \qquad 3.11$$

$$= \frac{h_D\,S(1-\epsilon)^2\,Z\,\rho\,\Phi_m}{\lambda} \qquad 3.12$$

The height of the drying zone can be obtained from equations (3.7) and (3.9);

$$Z = \frac{m\,a\,u\,M_o}{h_V\,a(1-\epsilon)t_m} = \frac{G\,X_2\,\lambda}{h_V\,a(1-\epsilon)t_m} \qquad 3.13$$

where Z is the height of the drying zone. Equations (3.10) and (3.13) can be used to predict the rate of drying and the height of the drying zone respectively for any material.

CHAPTER 4

DESIGN OF APPARATUS

CHAPTER 4 DESIGN OF APPARATUS

A flow sheet of the apparatus is shown in Fig.4.1. The apparatus was designed so that the weight of the column and its contents could be measured and recorded continuously as drying proceeded. The basic problem to be overcome in designing the column was twofold, i.e. to allow free movement of the column and yet prevent drying air from leaking out of the inlet to the column. These difficulties were overcome by using a mercury seal at the bottom of the column. The first design of the mercury seal is shown in Fig.4.2 . This seal had to be redesigned because of certain experimental difficulties mentioned on page 69 . The new design is shown in Fig.4.3.

A load cell, as shown in Plate 2, was used for continuously weighing the column. The column was suspended from one end of a beam which was supported on a knife-edge. A counter-balance was suspended from the other end of the beam. The counter-balance was used so that a load cell of range 0-1 Kg approximately could be used to determine the change in weight of a column weighing many kilograms.

Another problem encountered was that of the expansion of the apparatus when hot air passed through the system. So flexible bronze bellows were fixed in the pipework below the column and above the air heater.

The handy angle frame of the apparatus was placed on a concrete slab, which in turn was placed on blocks of compressed cork to minimize vibrations being transmitted to the apparatus through the floor.

A disc pelletizer shown in Fig.4.4 was used to roll pellets from iron ore concentrate, and a mixer, also shown

PLATE 1

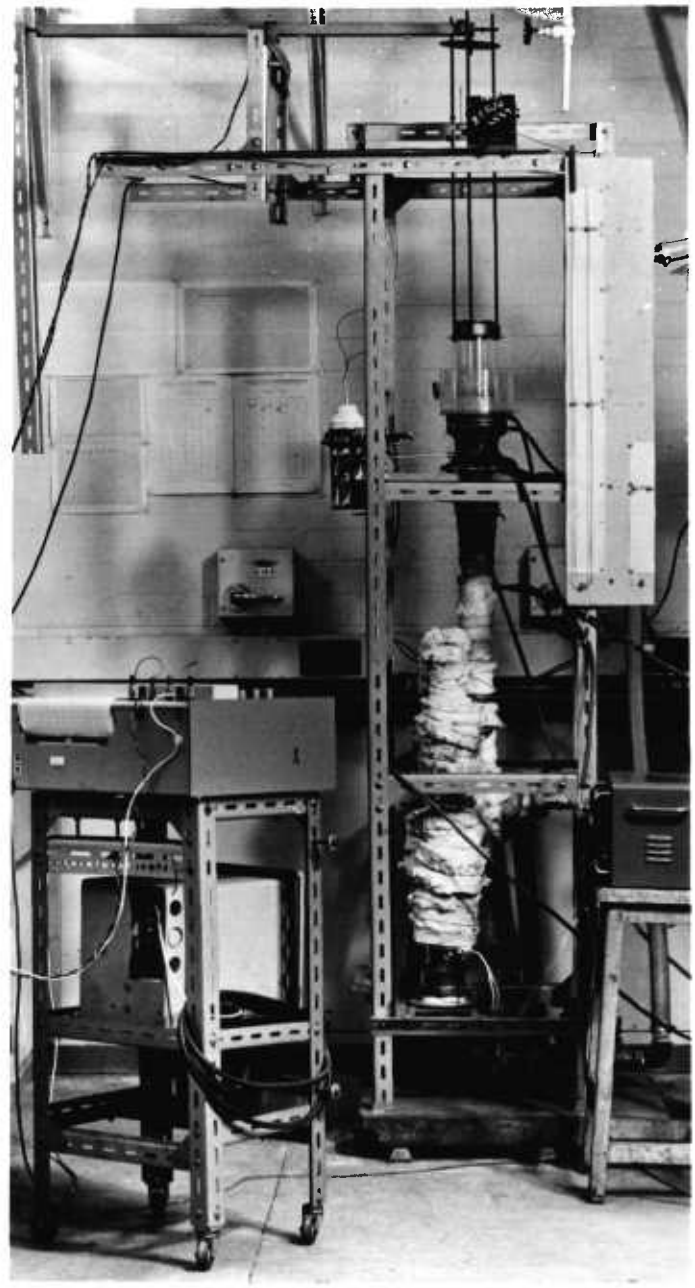

GENERAL VIEW OF THE APPARATUS

PLATE 2

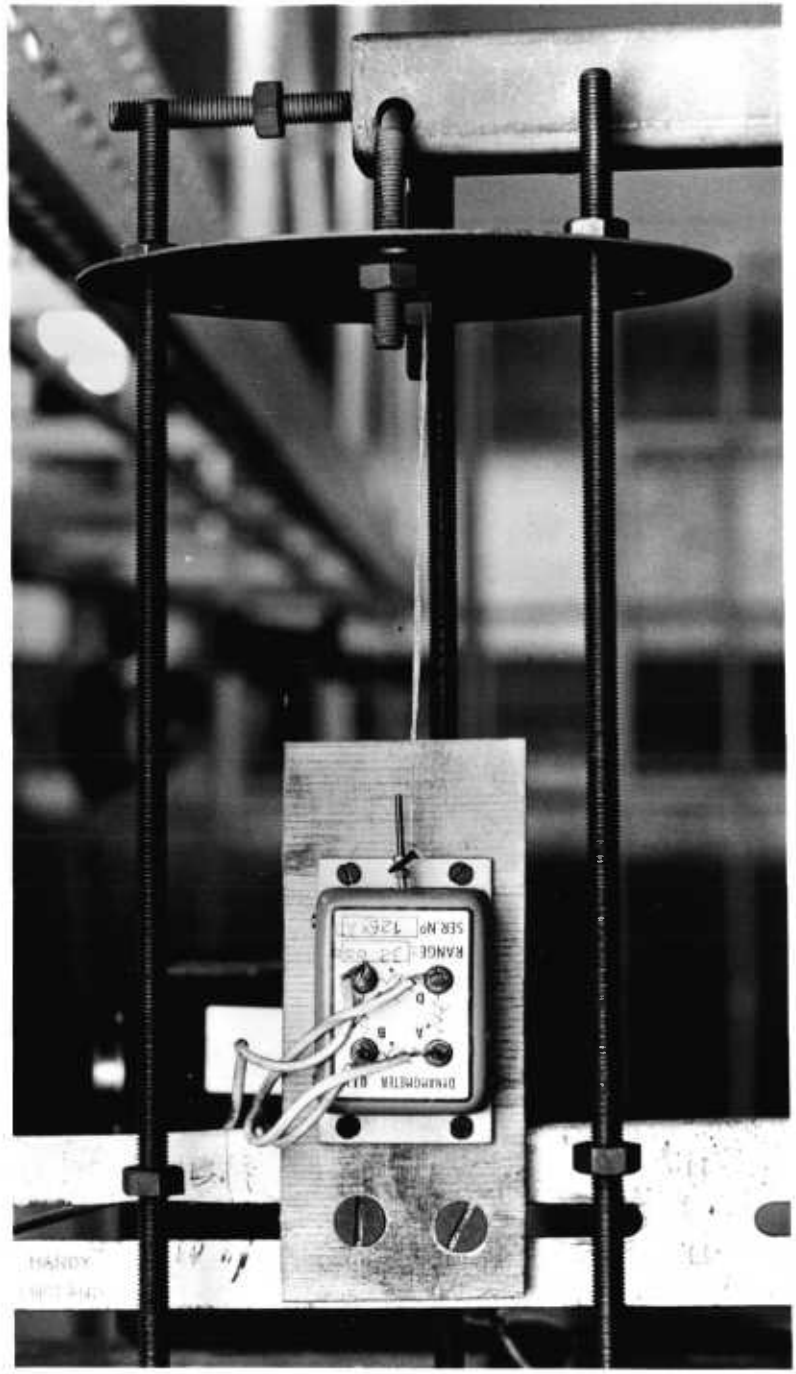

LOAD CELL AND BEAM ARRANGEMENT

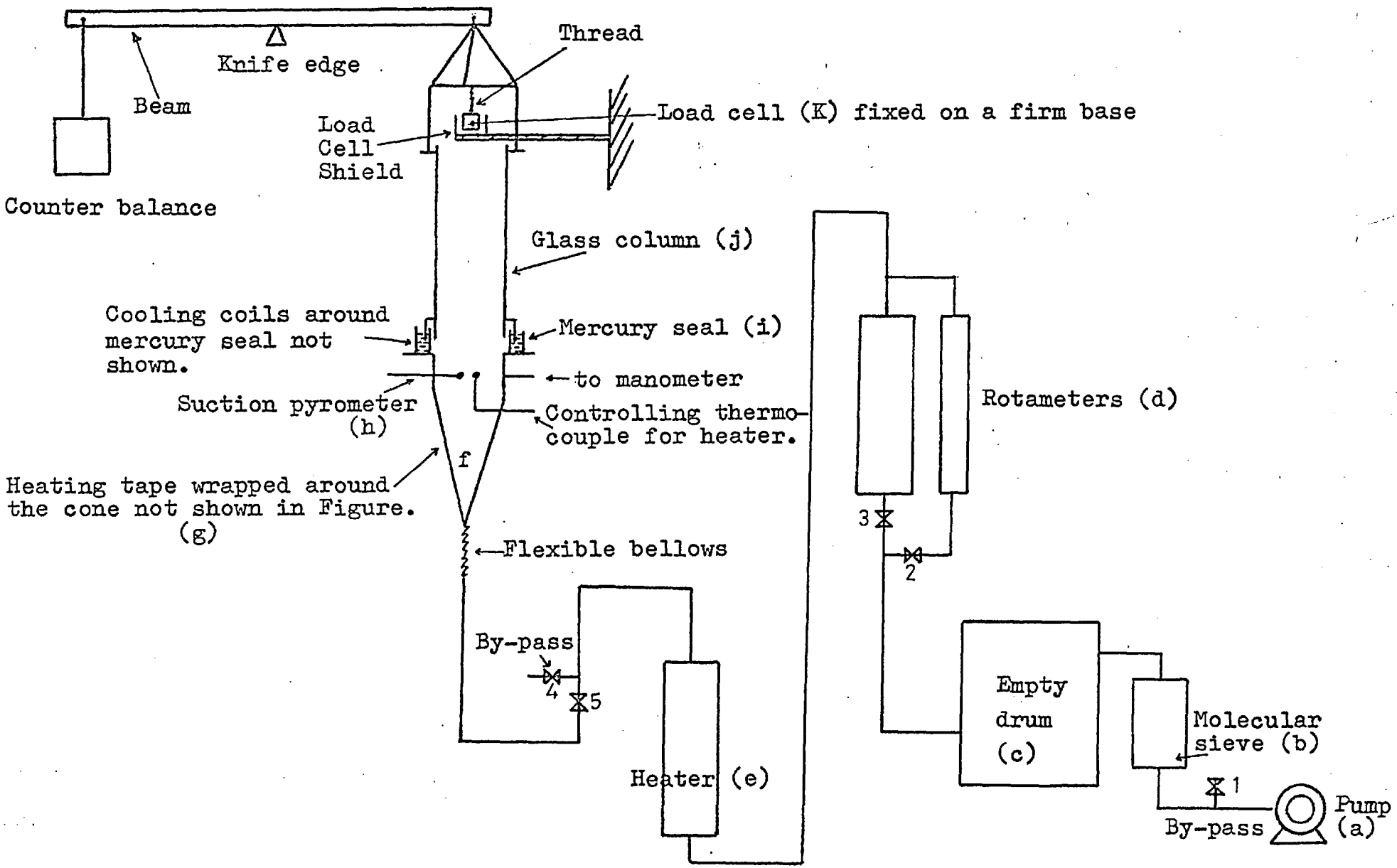

FIGURE 4.1 - Flow diagram of the apparatus

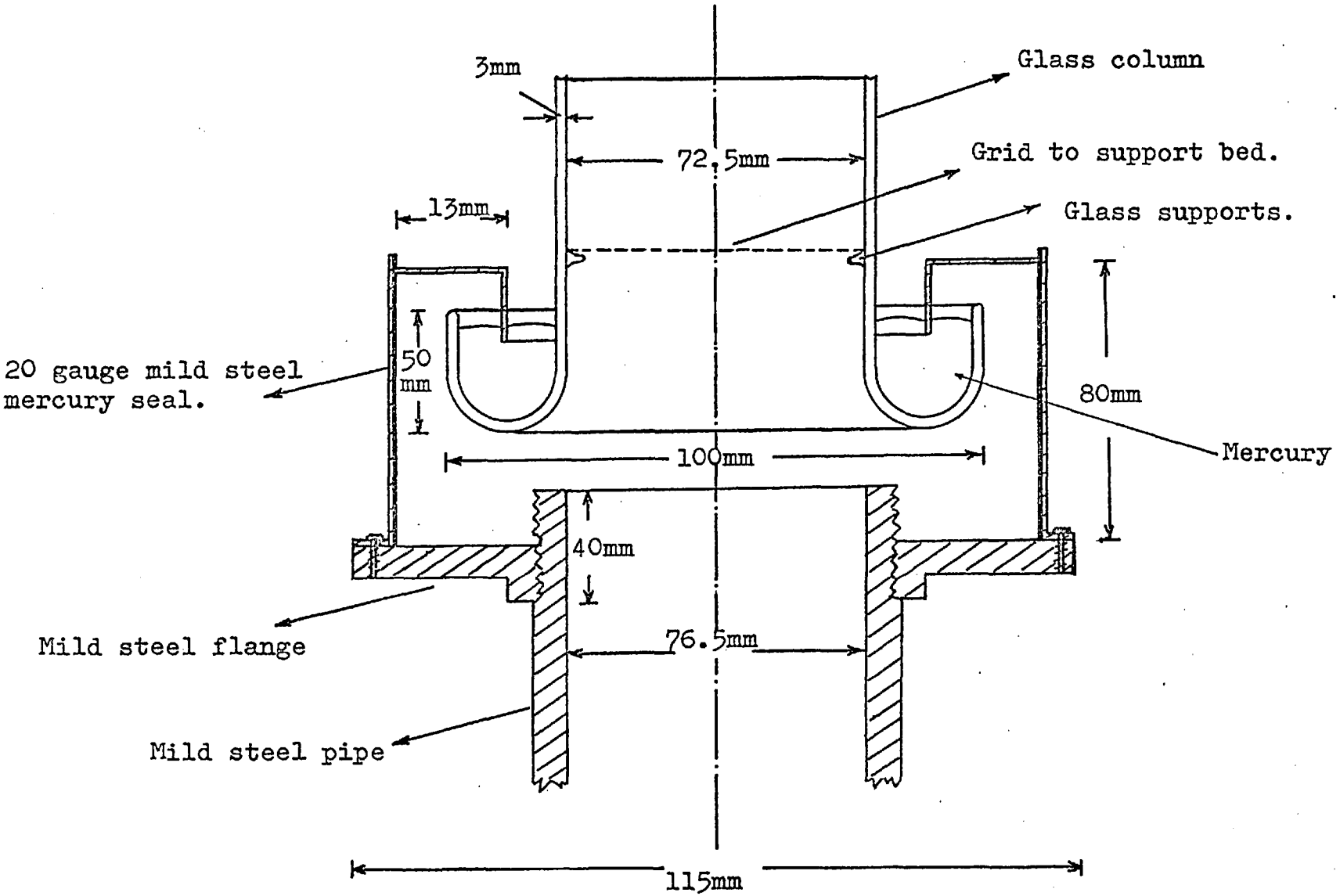

FIGURE 4.2 - Mercury Seal

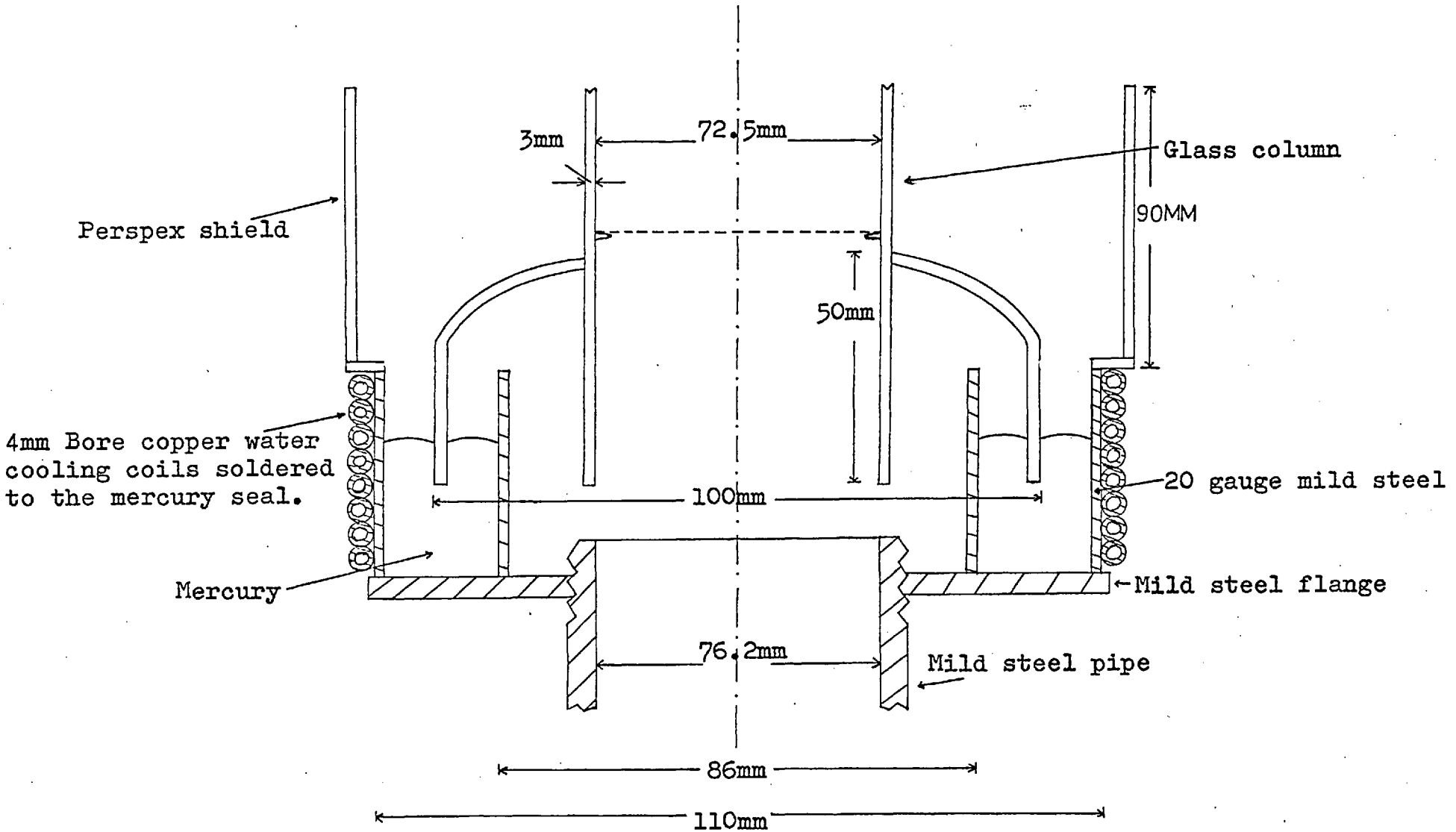

FIGURE 4.3 - Modified Mercury Seal

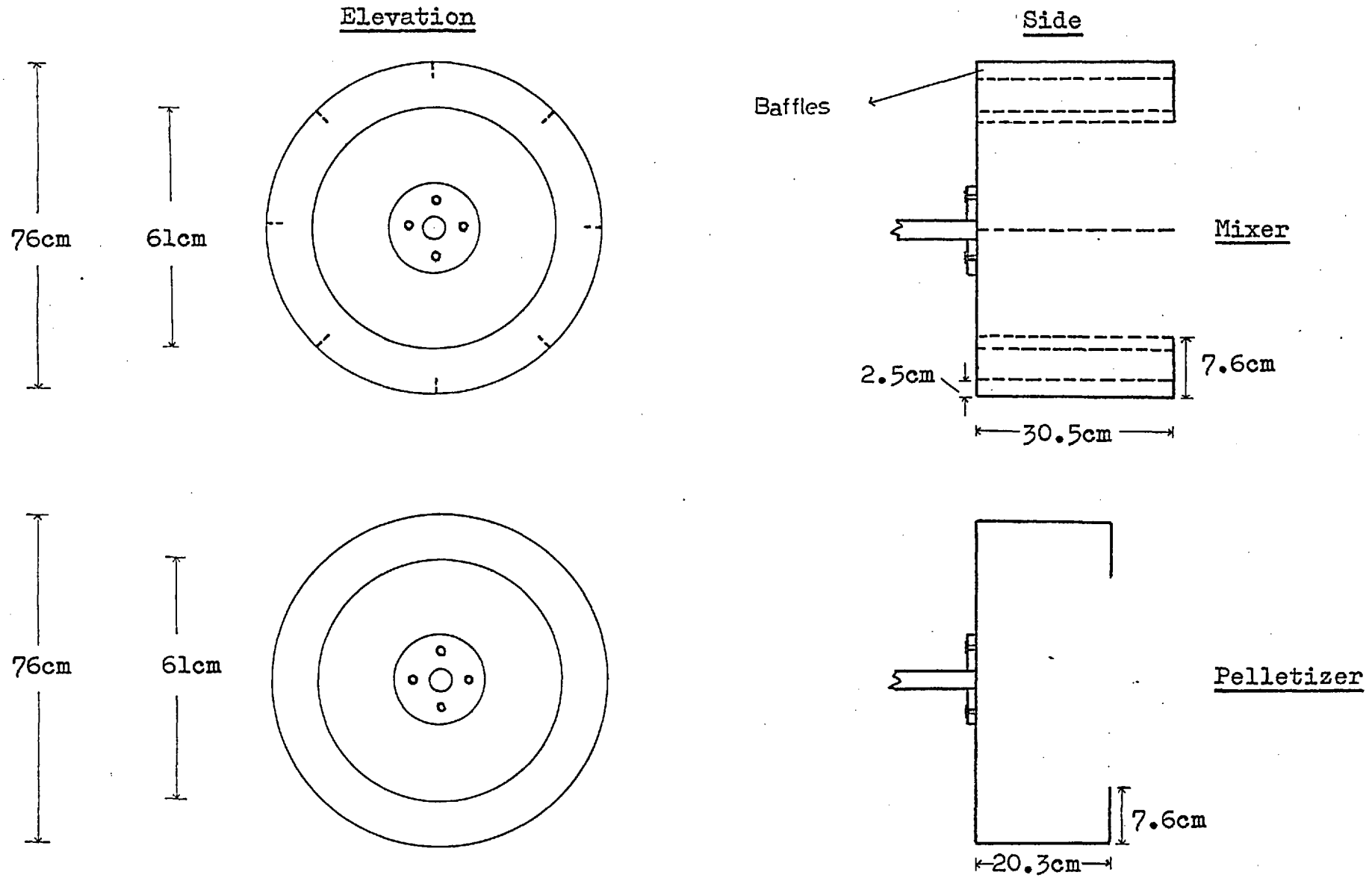

FIGURE 4.4 - Pelletizer and Mixer

in Fig. 4.4 , was used to prepare the raw sinter feed.

The apparatus is labelled in the flow sheet, Fig. 4.1 , and consisted of the following items :-

a) Pump

A rotary vane pump capable of delivering 0.02 m^3/s of air at 34.5 KN/m^2 was used.

b) Molecular Sieve Bed

Air from the pump was passed through a molecular sieve bed to remove any incoming moisture.

c) Drum

The air was then passed through an empty drum of 0.1 m^3 volume to damp down the pulsations from the pump.

d) Rotameters

Two rotameters were used, the smaller capable of measuring 8.3×10^{-4} m^3/s of air and the larger 2.91×10^{-3} m^3/s. By using a heavier float, the capacity of the larger rotameter was increased to 5×10^{-3} m^3/s.

e) Heater

An electric resistance heater of 1.5 KW was used to pre-heat the incoming air. The electrical power input to the heater was controlled by a suction pyrometer fitted at the inlet to the column, in conjunction with a three term thyristor temperature controller. The 7.6 cm internal diameter pipe of mild steel, housing the heater, was lagged with a 2.5 cm thick layer of Triton Kaowool. That part of the apparatus above the heater was made of copper and mild steel, and care was taken to design it, so that its thermal mass was as low as possible. The heater was designed on the following basis :-

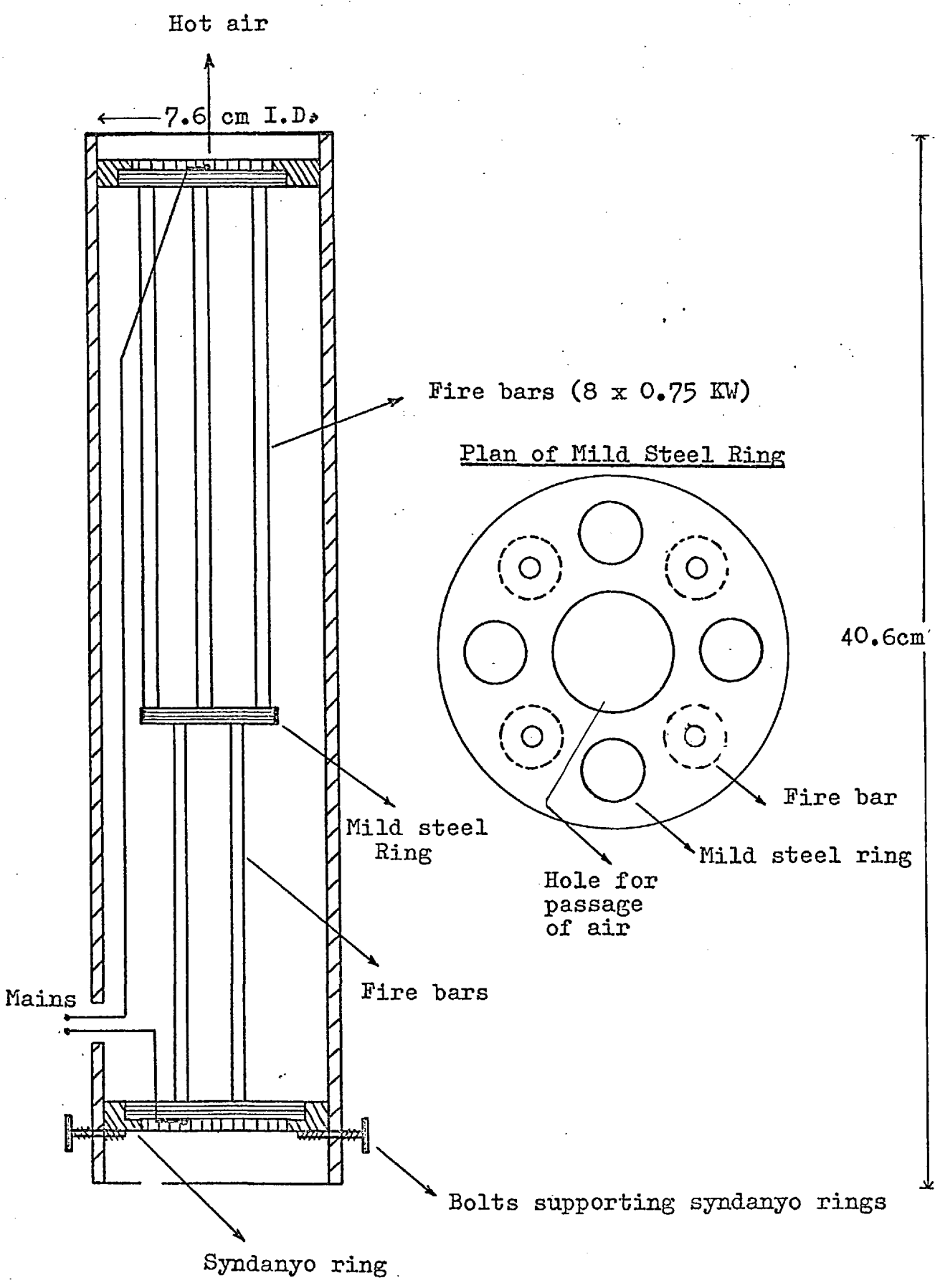

FIGURE 4.5 - Heater

An air flow rate of 6.7×10^{-3} m^3/s was required to be heated to 200°C. An overall heat balance was used to decide the electrical power requirements.

Area of cross-section of heater = 4.1×10^{-3} m^2.

Air flow rate to be heated to 200°C = 6.7×10^{-3} m^3/s at 20°C.

Density of air at 20°C = 1.2 Kg/m^3.

Mean specific heat of air between 20°C and 200°C = 1KJ/Kg°C.

Mass flow rate = $6.7 \times 10^{-3} \times 1.2 = 7.9 \times 10^{-3}$ Kg/s.

Rate of heat input required = $7.9 \times 10^{-3} \times 1.0 \times 180$ = 1.4 KW.

Therefore 1.4 KW are required to heat the air to 200°C.

A total of 8 fire bars of 750 W each were arranged, as shown in Fig. 4.5 , in two series of 4 in parallel. They gave 6.3 amps at 240 volts, as shown below :-

$$\text{Resistance of each bar} = \frac{(240)^2}{750} = 76.7 \text{ ohms}$$

And the resistance of all the elements

$$= 2 \times \frac{76.7}{4} = 38.4 \text{ ohms.}$$

$$\text{The current passing} = \frac{240}{38.4} = 6.25 \text{ amps.}$$

Therefore the power required = $240 \times 6.25 = 1.5$ KW.

f) Conical Inlet to Bed

The cone fitted below the bed had an angle of 10°, designed to give a uniform distribution of air velocity across the bottom of the bed. The angle of the cone was chosen to be similar to that of the outlet from a venturi

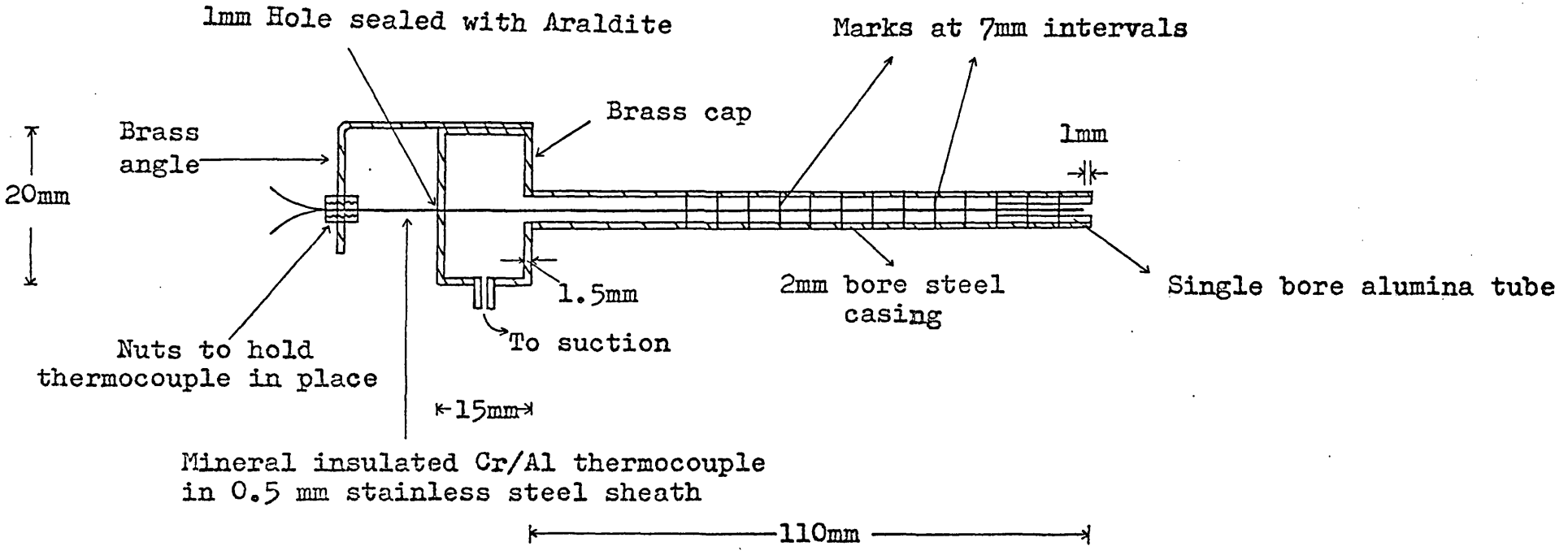

FIGURE 4.6 - Suction Pyrometer

meter, in order that a uniform distribution of velocity could be obtained in a short length of conical section of 0.3 m.

It was necessary to include flexible bronze bellows in the section between the heater and the cone, because as the apparatus expanded when heated air passed through the system, the level of the mercury seal was raised. This caused more of the column to dip into the mercury which in turn increased the tension on the load cell. This tension was recorded together with the tension caused by the loss in weight of the column, giving a high reading.

g) Heating Tape

Heating tape was wrapped around the cone between the mercury seal and the pipework above the heater. The tape was controlled by another suction pyrometer, fitted at an angle of 90° to the pyrometer used to control the heater but at the same distance from the bottom of the column. The heating tape was used to compensate for heat losses from the walls of the pipe and also to add extra heat to the air in the conical section between the mercury seal and the pipework above the heater. Two heating tapes capable of giving 0.75 KW and 2 KW were used. The 2 KW tape was used for higher temperatures and flow rates.

h) Suction Pyrometers

These consist of metal-clad mineral-insulated thermocouples, enclosed in steel tubes, with arrangement for drawing air past the thermocouple tips by suction, as shown in Fig. 4.6. This type of pyrometers were used because they give a more accurate reading of gas temperature

than open thermocouples, when radiation effects from the wall etc. to the thermocouple tip are significant. This is particularly so at low gas flow rates in the column. The pyrometers were fitted just below the bed, and could be moved across from centre to wall for measuring the temperature profile of the inlet gas stream.

i) Mercury Seal

This served the dual purpose of allowing the column to move freely along its vertical axis, and at the same time prevented any of the air, for drying, from leaking out of the system. The reason for choosing this design was to enable a load cell to be used, to record the changes in weight of the bed during drying. Hence the bed had to be freely suspended. The design of this seal is shown in Fig. 4.2.

The first experiments were carried out using silica gel. At the end of a run, the dried silica gel could be taken out of the top of the column with the help of a vacuum cleaner and fresh silica gel could be poured in. Later on when experiments with green pellets were started, it was found that the pellets were not strong enough to be poured into the column without breaking, and the column had to be detached from the system to pour in the pellets gently. Here the mercury at the bottom of the column presented a problem, apart from the fact that it was not very convenient to remove the column because the seal had to be unbolted from the flange supporting it. This operation not only took a long time, but it was also difficult to make the joint between the seal and the flange airtight. Another

shortcoming of this design was that at high drying temperatures, the temperature of the mercury in the seal also rose. To avoid evaporation of mercury and to save time and inconvenience, a new seal was designed and is shown in Fig. 4.3 . The new seal had copper cooling coils soldered around it. Water was continuously passed through them to keep the mercury cool during a run.

Another feature of both these seals was that they could be moved up or down slightly in order to make final adjustments in level.

A perspex shield was fixed on top of the mercury seal in order to prevent any mercury from blowing out.

j) Columns

The columns were made of pyrex glass tube of internal diameter 7.25 cm. The thickness of glass was 3 mm. Columns were made in various lengths to accommodate beds of heights 15, 23 and 30.5 cms. It was found that the columns had to be of the same height as the beds, otherwise condensation of water vapour occurred on the column walls above the bed, causing error in the weight loss recorded by the load cell. The lower end of each column was designed to fit the mercury seal as shown in Fig. 4.3 . Three protrusions were blown into the glass 5 cms above the bottom of the column, to support the wire mesh, which in turn supported the bed of the material to be dried. It was observed that the column did not remain vertical, and the bottom of the column always touched one side of the mercury seal. This was overcome by adding a small amount of lead to the mercury in order to reduce the surface tension of the mercury.

k) Load Cell, Beam and Counter Balance

The load cell, shown in Plate 2, was used for measuring the changes in weight of the column as moisture evaporated from the bed. It was sensitive enough to record changes in weight of one gram, and had a range of 0-900 grams. The input voltage of 4.5 V was supplied by a constant voltage source and the load cell gave an output of 18 mV approximately. The load cell was fixed on a firm base with a shield around it, in order to deflect hot air.

In the first design the column was counter-balanced by a weight suspended from two pulleys with ball bearings, but it was found that the system was only sensitive enough to indicate changes in weight of 10 grams in the weight of the bed. This lack of sensitivity was due to friction in the pulleys. So the system had to be changed to increase the sensitivity.

Instead, a beam was used, which was supported on a knife-edge of hardened steel, so there was negligible friction between the beam and the knife-edge. A thin copper wire was used initially to connect the load cell to one end of the beam, but a certain load was required to straighten the wire before weight losses were recorded. A fine nylon thread was then tried, but it stretched too much. Finally a polythene thread was selected, which stretched little, took negligible load to straighten out, and was strong enough for a load of 1 kg.

The other end of the beam was fitted with a hook for supporting weights which were used to counter-balance the

weight of the bed. A safety wire was passed over the beam and attached to the frame holding the apparatus, so that if the polythene thread snapped, the beam would be stopped immediately, before doing any damage to the column.

A dry cell battery and a zenor diode were used first instead of the constant voltage source, but it was difficult to maintain a constant voltage supply for more than one experiment.

1) Pelletizer and Mixer

A disc pelletizer was used to roll pellets of iron ore concentrate, and a mixer was used for preparing the sinter feed. Basically both the pelletizer and the mixer were drums. The pelletizer had a plain inner surface, while the mixer was fitted with baffles. Both drums could be attached to a motor, as shown in Plate 3. The dimensions of the drums are given in Fig. 4.4. The motor and the drum were mounted on a steel base, which could be raised or lowered, giving the axis of the drum an angle of up to 45° to the horizontal. By changing the drive sprockets, speeds ranging from 12-43 r.p.m. could be obtained.

A scraper was attached to the apparatus when rolling pellets which was used to prevent material from adhering to the inside of the drum. With the mixer, the scraping had to be done manually because the baffles interfered with a fixed scraper.

The following instruments were used with the apparatus:-

i) Potentiometer

An electric potentiometer capable of measuring $\pm$ 0.001 mV was used for calibrations.

PLATE 3

PELLETIZER

ii) Chart Recorder

A twin pen chart recorder continuously recorded the changes in weight and pressure drop in the bed.

iii) Micromanometer

A micromanometer capable of measuring 0.025 mm change in pressure was used for measuring the changes of pressure in the bed.

CHAPTER 5

EXPERIMENTAL TECHNIQUES

CHAPTER 5 EXPERIMENTAL TECHNIQUES

The procedures adopted to calibrate the apparatus, the preparations required prior to a run and the experimental procedure will now be outlined.

5.1 - Calibration Procedures

5.1.1 - Load Cell

The load cell was calibrated in situ as shown in Fig.4.1 . Calibrations were carried out with air flowing past the load cell at various temperatures and various flow rates. Fifty grams at a time were added to the counter-balance and the output voltage was measured with a potentiometer. Fresh weights were added when the potentiometer showed a steady reading.

It should be noted that the length of column dipping into the mercury would vary every time the column is removed and put back in position. The change in weight of the column would also alter its position in the mercury. A number of calibrations were carried out, but there was negligible difference in the various calibrations.

5.1.2 - Suction Pyrometers and Temperature Profiles

One of the suction pyrometers used was of known efficiency[37]. The other one was calibrated against it using the relation,

$$\text{Efficiency} = 1 - \frac{\text{error of pyrometer with suction}}{\text{error of pyrometer without suction}}$$

$$\text{or} \quad \text{Efficiency} = \frac{T_{suc} - T_{n.suc}}{T_t - T_{n.suc}}$$

$$\text{or} \quad T_t = T_{n.suc} + \frac{T_{suc} - T_{n.suc}}{\text{Efficiency}} \qquad 5.1$$

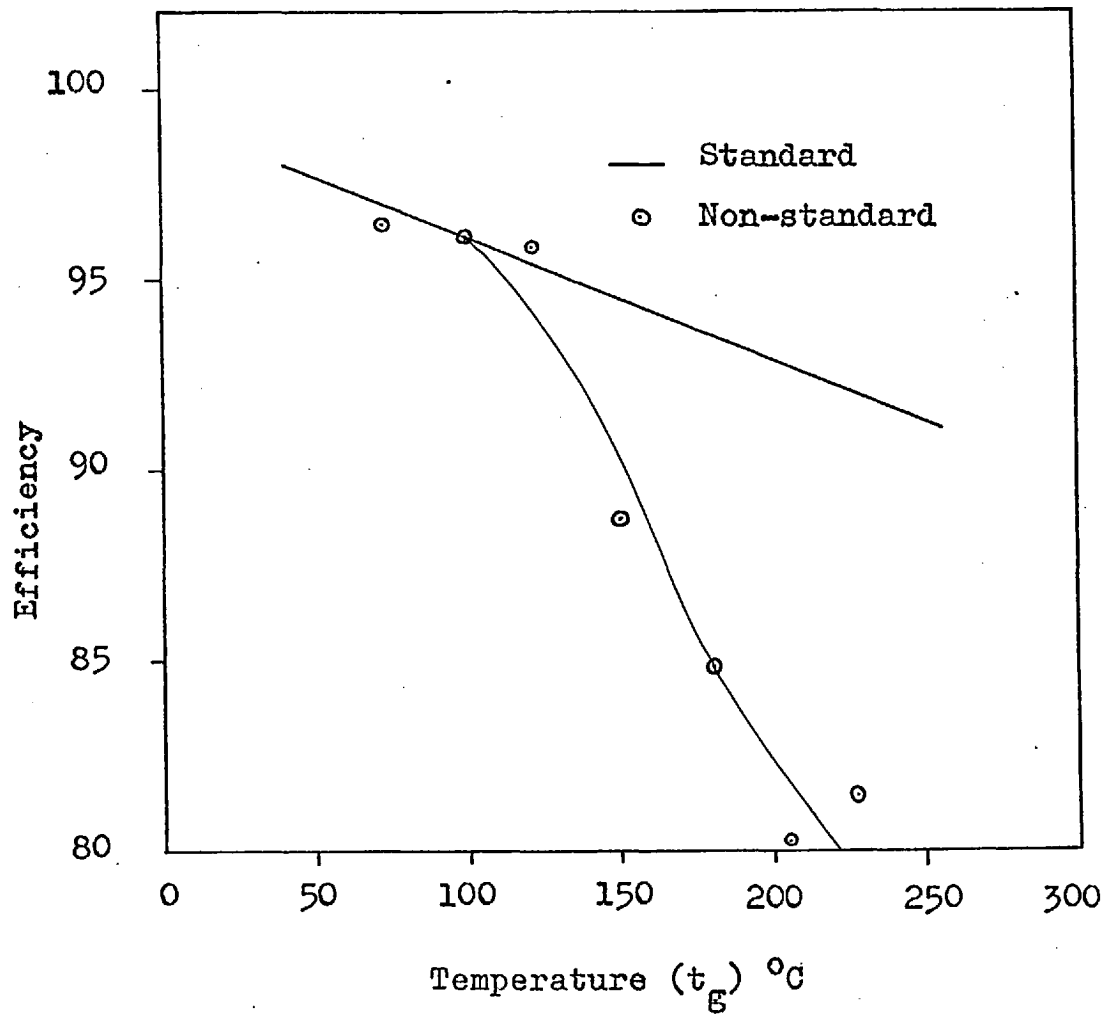

FIGURE 5.1 - Suction pyrometer calibration curve

The efficiency curves are given in Fig.5.1 . Both suction pyrometers had markings (Fig.4.6) on their enclosing steel tubes. One pyrometer was kept in a fixed position while the other was moved from wall to wall and recorded temperatures along its path. It was found from these movements that the heating tape had to be wrapped around a certain length of the conical section (Fig.4.1). If it was wrapped right down to the end of the cone, the centre temperature became much higher than the wall temperature. If the tape was wrapped around too short a length, it did not provide enough heat to raise the wall temperature to the required level.

The 2KW tape was used for air temperatures of $200^{o}C$, and also when flow rates of 1.2 m^3/sm^2 and higher were required.

5.1.3 - Micromanometer

Each diaphragm of the micromanometer was calibrated against a U-tube water manometer. The micromanometer was adjusted until the dial gave a full scale reading when the pressure difference corresponded to the maximum pressure difference specified on the diaphragm.

5.1.4 - Pressure drop across the bed

The pressure drop across the bed was calibrated in terms of load cell output for each run. The procedure will be outlined in the results chapter in terms of an actual example.

5.2 - Measurement of voidage

5.2.1 - Silica gel

The voidage of a bed of silica gel was determined by obtaining the true and bulk densities of silica gel. The true density was obtained by weighing a crystal of silica gel, and by measuring its volume using mercury. The bulk density was obtained by filling a glass column of known volume with silica gel and then weighing the silica gel afterwards. The voidage was obtained by using the relation

$$\epsilon = \frac{\rho_t - \rho_b}{\rho_t}$$

5.2.2 - Glass Balls

A glass column of known volume was filled with glass balls. The volume of the glass balls was determined by pouring them in a graduated cylinder and noting the volume of the water displaced. The voidage was obtained by using the relation

$$\epsilon = \frac{V_b' - V_s'}{V_b'}$$

5.2.3 - Green Pellets

Hot air was passed through a bed of dried green pellets and the data for this run (given in the Appendix 2 on page 184) was used in the Ergun equation (given on pg. 31) to calculate the voidage.

5.2.4 - Sinter Feed

The voidage was determined by filling a beaker with moist sinter feed and then adding water to it until

all the empty space in the beaker had been filled. From the amount of water added, the voidage was determined. The experiment was performed twice and the average of the two values was taken to be the voidage.

5.3.1 - Preparation of apparatus prior to a run

An experiment consisted of,

(a) preparing a sample of the material to be dried;

(b) pouring the sample into a pre-weighed column and weighing both the column and the sample;

(c) setting up the column;

(d) heating the air and then passing it through the bed.

(a) - Preparation of sample

The pelletizer or the mixer (both of which have been described in Chapter 4, page 72) was used, depending upon whether the material to be dried was pellets or sinter feed.

For both mixing and pelletization, the material was fed manually to the drum. The drum was rotated and water was sprayed continuously by hand from a polythene bottle onto the material. This process was continued until the material had absorbed sufficient moisture. By experience one could observe when the moisture content of the material was within half a percent of the desired moisture. After this the drum was stopped and the material which had gradually built up to a thick layer along the circumference was scraped off and broken into smaller particles. Any other large lumps rolling in the drum were also broken up, and the drum was revolved again. A further amount of water was added if necessary. In the

case of the sinter mix, the material had been thoroughly mixed by now and could be transferred to the column immediately. To prepare pellets, the material would begin to roll into pellets once the drum had started to revolve again. The diameter of the pellets depended upon the speed and angle of inclination of the axis of the drum. Pellets from 0.4 to 2 cm diameter could be prepared in this way. A scraper was attached to the apparatus when rolling pellets, but for preparing sinter feed, the scraping had to be done manually because of the presence of baffles inside the drum.

Moisture content of the solid being dried had to be within a certain range, as described below.

In the case of green pellets, if the moisture content was below 6%, then the pellets did not roll very well, and the ones which did roll, were difficult to handle because they were very brittle and also small particles kept falling out of the bed during the experiment. On the other hand if the moisture was above 8%, the surface of the pellets was wet, and when transferred to the bed, the pellets at the bottom of the bed dripped water prior to the start of experiment.

The sinter feed presented a problem of a different nature. If the moisture content was below 10%, the pressure drop across the bed was too high, i.e. exceeding the limits of the apparatus, whereas if it was above 15%, the bed lost its shape during the run and considerably lowered the pressure drop, i.e. below the initial pressure drop across the bed and gave erroneous results.

(a)1 - Preparation of other materials

Silica gel crystals were left in the atmosphere for about 36 hours prior to each run. In this time they reached a moisture content of approximately 14%.

Peas were taken from the freezer prior to each run and left in the atmosphere until all the ice had melted away and there were no water droplets on the surface. The peas were then transferred to the column and the drying experiment was performed.

Fired pellets were placed in a bath of water for about half an hour prior to each run, during which time they became saturated with water. Then they were taken out and left in the atmosphere until the excess surface moisture had evaporated.

(b) - Pouring the sample into a pre-weighed column

The pellets were sieved to remove any under or over-sized pellets and poured into a pre-weighed column. The column was weighed again on a solution balance to find the weight of the moist pellets.

The sinter feed after mixing could be transferred directly to the column.

(c) - Setting up the column

After weighing, the column was suspended from the beam, and was aligned vertically over the mercury seal, so that the column did not touch either the sides or the bottom of the mercury seal. The pump was switched on, the flow rate regulated to the required value, and air at room temperature allowed to pass through the bed. The weight

of the bed was then counter-balanced, so that the load cell indicated a slight positive reading. The reason for having a positive reading was threefold - (1) to take care of any zero error in the load cell, (2) to put tension in the polythene thread connecting the load cell to the beam, (3) to adjust the amount of column dipping into the mercury.

(d) - Heating the air

For each particular air temperature and flow rate required, the heater and the heating tape had to be left on prior to a run for a specific length of time. These times were found by experience, and had to be precise, because if the heater was left on longer than was necessary, the air temperature would go above the desired temperature and also raise the centre temperature considerably above the wall temperature. Similarly, if the heating tape was left on longer than necessary, the air temperature would go above the required temperature, and also raise the wall temperature higher than the centre temperature.

After the column had been aligned, the by-pass valve (4) was opened and valve (5) was closed (Fig. 4.1). The heater and the heating tape were switched on and the air was heated for the desired length of time before it was allowed to go through the bed.

The potentiometer and the constant voltage supply source to the load cell were switched on about 45 minutes before the start of each run, so that the output was stablised.

If for example air for drying was required at a flow rate of 0.6 $m^3/s\ m^2$ and 200°C, the pump and the main heater would be switched on, and the air would be allowed to escape into the atmosphere while being heated, via the by-pass valve (4). After 45 minutes the heating tape would be switched on in order to heat both the conical section and the stagnant air inside it. The temperature controller attached to the heater would be set at 200°C, while the heating tape controller would be set at 170°C. Fifteen minutes after switching on the tape, valves (4) and (5) would be reversed, and the temperature controllers set to 200°C. After 2-3 minutes, the suction pyrometers would show a steady inlet air temperature.

5.3.2 - Procedure during an experiment

As soon as heated air started to pass through the bed, drying commenced and the load cell and the micromanometer started indicating the changes in weight and pressure drop respectively, which were continuously recorded on the chart recorder. The run was continued until the load cell and the micromanometer showed constant readings. Then the heaters and the pump were switched off, the column removed and weighed.

CHAPTER 6

RESULTS

CHAPTER 6 RESULTS

6.1 - Calibrations

Before doing any experiments, the following calibrations were carried out:-

(a) Load Cell

The load cell calibration procedure is described in Chapter 5 on page 76. The calibration was linear and is shown in Fig.6.1. Other calibrations carried out at various inlet air temperatures and flow rates are shown in Figs.6.2 to 6.6 in Appendix 3.

(b) Suction Pyrometers

The calibration procedure is given in Chapter 5 on page 76, and the calibration curves are given in Fig.5.1.

6.2 - Temperature profiles across the inlet to the bed.

The procedure for measuring temperature profiles has been given in Chapter 5 on page 76. True temperatures were obtained by using the suction and non-suction temperatures and the relation given on page 76, and are plotted in Fig. 6.7.

6.3 - Sieve analysis and average particle diameter of sinter feed.

Particles above 9.5 mm were removed from the dry material which was then sieved to give the size analysis shown in appendix 5. This material was mixed thoroughly with water as described on page 80, and was then placed over a set of sieves of sizes -9.5 + 8 mm, -8 + 6.7 mm, -6.7 + 5.6 mm, -5.6 + 4.75 mm, -4.75 + 4 mm, -4 + 2.8 mm, -2.8 + 2 mm, -2 + 1 mm, -1 + 0.5 mm and -0.5 + 0.25 mm, and shaken mechanically for half an hour. On removing the sieves from the shaker, it was found that most of the material was on

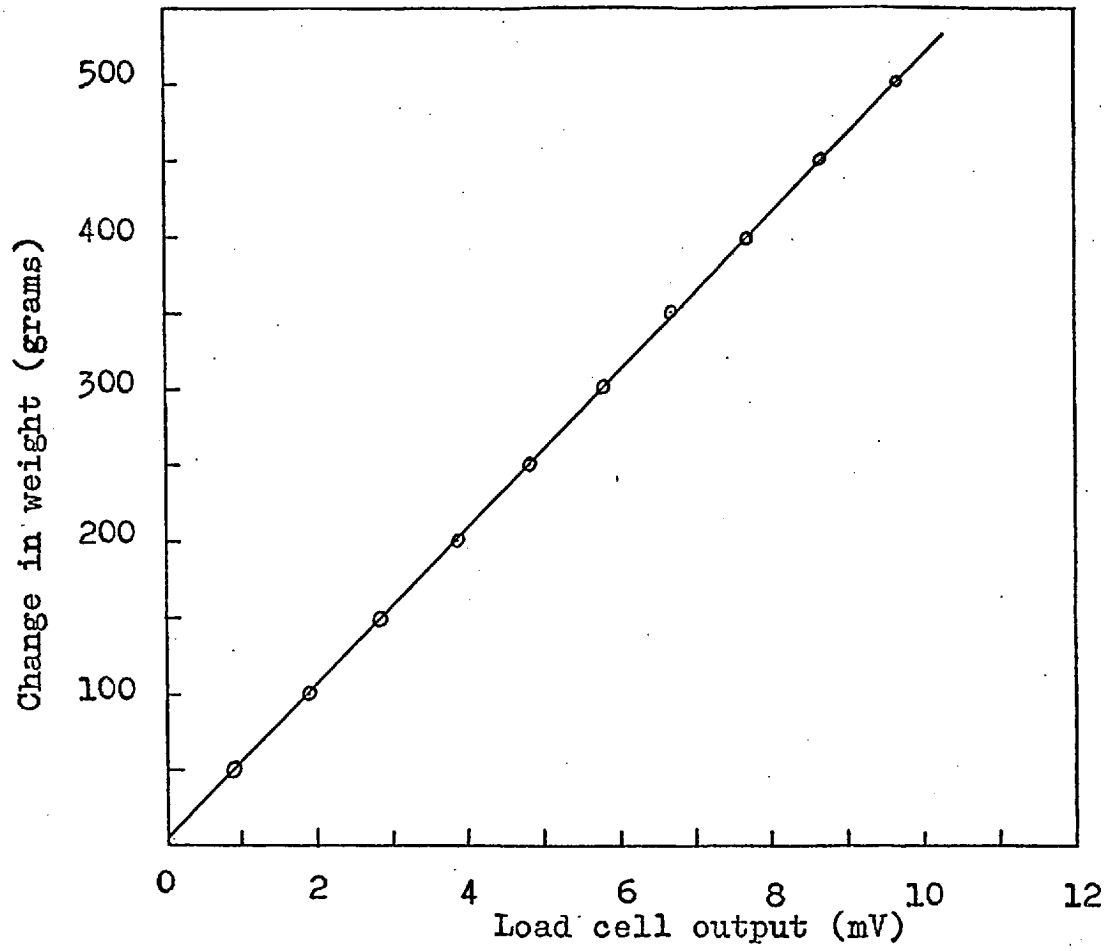

FIGURE 6.1 - Load Cell Calibration Curve

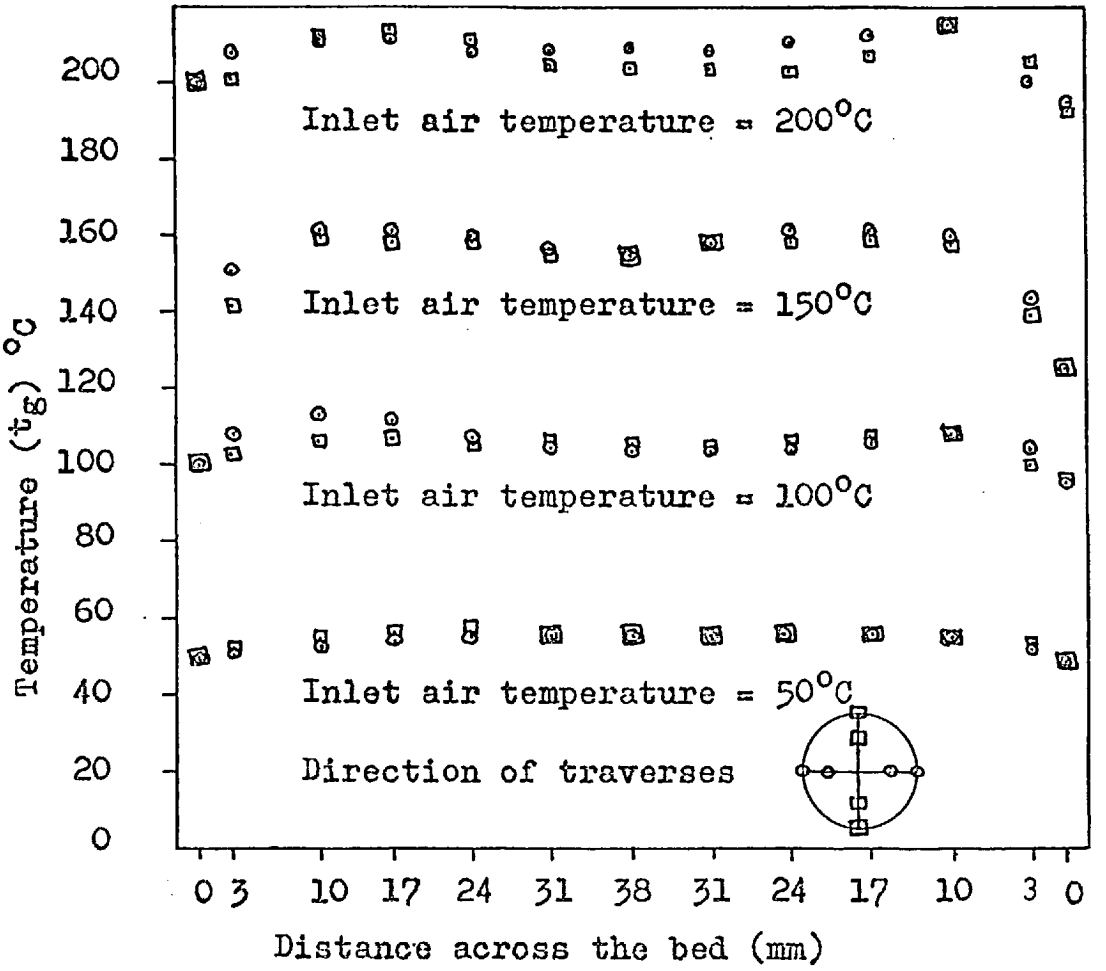

FIGURE 6.7 - Temperature profiles across the bed.

the 8 mm sieve and virtually nothing passed below the 2.8 mm sieve because of agglomeration. As this method of size analysis was unsatisfactory, the average particle diameter of the material had to be obtained by other means. The data of run No.31, and the Ergun equation given on page 31 was therefore used to obtain the mean particle diameter which was found to be 3.1 mm. The viscosity of air is given in appendix 4.2 on page 189.

6.4 - Voidage measurements

(a) - Silica gel

The measurement procedure has been given in Chapter 5, page 79. A value of 0.467 was obtained.

(b)(i) - Glass spheres

The measurement procedure has been given in Chapter 5, page 79.

Diameter of bed = 72.2 ± 0.2 mm

Height of bed = 152.4 ± 2.54 mm

Volume of spheres V'_s = 692 ± 1 cc (spheres and water)

− 300 ± 1 cc (water)

→ 392 ± 2 cc

$$\text{Voidage } \epsilon = \frac{V'_b - V'_s}{V'_b} = \frac{620.76 - 392}{620.76} = 0.368$$

V'_b (max) = 638.37 cc $\qquad$ V'_b (min) = 610.16 cc

V'_s (max) = 394 cc $\qquad$ V'_s (min) = 390 cc

$$\epsilon\ (\max) = \frac{V_b'(\max) - V_s'(\min)}{V_b'\ (\min)} = 0.389$$

$$\epsilon\ (\min) = \frac{V_b'(\min) - V_s'\ (\max)}{V_b'\ (\max)} = 0.354$$

(b)(ii) - Effect of voidage variation on pressure drop.

For a 30.5×10^{-2} m bed with an air flow rate of 0.4 $m^3/s\ m^2$ at 75°C, the pressure drop in mm of water, calculated from the Ergun equation given in Chapter 2, page 31.

with maximum voidage = 28.9 mm water gauge

with minimum voidage = 41.1 mm water gauge

with measured voidage = 34 mm water gauge

Percentage error upper limit = $\frac{7.1 \times 100}{34} = 20.9$

Percentage error lower limit = $\frac{5.1 \times 100}{34} = 15$

(c) - Sinter feed.

The procedure for measuring the voidage of sinter feed has been given in Chapter 5, page 79. Two voidage determinations were carried out:-

(i) volume of moist sinter = 600 cc

volume of water added = 189.6 cc

$$= \frac{189.6}{600} = 0.316$$

(ii) volume of moist sinter = 600 cc

volume of water added = 192.6 cc

$$= \frac{192.6}{600} = 0.321$$

The voidage was, therefore, taken to be equal to 0.32.

(d) - Green pellets

The measurement procedure is given in Chapter 5 , page 79 . A value of 0.401 was obtained.

6.5 - Moisture loss during pre-heating of air.

It was noted that from the time when the column was set in position over the mercury seal and before heated air was passed through the bed, the bed lost moisture. This loss of moisture is shown in Table 6.1, with bed height, inlet air temperature and time of pre-heating.

Experiment No.	Bed height m x 10^2	Inlet air Temperature (^oC)	Pre-heating time (min).	Moisture Loss (g)
1	7.6	100	12	2
2	15.2	100	12	2.5
3	15.2	150	35	4
4	15.2	150	35	5
5	15.2	150	35	4
6	15.2	200	60	4
7	15.2	200	60	5

Table 6.1 - Moisture loss with bed height, inlet air temperature and time of pre-heating.

6.6 - Pressure drop experiments.

Pressure drop experiments were carried out using glass balls, steel balls and silica gel crystals under various experimental conditions which will be detailed later.

The experimental values of pressure drop were compared with values which were calculated from Ergun's equation given on page 31. The calculated values were obtained as follows:-

Inlet air temperature = $25^{o}C$

Bed height = 0.152 m

Particle diameter = 6×10^{-3} m

Area of cross-section of bed = 4.13×10^{-3} m

Empty bed velocity (V) = 0.404 m/s

ϵ = 0.37

ρ_g = 1.185 Kg/m^3

μ_g = 1.8×10^{-5} Ns/m^2

$$\frac{\Delta P}{L} g_c = 150 \frac{(1-\epsilon)^2}{\epsilon^3} \frac{\mu_g V}{D_p^2} + 1.75 \frac{1-\epsilon}{\epsilon^3} \frac{\rho_g V^2}{D_p}$$

$$150 \frac{(1-\epsilon)^2}{\epsilon^3} \frac{\mu_g V}{D_p^2} = 150 \frac{(0.63)^2}{(0.37)^3} \frac{1.8 \times 10^{-5} \times 0.404}{(6 \times 10^{-3})^2} = 237.42 \text{ N/m}^3$$

$$1.75 \frac{1-\epsilon}{\epsilon^3} \frac{\rho_g V^2}{D_p} = \frac{0.63}{(0.37)^3} \frac{1.185 \times (.404)^2}{(6 \times 10^{-3})^2} = 701.62 \text{ N/m}^3$$

$$\frac{\Delta P}{L} g_c = 237.42 + 701.62 = 934.04 \text{ N/m}^2$$

$$\Delta P = 142.7 \text{ N/m}^2$$

$$= 14.5 \text{ mm water.}$$

A comparison of experimental and calculated pressure drop values is given in Table 6.2.

Expt. No.	Temp. (°C)	Bed Ht. (mm)	Flow Rate $m^3/s\ m^2$	Glass Balls Cal(mm)	Glass Balls Exptl	Steel Balls Cal(mm)	Steel Balls Exptl	Silica Gel Cal(mm)	Silica Gel Exptl
1	75	7.6	0.4	8.6	7.8	6.54	6	6.6	15
2	25	15.2	0.4	14.5	16	10.7	10.5		
3	50	15.2	0.4	15.9	16	12.1	11	for a 7.6mm	
4	75	15.2	0.2	5.52	6	4.2	4	bed with a	
5	75	15.2	0.4	17.2	18.5	13.2	12	flow rate of	
6	75	15.2	0.6	35.5	40.5	27.2	29	0.4 $m^3/s\ m^2$	
7	100	15.2	0.4	18.8	22	14.3	14	at 25°C.	
8	75	30.5	0.4	34.4	34				

Table 6.2 - Comparison of calculated and experimental values of pressure drop.

6.7 - Drying experiments.

Table 6.3 gives details of all the drying experiments carried out. The various materials used and the conditions under which the experiments were done are given in this table. Details of the various ores used to make the green pellets and sinter feed are given in appendix 5.

Expt No.	Material	Particle Size (mm)	Experimental Conditions: Bed Height ($m \times 10^2$)	Air Flow Rate ($m^3/s\ m^2$)	Inlet Air Temperature (°C)
1	Green Pellets	-8 + 5.6	7.62	0.6	150
2	"	"	15.2	0.4	"
3	"	"	"	"	"

Table 6.3 - Drying Experiments (Contd.)

Expt No.	Material	Particle Size (mm)	Experimental Conditions		
			Bed Height ($m \times 10^2$)	Air Flow Rate ($m^3/s\ m^2$)	Inlet Air Temperature (^oC)
4	Green Pellets	-8 + 5.6	15.2	0.6	150
5	"	"	"	"	"
6	"	"	"	"	"
7	"	"	"	"	"
8	"	"	"	0.9	"
9	"	"	"	"	"
10	"	"	"	1.2	"
11	"	"	"	"	"
12	"	"	"	"	"
13	"	"	"	1.4	"
14	"	"	"	"	"
15	"	"	"	"	"
16	"	"	"	0.6	"
17	"	"	"	"	50
18	"	"	"	"	100
19	"	"	"	"	"
20	"	"	"	1.2	200
21	"	-5.6 + 4	"	0.6	"
22	"	"	"	"	150
23	"	"	"	"	"
24	"	-9.5 + 8	"	"	"
25	"	"	"	"	"

Table 6.3 - Drying Experiments (Contd.)

Expt No.	Material	Particle Size (mm)	Experimental Conditions		
			Bed Height ($m \times 10^2$)	Air Flow Rate ($m^3/s\ m^2$)	Inlet Air Temperature (^oC)
26	Green Pellets	-8 + 5.6	22.86	0.6	150
27	"	"	"	"	"
28	"	"	30.48	"	"
29	"	"	"	"	"
30	Sinter Mix	3.1	7.62	"	100
31	"	"	"	"	150
32	"	"	"	"	200
33	"	"	"	0.4	150
34	"	"	"	"	"
35	"	"	"	"	"
36	"	"	"	0.7	"
37	"	"	15.24	0.4	"
38	Peas	7	7.62	0.6	"
39	"	"	15.24	"	"
40	"	"	"	"	"
41	"	"	"	"	200
42	Silica Gel	6	7.62	"	150
43	"	"	"	"	"
44	Fired Pellets	10	15.24	"	"

Table 6.3 - Drying Experiments.

Typical experiments with their experimental and calculated data, carried out with various materials under

different experimental conditions are shown in Table 6.4.

Inlet and outlet air temperatures to the drying zone were calculated as follows :-

The humidity of the exit air x_2 was obtained from the experimental drying rate. Knowing x_2, the temperature of the exit air can be obtained from tables[38] which give the data for saturated air. The total enthalpy of exit air can also be obtained from these tables. According to assumption No.6 of the model, the enthalpy at the inlet to the drying zone will be the same as the total enthalpy at the outlet. The temperature of the inlet air can be obtained from the enthalpy of the inlet air, if the specific heat of dry air is known.

The height of the drying zone was calculated using Eqn.(3.13) given on page 55. Values of the heat transfer coefficient h_v were obtained from eqn.2.36 on page 37 using the data in appendix 4.

6.8 - Calculation procedure for drying experiments.

The calculation procedure is illustrated by a typical run, experiment No.4, chosen because its inlet air temperature and flow rate lie in the middle of the temperature and flow rate ranges used in this work.

From Appendix 1 , the following results are obtained.

Weight of column	=	610 g
Weight of column + wet material	=	1814 g
Weight of column + dry material	=	1726 g
Weight of wet material	=	1204 g
Weight of dry material	=	1116 g
Weight of moisture	=	889 g
Percentage moisture (dry basis)	=	7.9

Expt. No.	Experimental Conditions			d. rate	sp. d. rate	Flow rate	x_2 = d. rate / flow rate	t_{g_2} cal.	t_{g_2} exptl.	ϕ_{g_2}	$C_{p_{air}}$	t_{g_1} cal.	z	h_V	t_m	m M_o
	Bed Ht. (cm)	Flow rate $\frac{m^3}{s \times m^2}$	Temp. (^oC) t_{g_o}	$\frac{Kg}{s} \times 10^6$	$\frac{Kg}{m^2 s} \times 10^3$	$\frac{Kg}{s} \times 10^3$	$\times 10^2$	(^oC)	(^oC)	KJ/Kg		(^oC)	(m) $\times 10^2$	$\frac{KW}{m^3\ ^oC}$	(^oC)	$\frac{Kg}{m^3}$
16	15.2	0.6	50	31.7	7.7	2.963	1.07	15	-	42	1.008	41.7	-	-	-	122.8
17	15.2	0.6	100	71.2	17.2	2.963	2.4	28	-	89.8	1.012	88.7	2.7	88.4	28.2	129
4	15.2	0.6	150	101.3	24.5	2.963	3.42	34	32	122	1.018	119.8	2.6	89.5	43.8	133.9
19	15.2	0.6	200	110.2	26.7	2.963	3.72	35.5	-	132	1.026	128.6	2.9	76.5	47.7	125.9
2	15.2	0.4	200	61	14.8	1.975	3.09	32	-	110.7	1.018	108.7	2.1	76.1	38.3	127.4
8	15.2	0.9	200	125	30.3	4.44	2.81	30.5	-	102.43	1.018	100.6	3.7	95.1	34.4	122.8
11	15.2	1.2	200	173.2	41.9	5.926	2.92	31	-	105.09	1.018	103.2	4.3	109.6	35.7	127.4
13	15.2	1.4	200	208.3	50.4	6.91	3.01	31.5	-	107.87	1.018	106	4.7	118	37	127.4
33	7.6	0.4	200	62.8	15.2	1.975	3.18	32.5	-	113.5	1.018	111.5	.32	431.6	39.7	192.9
31	7.6	0.6	200	73.5	17.8	2.963	2.48	28.3	-	92.3	1.018	90.7	.45	481.7	29.2	153
36	7.6	0.8	200	94.5	22.9	3.95	2.39	27.7	-	90	1.018	88.4	.57	525	27.8	168.9
30	7.6	0.6	100	62.2	15.1	2.963	2.09	25.6	-	78.6	1.012	77.7	.52	464	22.3	177

Continued

Table (Continued)

Expt. No.	Experimental Conditions			d. rate	sp. d. rate	Flow rate	×2 = d. rate / flow rate	t_{g_2} cal.	t_{g_2} exptl.	ϕ_{g_2}	$C_{p_{air}}$	t_{g_1} cal.	Z	h_V	t_m	$m M_o$
	Bed Ht. (cm)	Flow rate $\frac{m^3}{s \times m^2}$	Temp. (^oC) t_{g_o}	$\frac{Kg}{s} \times 10^6$	$\frac{Kg}{m^2 s} \times 10^3$	$\frac{Kg}{s} \times 10^3$	$\times 10^2$	(^oC)	(^oC)	Kj/Kg		(^oC)	(m) $\times 10^2$	$\frac{KW}{m^{3o}C}$	(^oC)	$\frac{Kg}{m^3}$
32	15.2	0.6	200	109.8	26.6	2.963	3.7	35	-	129.4	1.026	126.2	.48	426	46.5	143.4
38	15.2	0.6	150	87.7	21.2	2.963	2.96	31	-	105.09	1.018	103.2	2.8	86.9	35.7	450.2
44	15.2	0.6	150	84.5	20.5	2.963	2.85	30.5	-	102.43	1.018	100.6	4.9	49.3	34.4	111.5
42	7.6	0.6	150	50.7	12.3	2.963	1.71	22	-	64.57	1.018	63.4	5.3	80	13.4	95.6

Table 6.4 - Typical Drying Experiments.

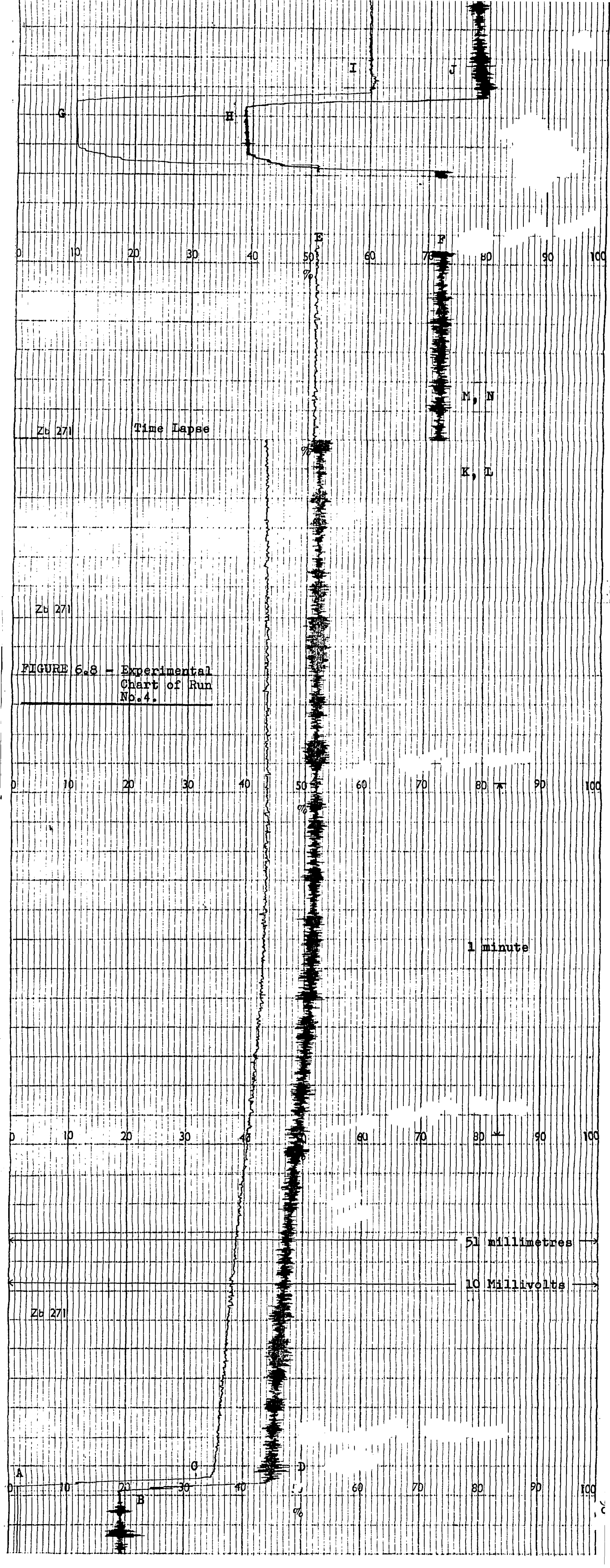

FIGURE 6.8 - Experimental Chart of Run No.4.

FIGURE 6.8 - Experimental chart of run no.4.

From the load cell calibration curve given in Fig. 6.1 ,

1 mV of load cell output = 50.8 g

The load cell output in grams during the experiment can now be evaluated from the chart recorder data for experiment No.4, which is given in Fig. 6.8.

Points A and B in Fig. 6.8 represent the manometer and the load cell readings respectively before the start of the run. As soon as the air is passed through the bed, the manometer and the load cell readings rise to points C and D respectively. Points E and F represent the final readings of the manometer and the load cell when there are no further changes in manometer or load cell readings.

Points G and H represent the manometer and the load cell readings respectively at some flow rate X, and points I and J at another flow rate Y. The values of X and Y are immaterial, but these four readings can be used to calculate the load cell reading equivalent to 1 mm of water in the manometer. Because the experimental chart was very long, it has been cut between points K, L and M, N for convenience. There were no changes in the trends of the readings between points K, L and M, N.

Points C and D were taken to be the initial values of the manometer and load cell readings at the start of the run. Prior to point A, the manometer output was a straight line, whereas during the experiment from point C onwards, the line was wavy. This is because small fluctuations occur in the air flow rate through the bed due to pulsations from the pump. The fluctuations in the load cell output are more pronounced and are probably caused by a pulsating

air flow together with transmission of vibrations from the pump via the floor, even though the apparatus was mounted on a vibration absorbing slab. At point G, the manometer reading is without noticeable fluctuation. This is due to the small flow rate of air passing through the bed.

The force on the load cell is equated to the sum of the upthrust due to air flow and the weight loss due to drying. The procedure for correcting the load cell reading for the upthrust on the bed will now be described. At the end of the experiment, the manometer reading was noted and then the flow rate was changed in order to change the pressure drop across the bed. This change in pressure drop was then equated to the change in the load cell reading, and from this, the mV reading equivalent to 1 mm of water in the manometer was calculated. In this example, 1 mm of water in the manometer ≡ an upthrust of 7.9 g. This calculated value was then used to correct the load cell reading by evaluating the pressure drop change during the run in terms of force on the load cell in grams. The readings obtained from the chart (Fig.6.8) are shown in Table 6.5.

Time min.	Pressure Drop	Load Cell Output		Upthrust due to pressure drop	Moisture Evaporated	Residual Moisture
	mm of H_2O	mV	g	(g)	(g)	(g)
0	0.0	0	0	0	0	80
1	3.07	0.4	20	24	-4	84
2	4.42	0.77	39	35	4	76
3	4.17	0.8	41	33	8	72

Time min.	Pressure Drop mm of H_2O	Load Cell Output		Upthrust due to pressure drop (g)	Moisture Evaporated (g)	Residual Moisture (g)
		mV	g			
4	4.09	0.9	46	32	14	66
5	4.11	1.02	52	33	19	61
6	4.17	1.16	59	33	26	54
7	4.39	1.32	67	35	32	48
8	4.67	1.47	75	37	38	42
9	4.88	1.64	83	39	44	36
10	5.23	1.81	92	41	51	29
11	5.64	1.97	100	45	55	25
12	6.15	2.15	109	49	60	20
13	6.55	2.31	117	52	65	15
14	6.91	2.46	125	55	70	10
15	7.37	2.61	133	58	75	5
16	7.72	2.73	139	61	78	2
17	8.03	2.77	141	63	78	2
18	8.23	2.84	144	65	79	1
19	8.23	2.85	145	65	80	0
20	8.28	2.85	145	65	80	0
21	8.28	2.86	145	65	80	0

Table 6.5 - Data for Experiment No.4.

In this run, the total moisture found by weighing the bed before and after the experiment was 88 g. So the actual moisture is 88-4 = 84 g, where 4 g is subtracted as explained

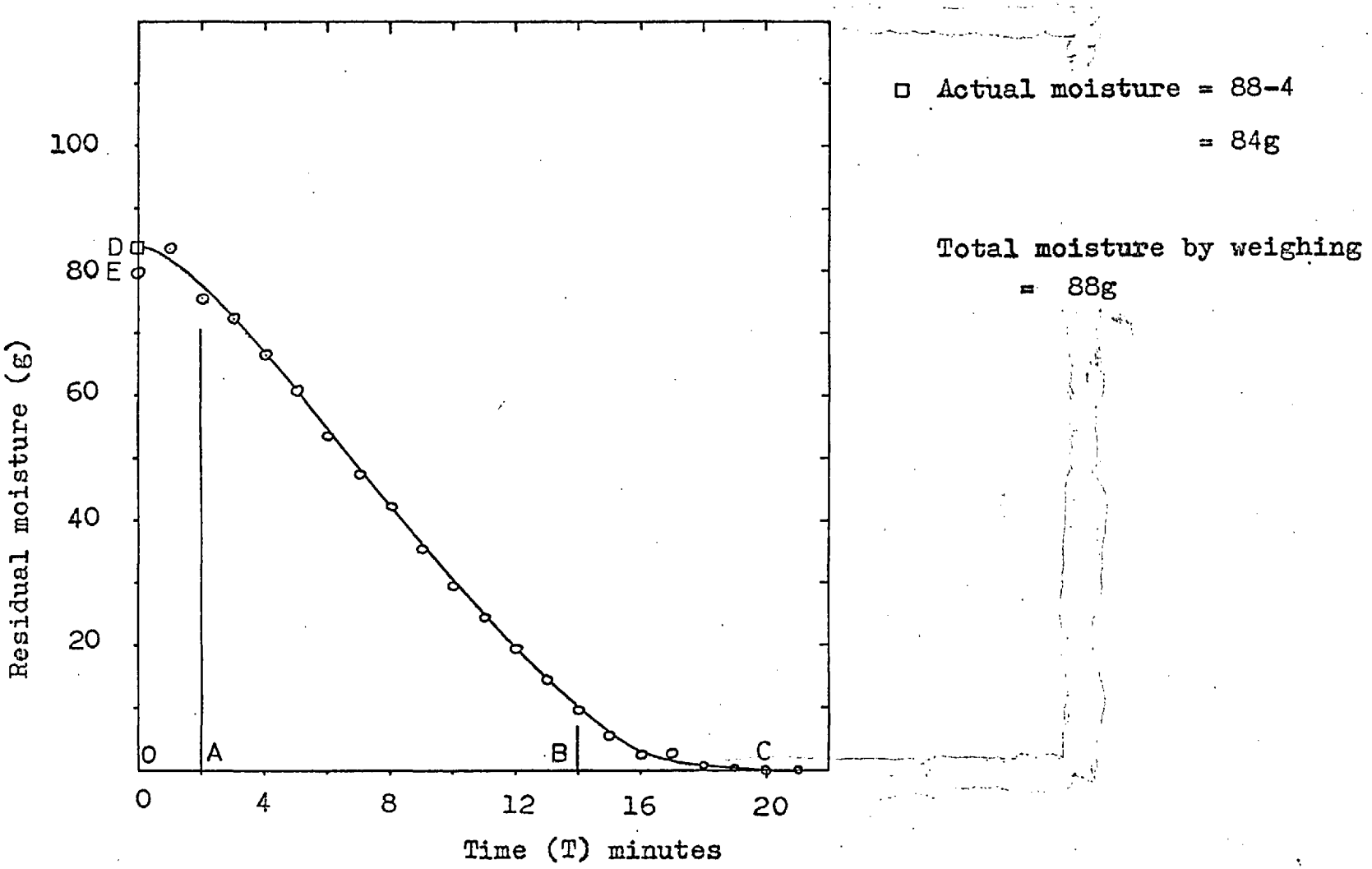

FIGURE 6.9 - Residual moisture against time plot for Run No.4.

on page 90 . However, the total moisture given by the load cell is 80 g. The plot of residual moisture against time obtained from this experiment is shown in Fig. 6.9. From the residual moisture against time curves / of Expt.Nos.4,5 & 6,which were carried out under similar conditions/, fig (6.14) it can be seen that reproducibility is good, ⊛ The results of experiments 1 - 44 are given in Appendix 1 as tables of manometer readings in mm of water, and load cell readings in mV in terms of time.

6.9 - Drying experiments with sinter feed.

The experimental procedure and the procedure for calculation was the same for this set of experiments as for green pellets.

6.10 - Drying experiments with other materials.

Two similar experiments were carried out with silica gel crystals and the results are given in Appendix 1 .

Four further experiments were carried out with peas and the results are given in Appendix 1 .

One experiment was done with fired pellets/and the result is shown in Appendix 1 . (data in appendix 5)

6.11 - Visual observations.

(i) In all experiments some colour differences existed between dry and wet material. For example, in the case of green pellets, the wet material was black and the dry material was grey. A drying zone of intermediate colour could be seen between the wet and dried pellets, but the height of the drying zone could not be determined accurately because the boundaries of the drying zone were ill-defined. The height of the zone was estimated to be about 30 mm.

⊛ and that the constant drying rates are reproduced within ± 0.22 g/min.

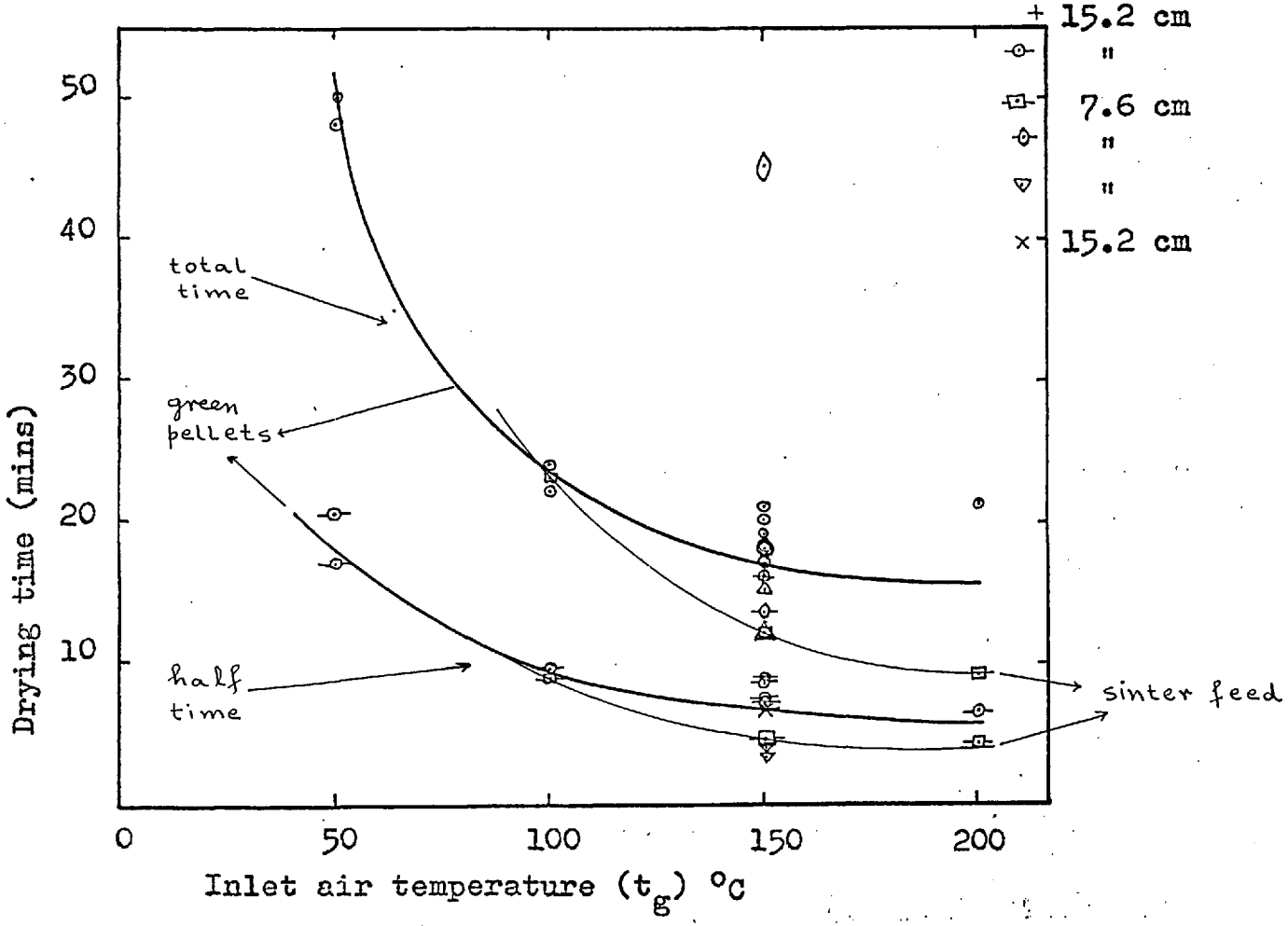

FIGURE 6.10 - Effect of inlet air temperature on the drying times.

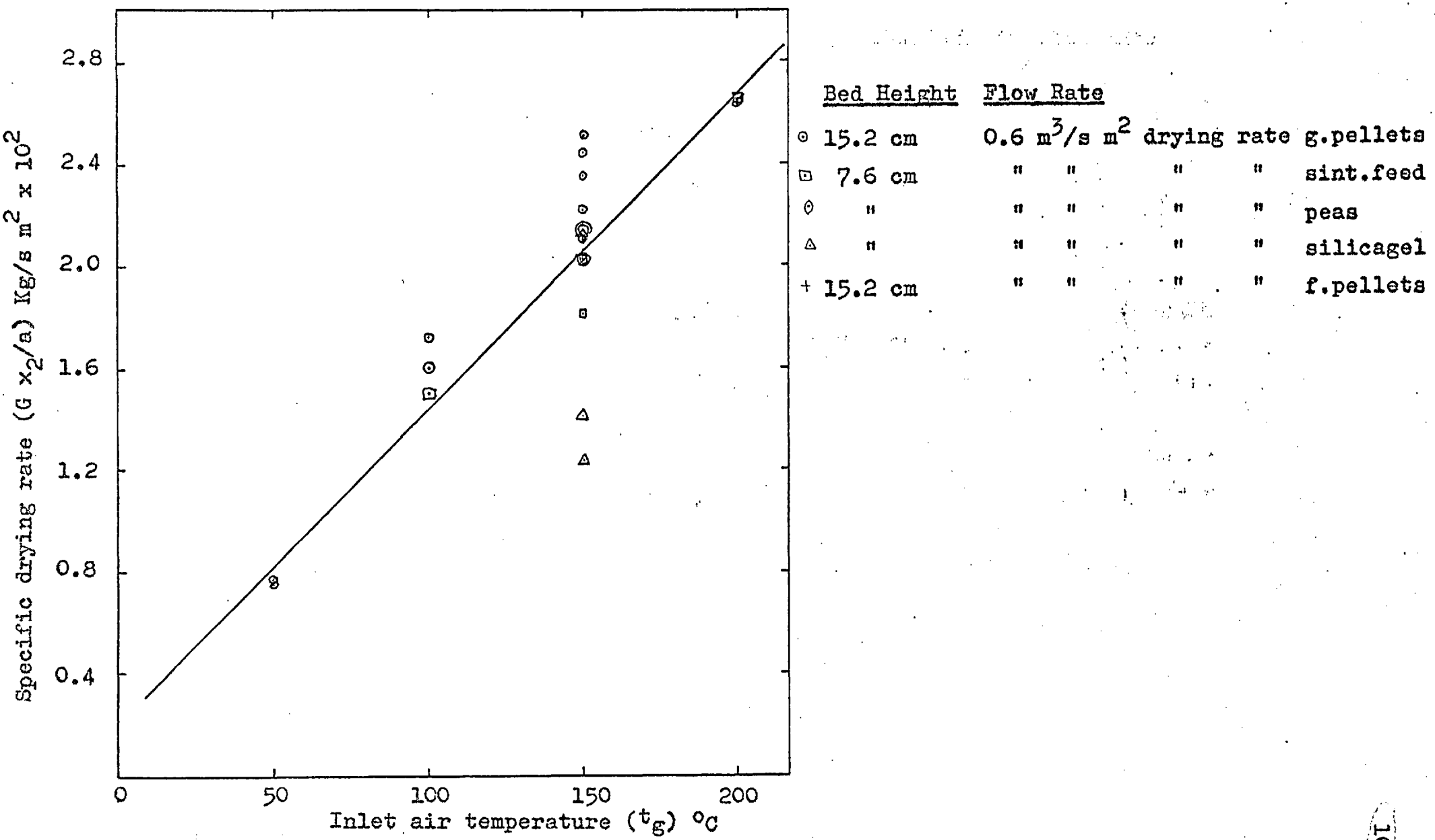

FIGURE 6.11 - Effect of inlet air temperature on the specific drying rate.

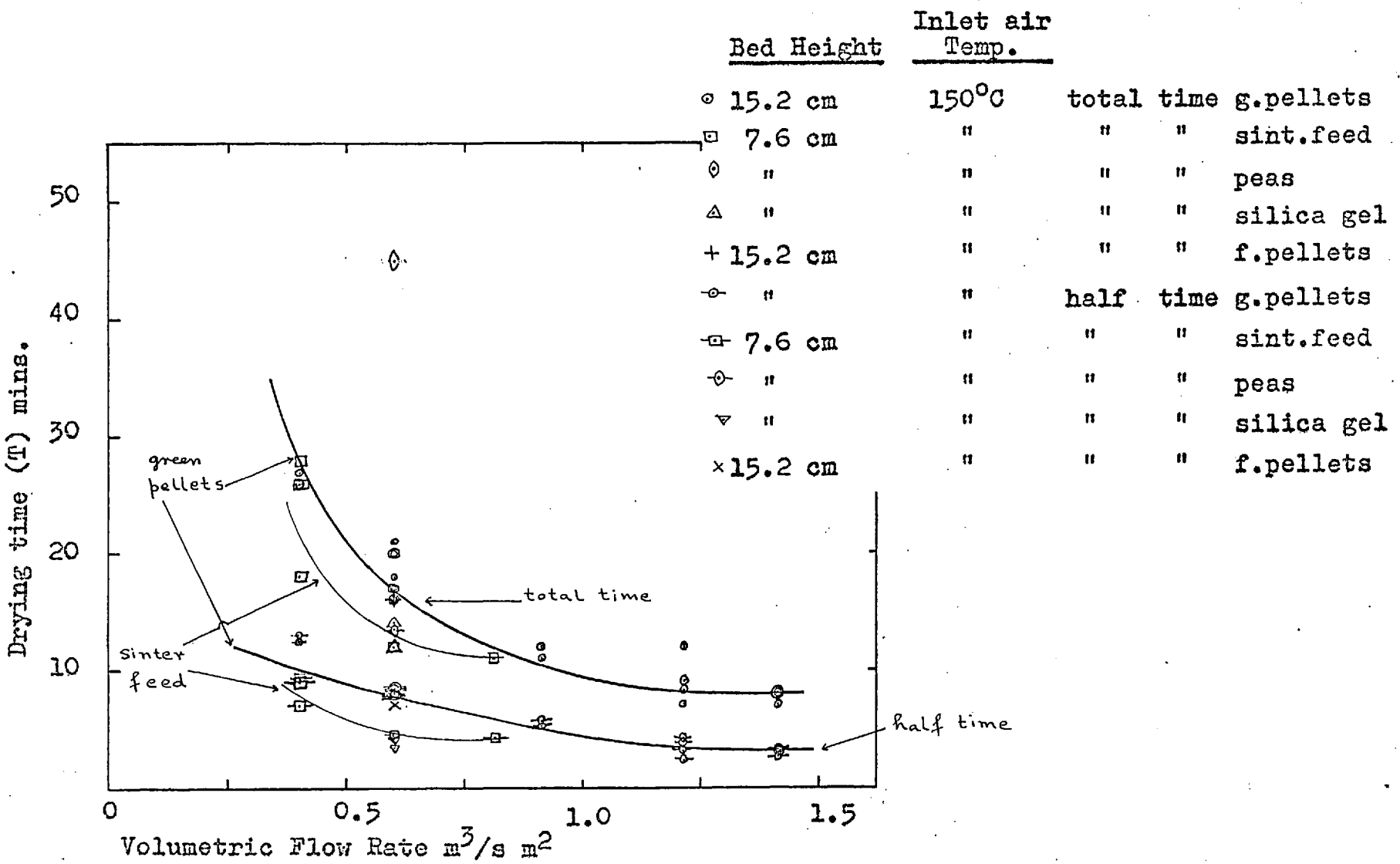

FIGURE 6.12 - Effect of air flow rate on the drying times.

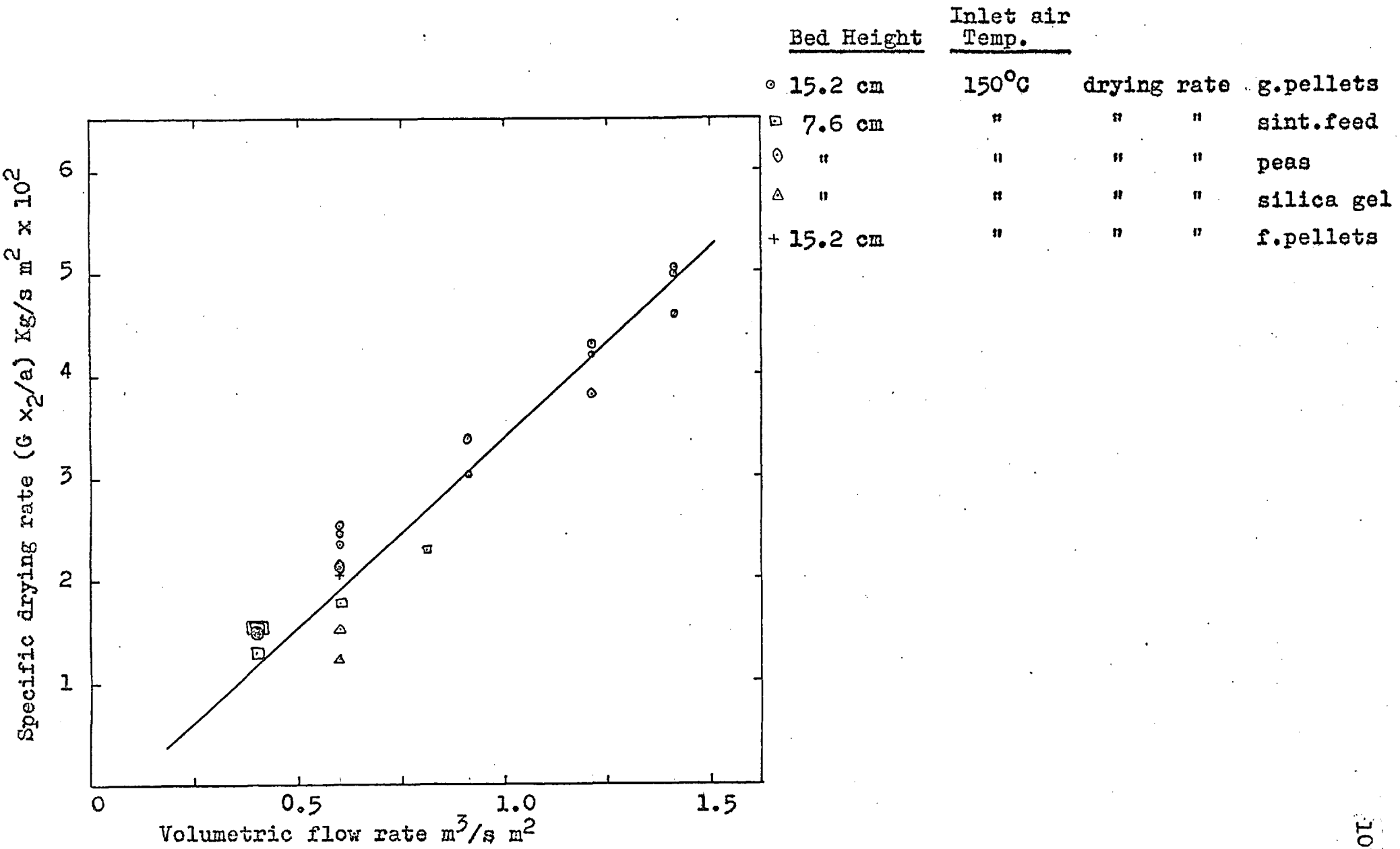

FIGURE 6.13 - Effect of air flow rate on the specific drying rate.

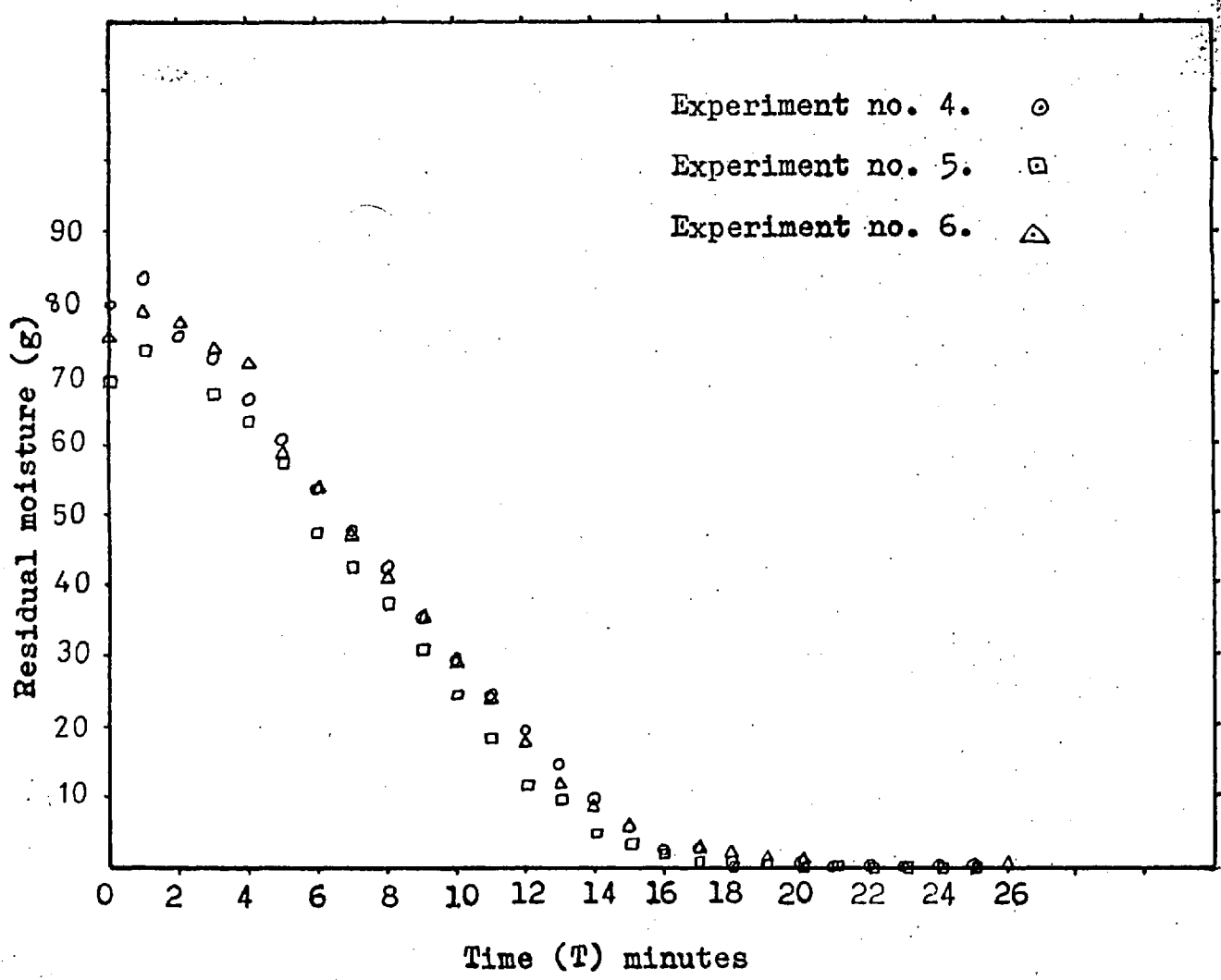

FIGERE 6.14-Residual moisture against time curves of experiments numbers 4,5 and 6.

(ii) Peas shrank in size during an experiment until at the end of the run, the bed height had been reduced to about two-thirds of its original height. The surface of the peas also became rough and dented. When the bed had almost completely dried, it was possible to detect a slight movement in the top layer of the bed, which would indicate that there was a tendency to fluidize.

6.12 - Comparison of various materials.

The effect of inlet air flow rate on the rate of drying, and on half and total drying times of green pellets, sinter feed, fired pellets, silica gel and peas is shown in Fig. 6.13 and 6.12 respectively.

Similarly, the effect of inlet air temperature on the rate of drying, and on half and total drying times of green pellets, sinter feed, fired pellets, silica gel and peas is shown in Fig. 6.11 and 6.10 respectively.

The effect of pellet size on the rate of drying of green pellets is shown in Table 6.6.

The effect of initial moisture content and material on the rate of drying of various materials is shown in Table 6.8.

The effect of bed height on the rate of drying of different materials is shown in Table 6.7.

Expt. No.	Pellet Size	Material	mM_o (kg/m^3) x 10^{-2}	h_v $KW/m^3\ ^oC$	Drying Rate (kg/s) x 10^4
24	-9.5 + 8	G.Pellets	1.3	100	0.95
4	-8 + 5.6	"	1.4	89.5	1.01
6	-8 + 5.6	"	1.3	89.5	0.97
22	-5.6 + 4	"	1.3	80.5	0.82

These experiments were carried out at an inlet air temperature of 150°C and an inlet air flow rate of 0.6 $m^3/s\ m^2$.

Table 6.6 - Effect of pellet size on the rate of drying of green pellets.

Expt.No.	Bed Ht. m x 10^2	Flow Rate ($m^3/s\ m^2$)	Material	mM_o (kg/m^3) x 10^{-2}	Drying Rate (kg/s) x 10^4
1	7.6	0.6	G.Pellets	1.3	0.87
4	15.2	"	"	1.4	1.01
26	22.9	"	"	1.3	0.87
28	30.5	"	"	1.4	0.95
33	7.6	0.4	Sinter Feed	2.1	0.63
37	15.2	"	"	1.8	0.63
38	7.6	0.6	Peas	4.7	0.88
39	15.2	"	"	4.8	1.23

These experiments were carried out at an inlet air temperature of 150°C.

Table 6.7 - Effect of bed height on the rate of drying of various materials.

Expt.No.	Bed Height m x 10^2	Material	mM_o (kg/m^3) x 10^{-2}	Drying Rate (kg/s) x 10^4
4	15.2	G.Pellets	1.4	1.01
5	15.2	"	1.3	1.05
6	15.2	"	1.3	0.97
31	7.6	Sinter Feed	1.7	0.83
42	7.6	Silica Gel	1.1	0.51
44	15.2	G.Pellets	1.2	0.84
38	7.6	Peas	4.7	0.88
39	15.2	"	4.8	1.23
40	15.2	"	4.9	1.21

These experiments were carried out at an inlet air temperature of 150°C and an inlet air flow rate of 0.6 $m^3/s\ m^2$.

Table 6.8 - Effect of mM_o and material on the rate of drying.

CHAPTER 7

DISCUSSION OF RESULTS

CHAPTER 7 DISCUSSION OF RESULTS

7.1 - Apparatus and Experimental Procedure

Before discussing the results of the drying experiments, the effect of the following factors on the experiments will be discussed.

(i) Pressure drop across the bed.

(ii) Heat losses from the bed.

(iii) Temperature profiles of the air entering the bed.

(iv) Conditions at the start of the experiment.

(i) Pressure drop across the bed.

Experimental pressure drops across the bed for steel and glass balls were compared with the values calculated from the Ergun equation given on page 31 , and are shown in Chapter 6 , page 92. The agreement between the experimental and calculated values was good except in the case of granular materials, in which case it was difficult to obtain the effective particle diameter. The assumptions made by Ergun in developing his equation are therefore also obeyed by this system, i.e.

(a) velocity profiles of the drying air are uniform across the bed;

(b) there is negligible wall effect;

(c) there is only point contact between the particles;

(d) the flow is adiabatic, in the steady state, and incompressible.

Assumptions (a) and (b) are important because the results of the drying experiments would be affected if

significant wall effects or variations in velocity profile existed. The results at an inlet air temperature of 100°C in the steady state also show that the above assumptions hold at this temperature. The variation in voidage is much greater for glass balls than for steel balls, and this would account for the better agreement obtained between calculated and experimental pressure drops for steel balls.

Another purpose of the pressure drop experiments was to check if the system was functioning properly, i.e. any gas leaks, friction between any moveable parts, effect of mercury seal, etc. Since the agreement between experimental and calculated pressure drops was good, it can be concluded that there were no defects in the general functioning of the system.

(ii) Heat losses from the bed.

The heat losses from the bed, excluding the enthalpy of the outlet air, will be caused mainly by natural convection and radiation from the glass walls of the container.

In the steady state,

Rate of heat conduction through the wall = rate of heat loss by radiation + rate of heat loss by natural convection.

i.e. $Q'_C = Q'_{nat.convec.} + Q'_{radiation.}$

a) Natural Convection

The maximum rate of heat loss by natural convection from the walls will occur when all the moisture from the

bed has been removed and the outlet air temperature approaches the inlet air temperature, i.e. the steady state has been achieved. It is necessary to determine whether laminar natural convection or turbulent natural convection correlations should be used. A sample calculation follows for experiment no.4 (data on page 163), in which it is assumed that the surface temperature of the container is at the inlet air temperature of 150°C. The relationship for natural convection from vertical cylinders given by McAdams[39] has been used in the following calculation.

Height of the column (L) = 0.152m = 0.5 ft

Diameter of column (D) = 0.07m = 0.25 ft

Assume wall temperature (t_w) = 150°C = 302°F

Room temperature (t_r) = 20°C = 68°F

Temperature difference Δt = 130°C = 234°F

Film temperature $\frac{t_w+t_r}{2}$ = $\frac{302+68}{2}$ + 460 = 645°F

Thickness of glass column (t') = 3×10^{-3}m

Thermal conductivity of glass (K_{gl}) = 1.26×10^{-3} KW/m°C

$$Nu_f = A(Gr_f\ Pr_f)^n$$

$$= A\ x^n = (\theta\ L^3 \Delta t)^n \qquad \text{for air}$$

$$\theta = 6 \times 10^5\ ft^{-3}\ F^{-1}$$

$$L^3 \Delta t = 29.2\ ft^{-3}\ {}^oF$$

Therefore $x = 1.7 \times 10^7$

Hence the flow is laminar and the relevant

correlation[39] is

$$h_c = 0.29 \left(\frac{t_w - t_r}{L}\right)^{0.25} \quad \text{BTU/hr ft}^2\,^{\circ}\text{F} \qquad 7.1$$

$$= 1.57 \times 10^{-3} \left(\frac{t_w - t_r}{L}\right)^{0.25} \quad \text{kW/m}^2\,^{\circ}\text{C} \qquad 7.2$$

b) Radiation

The following equation for radiation from the wall will be used

$$Q'_{radiation} = e \sim \left[(t_w + 273)^4 - (t_r + 273)^4\right]$$

where

$$e = 0.94^{(41)}$$

and

$$\sim = 5.67 \times 10^{-8} \quad \text{W/m}^2\,^{\circ}\text{K}^4$$

c) Conduction

The rate of conduction through the wall is given by

$$Q'_{conduction} = \frac{K_{gl}}{t'} (t_{g_o} - t_w)$$

therefore

$$\frac{K_{gl}}{t'}(t_{g_o} - t_w) = h_c(t_w - t_r) + e\sim\left[(t_w+273)^4 - (t_r+273)^4\right]$$

or

$$\frac{K_{gl}}{t'}(t_{g_o} - t_w) = 1.57 \times 10^{-3}\left(\frac{t_w - t_r}{L}\right)^{0.25} (t_w - t_r)$$

$$+ e \sim\left[(t_w+273)^4 - (t_r+273)^4\right]$$

Substituting for K_{gl}, t', t_{g_o} = 150°C, L, t_r, e and α and solving for t_w by trial and error gives

$$t_w = 145^{\circ}C$$

Rate of heat loss in steady state

$$= Q'_{conduction} \times \text{surface area of column}$$

$$= \frac{K_{gl}}{t'} (t_{g_o} - t_w) \pi D L$$

$$= 76 \text{ W}$$

Alternatively, the maximum rate of heat loss from the system can be calculated because the outlet air temperature obtained from experiment number 4 was 129°C in the steady state.

Inlet-outlet air temperature (Δt) = 150-129 = 21°C

Therefore

Rate of heat loss = $G c_p \Delta t$ = 63 W.

The two methods of calculation give heat loss values which are in reasonable agreement. The heat loss calculated by the first method does not include heat lost to the mercury seal, whilst the second method includes heat lost to the seal.

The rate of heat input from the inlet air

$= G\ C_p\ (t_{g_o} - 20)$

$= 392$ W.

The maximum rate of heat loss from the column (steady state heat loss) is therefore about 16 % of the total heat input to the bed, and the average rate of heat loss will therefore be 8% of the heat input.

The container should absorb an insignificant proportion of the heat input to the bed. The thermal capacity of the container including the mercury seal

= mass of container x specific heat

= 0.610 x 0.96 = 0.586 KJ/°C.

The container attains a temperature of 147.5°C and therefore the maximum amount of heat absorbed by the container

= 0.586 x 147.5 = 86.5 KJ.

The heat absorbed by that part of the container surrounding the bed is less than 86.5 KJ and is given by

$$86.5\ \frac{\rho_{gl} \pi D t' L}{610}$$

(where $\pi Dt'L$ is the volume of the glass surrounding the bed)

$$= 86.5 \times \frac{218}{610} = 31 \text{ KJ}$$

The total heat input to the bed for a drying time of 21 minutes = 392 x 21 x 60 = 490 KJ.

The heat absorbed by the container is therefore 17.5% of the total heat input, but the heat absorbed by that part of the container surrounding the bed is only 6.0% of the total heat input.

All the above estimates of the rate of heat loss and of the amount of heat absorbed are likely to be higher than in actual practice because the inside wall temperatures were taken to be equal to the inlet gas temperature of 150°C. In fact wall temperatures will be lower than this.

(iii) Temperature profiles of the air entering the bed.

The method of obtaining the temperature profiles is given in Chapter 5, page 76. Since both suction pyrometers controlled the inlet air temperature, therefore when one of them was used for measuring the temperature profile and moved from one wall to the other, neither of the pyrometers was maintaining the temperature at the wall and by the time the traverse was completed, the temperature of the wall in which direction the pyrometer was moving, had fallen below its actual value. This effect was reversed when the pyrometer was brought back to its original position. The time taken for each traverse was about one minute.

Apart from a 4mm zone next to the wall, temperature variation of the air entering the bed was within ±5°C of the required value. This 80% of the air was heated to the set temperature ±5°C.

(iv) Conditions at the start of the experiment.

Before the air is passed through the bed, the load cell and the manometer outputs are steady at points A and B shown in Fig. 6.8. As soon as the air enters the bed, readings A and B jump to points C and D respectively in less than 1 second. These rapid changes are equivalent to a load cell reading of 127 g and to an upthrust on the bed of 134 g. These two values of 127 g and 134 g should

be the same, since virtually no moisture has been evaporated. The difference of 7 g could be due to a number of reasons :-

1) It is not possible to determine exactly the starting points of the load cell and the manometer readings on the chart, though they would be expected to be close to points C and D, between A and C, and B and D respectively.

2) It takes up to 2 seconds to open valve (5) and close valve (4) (Fig. 4.1), in order to direct the air from the by-pass to the bed. The amount of moisture that is removed from the bed during this time can be estimated. The moisture removed from the bed in 2 seconds for run No. 4, is given by

$$m.a.u.M_o.T = 0.2 \text{ g}$$

Therefore the moisture removed from the bed during this time cannot account for the discrepancy of 7 g between the load cell reading and the manometer reading.

3) The manometer reading is calibrated in terms of the load cell reading, as explained on page 100 Chapter 6 . This calibration can only be carried out when drying has been completed, otherwise moisture losses would affect the load cell reading. However it is assumed that the dry bed calibration also applies to the wet bed. The error involved in the calibration can be estimated because the load cell error is $\pm$ 2 g due to fluctuations, and the manometer error is $\pm$ 1 g. This gives a total of $\pm$ 6 g according to the calibration procedure on page 99 Chapter 6 . This accounts for most of the 7 g error at the start of the experiment.

4) The instrument response times of the micromanometer and the load cell are very small and are unlikely to influence the results. The chart recorder with a response time of 1 second full scale deflection would affect both readings to the same extent and is in any case fast enough to have a negligible effect.

5) The time taken for an element of air to reach the top of the bed could influence the pressure drop reading immediately after time zero. The time for this element to reach the top of the bed is given by

$$\frac{L}{v/\epsilon} = 0.1 \text{ S.}$$

This time interval can be ignored because it is negligible compared to the time taken to switch the valves.

7.2 - A typical residual moisture against time plot.

Fig.6.9 is a typical residual moisture against time plot. This graph can be divided into three parts, i.e.

OA - Period of increasing moisture content.

AB - Constant drying rate period.

BC - Falling drying rate period.

OA - Period of increasing moisture content.

During the first 1 - 2 minutes of the run, the residual moisture 'increases'. There does not appear to be any obvious reason for this but it could be associated with the following observations :-

(i) Air enters the bed initially at about 130°C and takes 2 - 3 minutes to reach the required temperature of 150°C.

(ii) During this period, the drying zone may not be fully established.

The initial period OA is not well defined and varies

from run to run. The increase in moisture content shown in Fig.6.9 is not obtained in every run, but most runs show either this effect or negligible loss of moisture in the first two minutes.

AB - Constant drying rate period.

As soon as the unstable period OA is over, the constant drying rate period begins. The rate of drying remains approximately constant (averaging 6.08 g/min) until 14 minutes after the start of the experiment. This is so, according to the model, because the drying zone is within the bed

According to the model of the drying process given in Chapter 3, the drying rate should be constant because the air is assumed to leave the bed saturated at a constant temperature.

BC - Falling drying rate period.

The drying rate at point B starts to decrease and approaches zero at about position C. This falling rate period can be explained by referring to the model. At point B, the front of the drying zone has reached the top of the bed. As soon as the zone starts to move out of the bed, the drying rate falls off. This is confirmed by Fig.7.1 of the actual experimental chart, which shows that the outlet air temperature increases during this period.

The total moisture obtained by weighing the column before and after the experiment excluding the weight loss during pre-heating

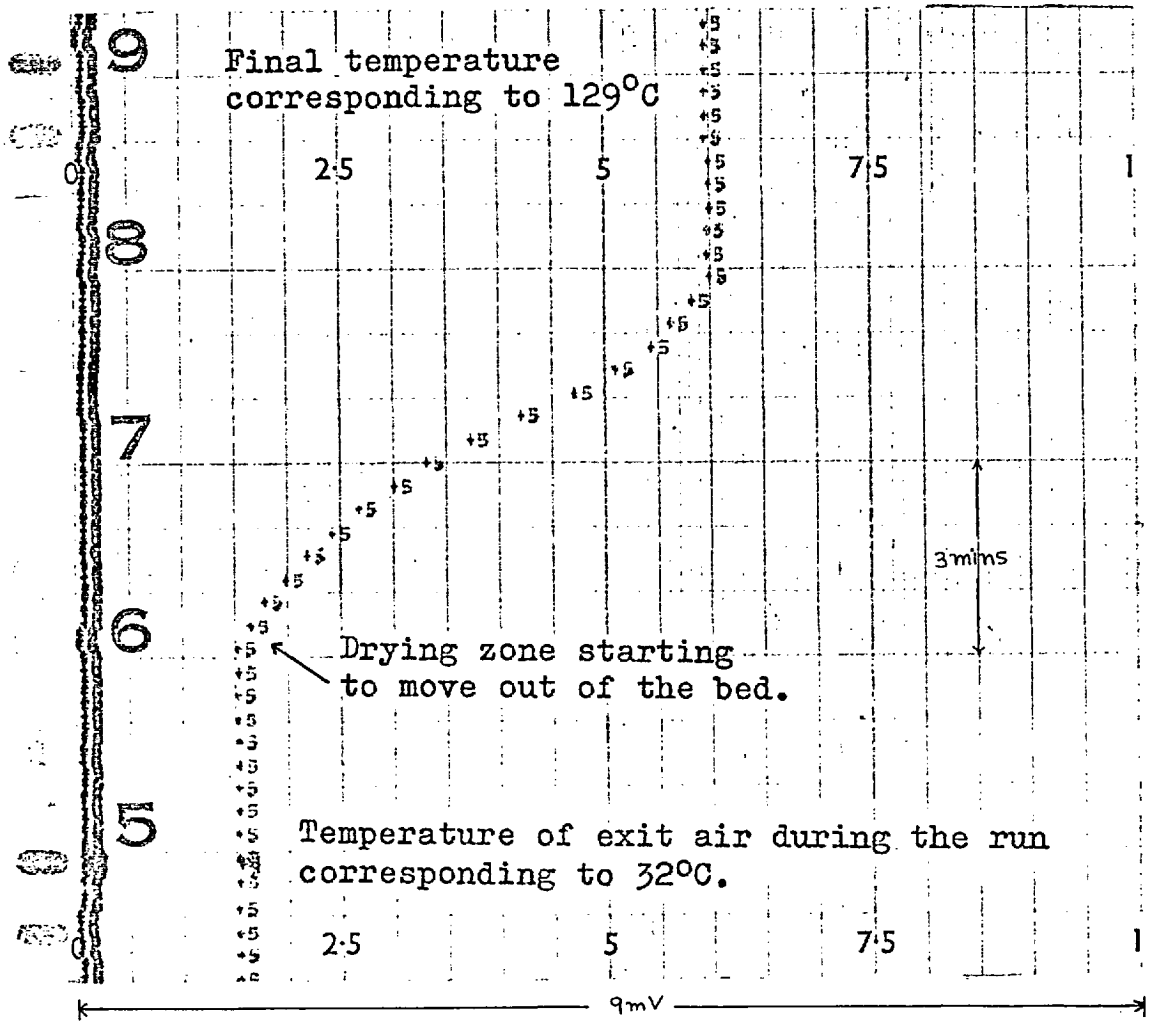

FIGURE 7.1 - Exit temperatures of Run No.4.

is indicated by point D on Fig. 6.9. Point D is a more accurate starting point than point E, because point E includes the errors encountered at the start of the run.

7.2.1 - Up-thrust on the column

The force on the column due to pressure drop was obtained experimentally as explained on page 100. However it can also be obtained theoretically as follows, using the data of experiment No. 4 obtained from the experimental chart shown on page 98

Initial load cell reading = 4.4 mV - 1.9 mV

= 2.5 mV = 127 g.

Initial pressure drop reading = 17.7 mm - 0.8 mm of water

= 16.9 mm

= 1.69 g/cm^2

Cross sectional area of column and mercury seal on which the air is exerting pressure

$$= \frac{\pi \times D^2}{4} = 70.8 \text{ cm}^2$$

where D = 9.5 cm.

Therefore force on the column = 1.69 x 70.8 = 120 g.

This method underestimates the force on the bed by about 5% whereas the empirical method mentioned on page 100 overestimates it by about 5%.

7.2.2. - Pressure drop against time plot.

Pressure drop against time curves for green pellets, sinter feed and peas are shown in Fig. 7.2 . This data was obtained from run Nos.4, 35 and 39 given in Appendix 1, pages 163, 179 and 181 respectively.

The pressure drop across beds of all the materials rises in the first 2-3 minutes which is due to the inlet air temperature increasing from about 130°C to 150°C, as explained in Section 7.2 of this chapter. Between 2 and 3 minutes, the pressure drop curve for green pellets falls slightly which could be due to the inlet air temperature over-shooting the required temperature and then decreasing to the required value. From 3 minutes onwards, the pressure drop goes on rising due to the heating of the bed.

In the case of peas, the pressure drop starts to decrease after 3 minutes, which could be due to the expansion of the bed resulting from the peas losing weight. This causes an increase in voidage.

The drying of sinter feed could cause fines to fall through the bed. This would decrease the voidage, and consequently result in a fall in pressure drop. From 24 minutes onwards, heating of the bed causes the pressure to rise again.

7.3 - Influence of process variables.

The effect of the process variables on the drying rate and drying time will now be discussed.

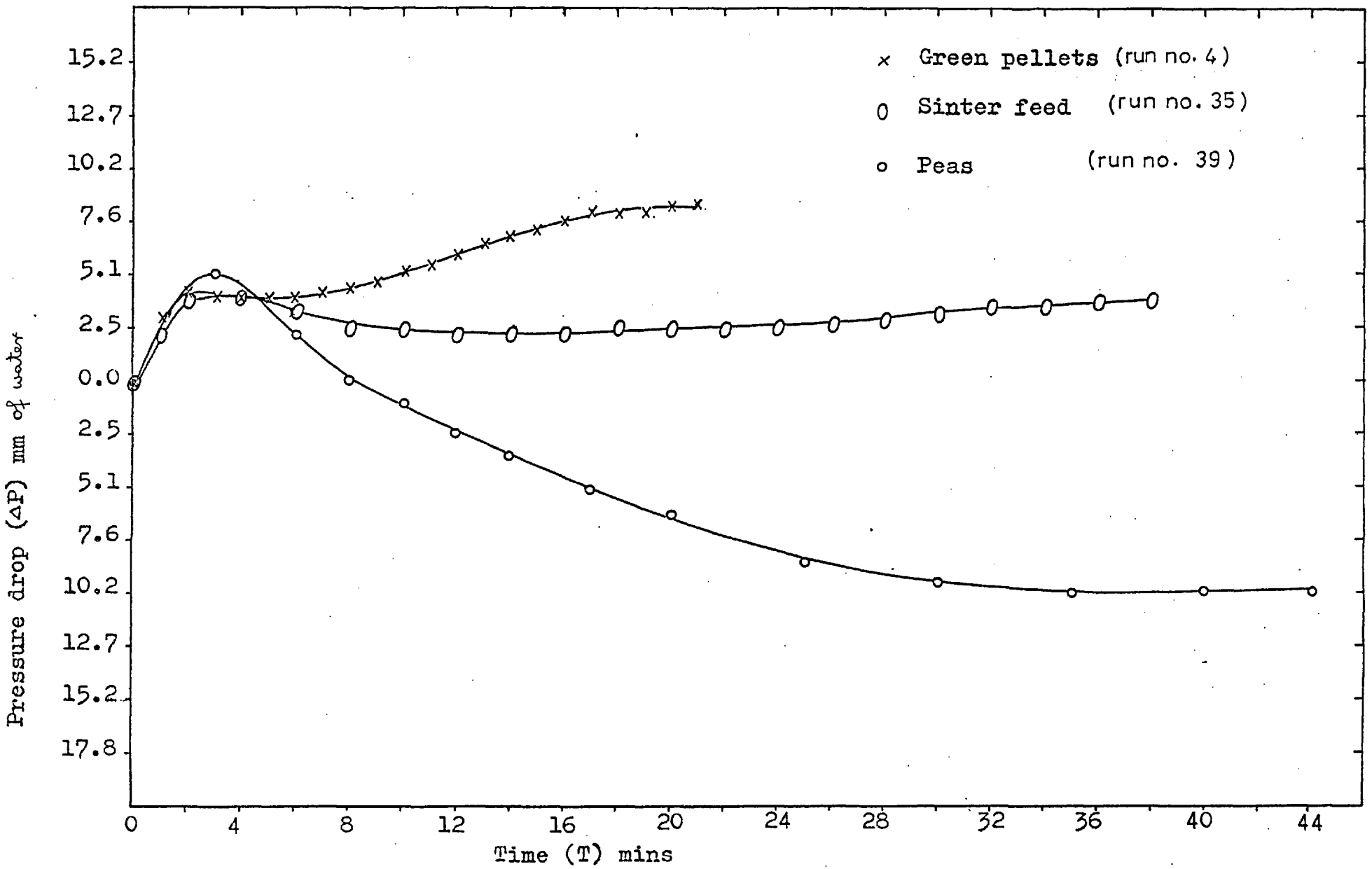

FIGURE 7.2 - Pressure drop during a run against time plot for different materials.

7.3.1 - Inlet air flow rate.

Considerable scatter exists about the curve of air flow rate against drying time shown in Fig. 6.12. At the end of an experiment, the residual moisture against time curve gradually tails off (Fig. 6.9) and it is difficult to decide the exact time when all the moisture has been evaporated. So a second curve of flow rate against half drying time, i.e. time for half of the moisture to be removed, was plotted.

The half drying time could be determined with greater accuracy because the drying rate is constant when half drying has been accomplished, i.e. in region A B in Fig. 6.9. The general trend of both curves is the same and indicates that the drying time decreases as the flow rate is increased. There is a large reduction in drying time when the flow rate increases from 0.4 $m^3/s\ m^2$ to 0.6 $m^3/s\ m^2$ but as the flow rate is increased further, the reduction in drying time becomes correspondingly smaller. The flow rate against drying rate curve in Fig. 6.11 shows that the drying rate increases as the flow rate increases. The graph of flow rate against drying rate in the constant rate period, shown in Fig. 6.13, is linear with a slope of $\frac{\rho_g x_2}{a}$ indicating that the humidity x_2 of the outlet air is independent of flow rate under the experimental conditions used for this work.

The drying rate of silica gel is lower than other other materials because the process of drying silica gel is endothermic.

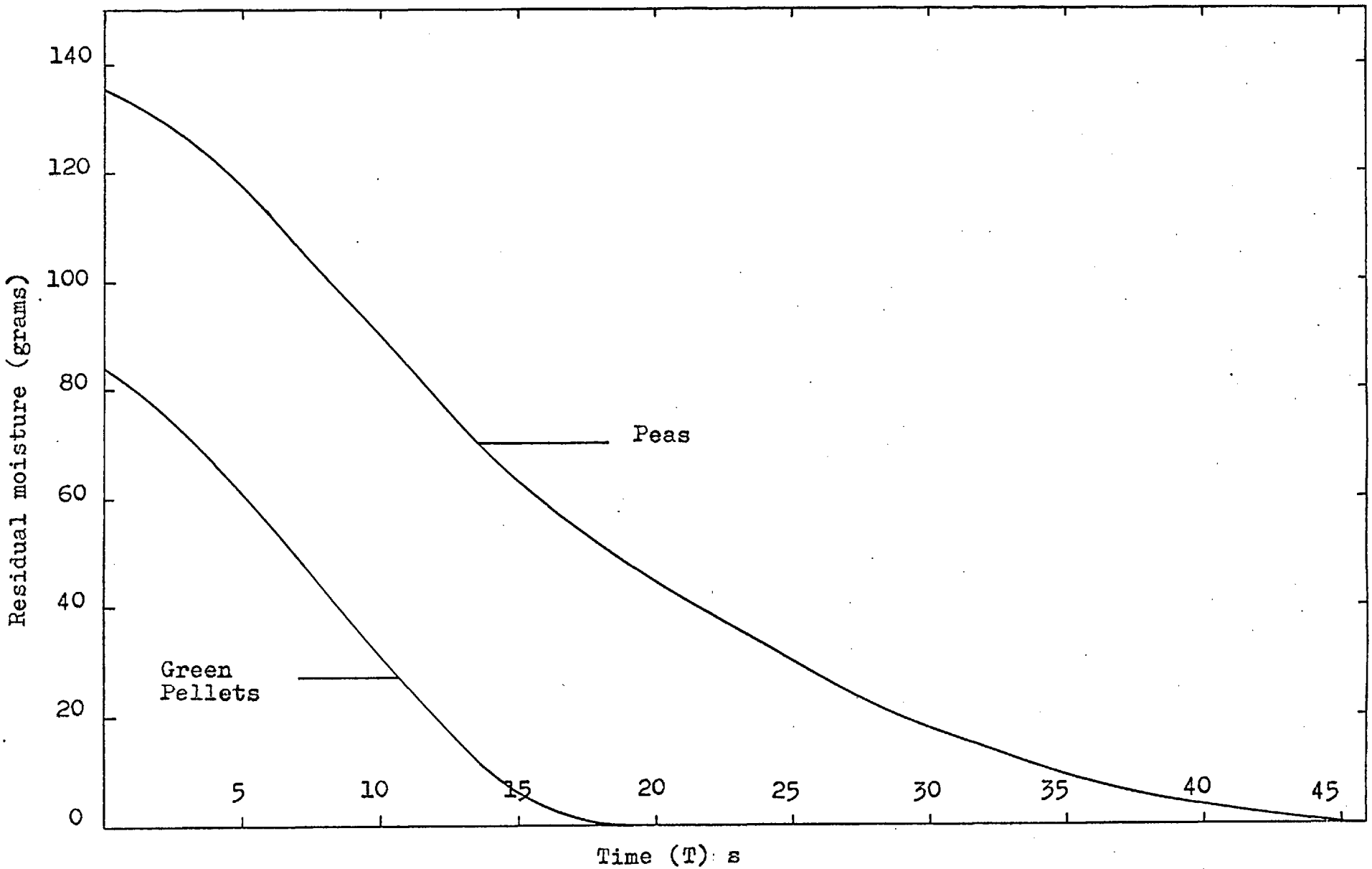

FIGURE 7.3 - Residual moisture against time plot.

7.3.2 - Inlet air temperature.

Inlet air temperature was plotted against half and total drying times as is shown in Fig. 6.10 . There is a considerable decrease in drying time as the temperature rises from 50°C to 100°C. However the reduction in drying time becomes less marked when air temperatures in excess of 100°C are used.

Inlet air temperature was also plotted against the drying rate for the constant rate period and is shown in Fig. 6.11. The plot shows that the drying rate is a linear function of temperature for all materials except silica gel which has a lower rate of drying, as explained in Section 7.3.1 of this chapter.

7.3.3 - Initial moisture content and material.

The effect of M_o and material on the rate of drying is shown in Table 6.8. The drying rates of most of the experiments are the same within experimental error. The drying rate of silica gel is lower as explained in Section 7.3.1 of this chapter. The drying rates of experiments Nos.39 and 40, i.e. 15.2×10^{-2} m beds of peas, are higher because the residual moisture against time curve (Fig.7.3) exhibits a long tail which tends to shorten the constant rate period. The slope of the curve in the constant rate period is therefore difficult to assess and drying rates are subject to large errors. The reasons for this type of behaviour could be :

(a) The structure of the material is very different from that of green pellets and sinter feed. In peas it is likely that considerable resistance to mass transfer could lie in the solid because pore sizes are likely to be much smaller.

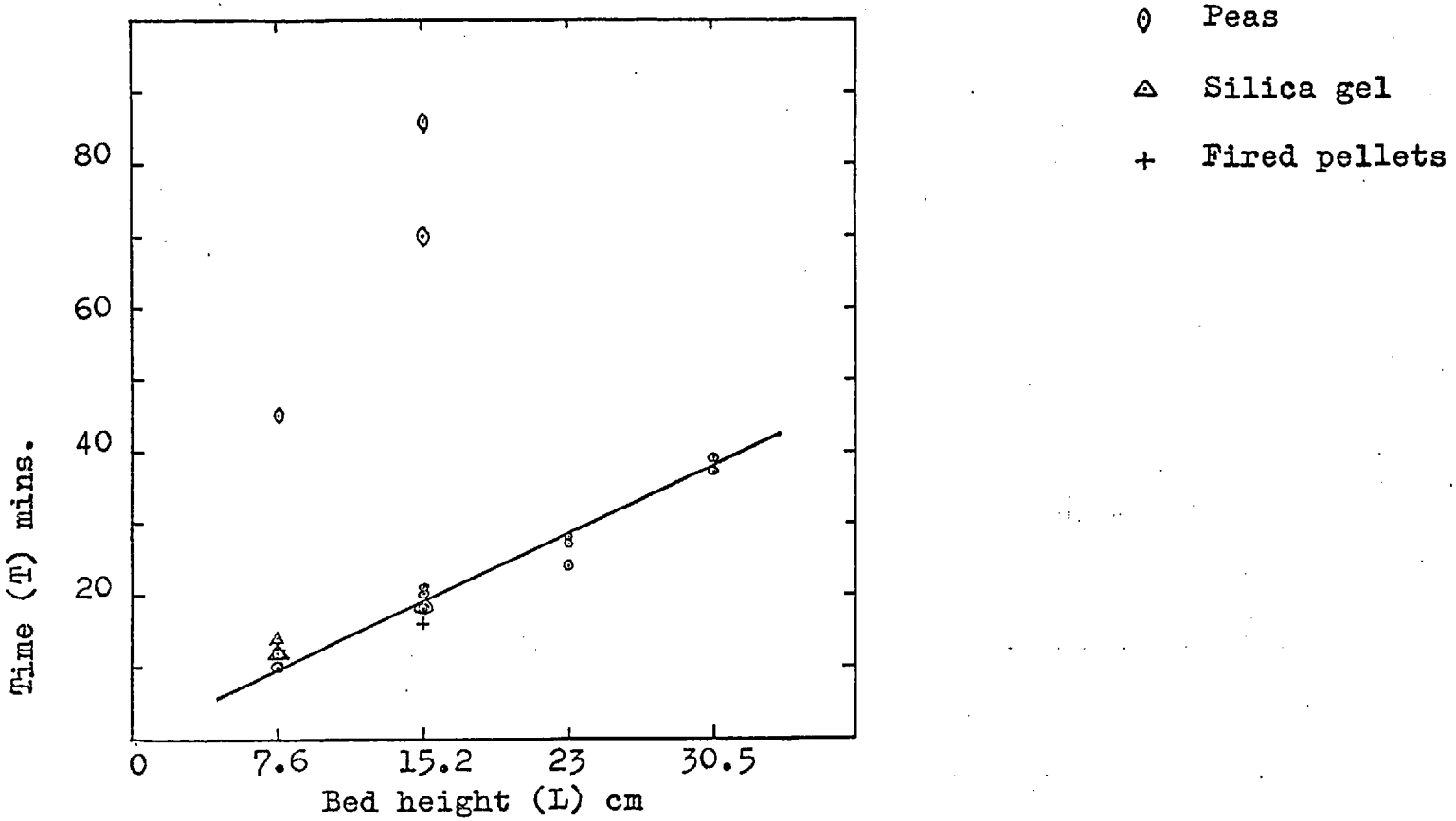

FIGURE 7.4 - Bed height against time plot for different materials.

b) Peas change their shape during drying, as mentioned on page 109. This would change the voidage of the bed and the value of the heat transfer coefficient as drying proceeded.

7.3.4 - Pellet size.

The effect of pellet size on the rate of drying is shown in Table 6.6. As can be seen, the pellet size has no effect on the rate of drying within the range of the particle sizes used in this work.

7.3.5 - Bed height.

The effect of bed height on the rate of drying is shown in Table 6.7 . As is apparent from the table, the bed height has no effect on the rate of drying of various materials within limits of experimental error, except for the drying rates of silica gel and peas, as explained in Sections 7.3.1 and 7.3.3 of this chapter respectively.

The effect of bed height on total drying time is shown in Fig. 7.4. It can be seen that the total drying time is a linear function of bed height.

7.4 - Voidage.

(a) - Green pellets.

The voidage of steel spheres used in the early part of this work was found to be 0.39, whereas that of glass balls was found to be 0.37. Although the steel and glass spheres were of approximately the same size, i.e. 6 mm, the glass balls were not perfectly spherical and therefore are likely to have been more compactly packed

than the steel spheres, giving a lower voidage. As the green pellets were not perfect spheres either, it would be expected that they would have a voidage lower than 0.4. But as they were of a larger size than 6 mm, giving a lower ratio of particle diameter to bed diameter and increasing the amount of air passing along the walls of the column because of lower resistance to flow there, they would be likely to have a larger voidage. These two opposing effects were found to cancel each other out as confirmed by using the data of a dry pellet** , substituted in the Ergun equation given on page 31 , to calculate the voidage. A value of 0.401 was obtained for the green pellets.

(b) - Sinter Feed.

The experimental procedure for obtaining the voidage of sinter feed is given on page 79 , Chapter 5 . The voidage of sinter feed could not be obtained theoretically because it was not possible to determine the effective particle diameter or specific surface for sinter feed. The experimentally obtained voidage was 0.32.

(c) - Other Materials.

(i) - Fired pellets.

These pellets were similar to green pellets in shape and therefore a value of 0.4 was used for the voidage.

(ii) - Peas.

Although the voidage of peas did not remain constant during the drying experiments and it was not possible to assess the change in voidage, peas were also similar to green pellets in sphericity and therefore the voidage was

** run(given in appendix 2)

assumed to be 0.4. The voidage may have altered near the end of a run because of the bed's tendency to fluidize.

(iii) - Silica gel.

The procedure for obtaining the voidage of silica gel is given on page 79 , Chapter 5 . A value of 0.467 was obtained.

7.5 - The Model

7.5.1 - Prediction of the rate of drying

Equation (3.10) of the model given on page 54 gives the rate of drying. This equation cannot be used directly to predict drying rates unless h_v, $\bar{z}$ and t_m are known. The heat transfer coefficient h_v can be obtained by using Rowe and Claxton's [19] relationship as explained on page 37 Chapter 2 . The height of the drying zone $\bar{z}$ can be obtained from the relationship given by Allerton [34] (page 45), From the graph plotted for experiment No.4, (Fig 6.9) and from the data of other experiments given in Appendix 1 , it is apparent that the start of the falling rate period cannot be determined accurately. Similarly the total drying time cannot be determined accurately. This method for calculating $\bar{z}$ was found to be unsatisfactory because of too much scatter as can be seen from Fig. 7.5. The height of the drying zone can be obtained accurately by using Eq.(3.13) of the model, given on page 55, but some experimental data has to be used to evaluate it. The log mean temperature difference, t_m, can be calculated from the inlet and outlet temperatures to the drying zone as explained on page 95, Chapter 6 , but these temperatures

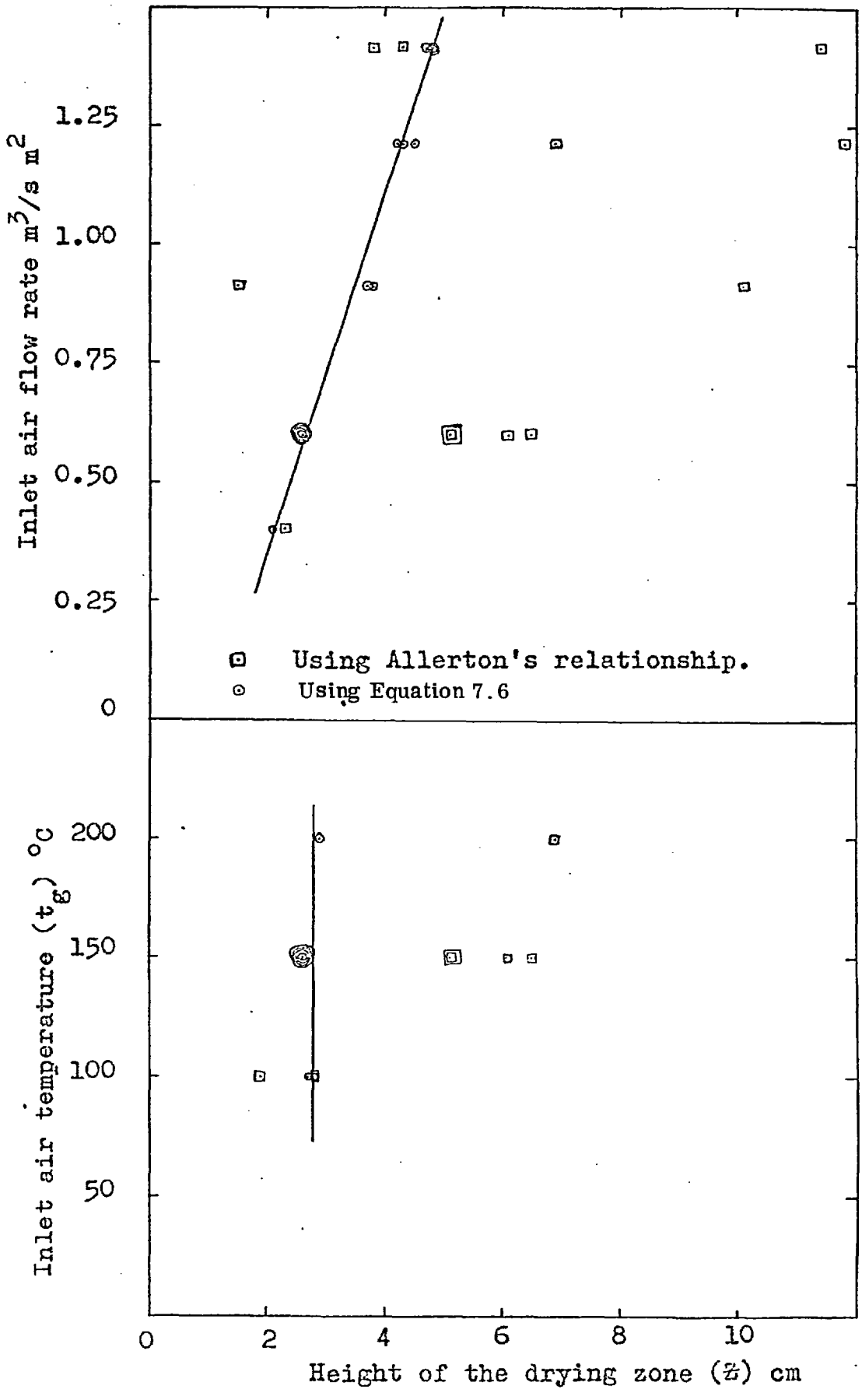

FIGURE 7.5 - Plot of inlet air temperature and flow rate against height of the drying zone for green pellets.

cannot be obtained without the use of experimental data. Therefore $\mathcal{Z}$ and t_m had to be expressed as empirical relations involving process variables.

Inlet air temperature t_{g_o} is plotted against t_m in Fig.7.6 at different inlet air flow rates and for different materials. Although there is considerable scatter, a good fit for all the points would be the straight line shown in Fig.7.6. The figure also indicates that t_m is largely independent of both the flow rate and the material to be dried. From this figure,

$$t_m = 0.21 \quad t_{g_o} + \quad 5.1 \qquad 7.4$$

The line drawn through the points in figure 7.6 was obtained by a least square regression analysis on the data for green pellets, fired pellets and sinter feed. The correlation coefficient for the linear equation is 0.74 and the standard deviation is 3.84. The standard error in the slope is 0.023 i.e. 11%. This gives a standard error in the intercept of ±3.2 .

The values of $\mathcal{Z}\ h_v$ are plotted against $G/_a$ in Fig.7.7 for various materials at different inlet air temperatures. Although there is some scatter, the best fit is a straight line passing through the origin. Since values for various temperatures have been plotted and lie on or close to the line, $\mathcal{Z}\ h_v$ can be said to be largely independent of temperature and the material to be dried. From Fig.7.7

$$\mathcal{Z}\ h_v = 3.29\ \frac{G}{a} \qquad 7.5$$

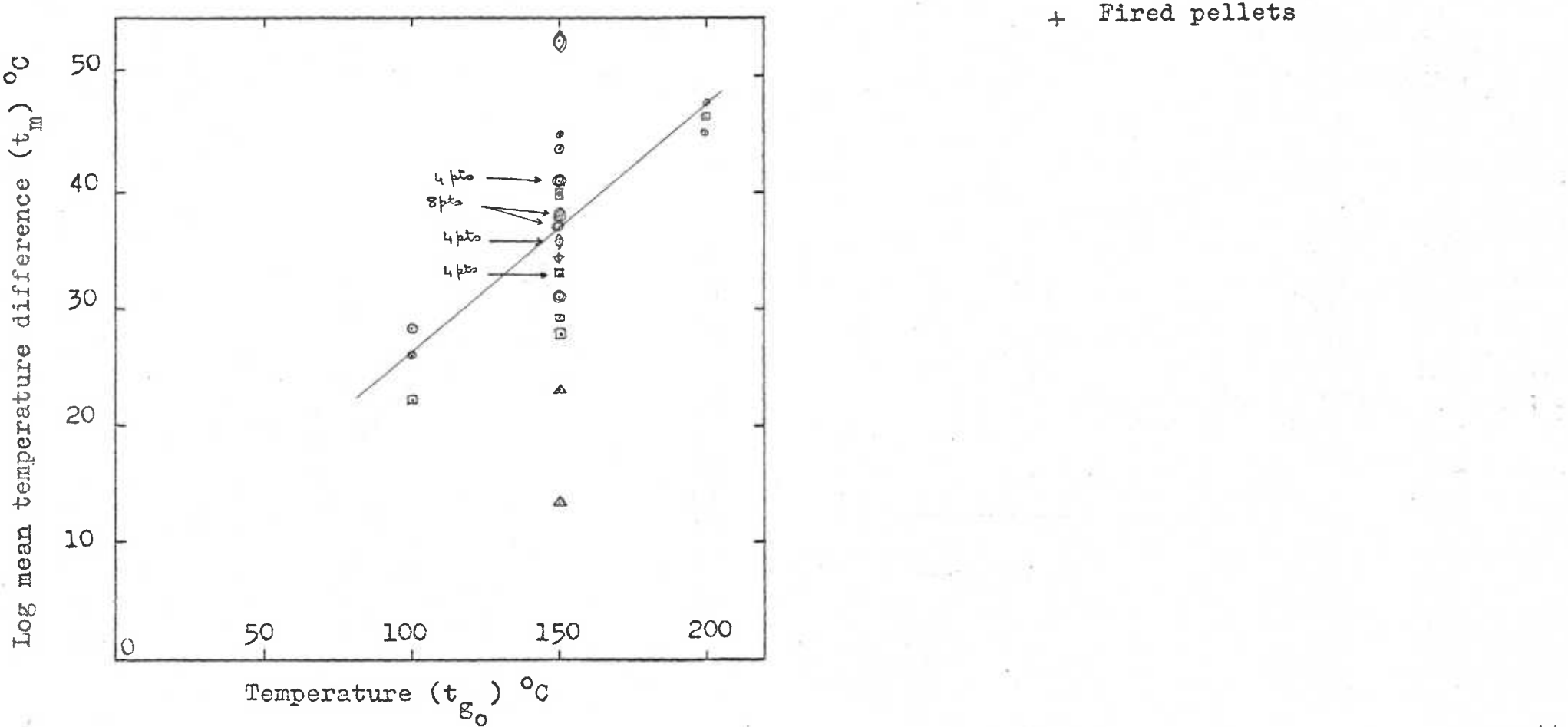

FIGURE 7.6 - Plot of log mean temperature difference against inlet air temperature.

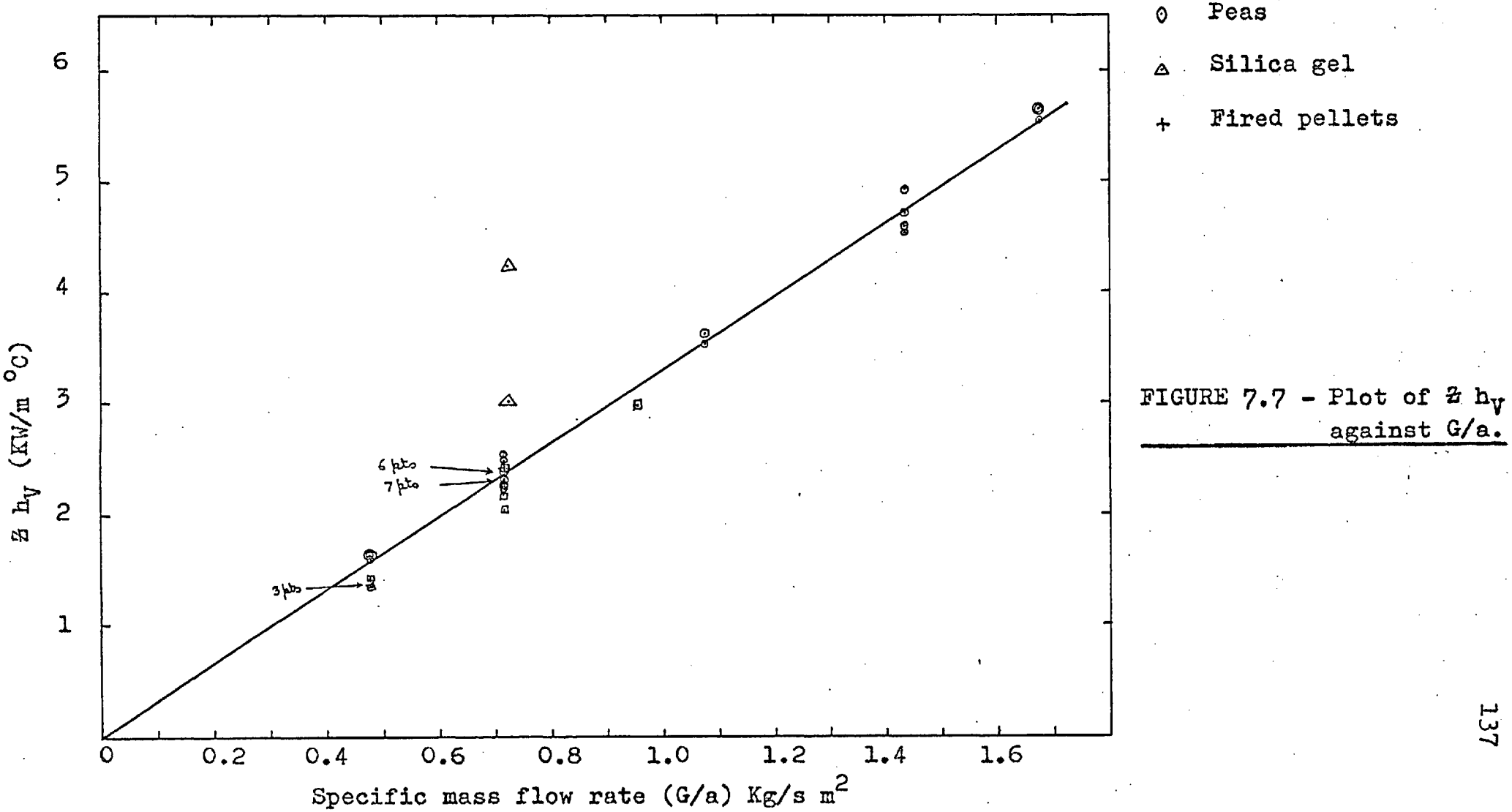

FIGURE 7.7 - Plot of Σh_V against G/a.

The linear relationship between Σh_v and $\frac{G}{a}$ shown in Fig. 7.7 is also empirical. In this case there is some justification for the line to pass through the origin because the equation of the model (3.9) shows that $\Sigma h_v = o$ when $\frac{G}{a} = o$. The error in obtaining Eqn.(7.5) from Fig. 7.7 is small and is judged to affect the constant 3.29 by $\pm$ 1%.

Values of t_m and Σh_v can be substituted in Eqn.(3.9), giving

$$\frac{G x_2}{a} = 0.69 \quad \frac{G}{a}(1 - \epsilon)\frac{(t_{g_o} + 24)}{\lambda}$$

$$\text{or} \quad \frac{G x_2}{a} = 2.8 \times 10^{-4} \quad \frac{G}{a}(1 - \epsilon)(t_{g_o} + 24) \qquad 7.6$$

Introducing the errors discussed above, the numerical constants in Eqn.(7.6), become $2.8 \times 10^{-4} \pm 0.3 \times 10^{-4}$ and 24 ± 15. This equation can be used to predict the rate of drying of any material.

From Eqn.(7.5) and Eqn.(3.6), given on page 54

$$u = \frac{2.8 \times 10^{-4}(1 - \epsilon)(t_{g_o} + 24)}{m M_o} \frac{G}{a} \qquad 7.7$$

where u is the velocity of the drying zone.

The errors in the numerical constants in Eqn.(7.7) are identical to those in Eqn.(7.6).

7.5.2 - Velocity of the drying zone.

Figure 7.8 is a theoretical plot based on the model (eq. 7.7), between the velocity of the drying zone and specific mass flow rate. Lines have been drawn for various values of inlet air temperature and $\frac{mM_o}{\epsilon}$. This plot can be used for obtaining the specific rates of drying of any material under the range of experimental conditions used for this work if $\frac{G}{a}$, $\frac{mM_o}{\epsilon}$ and t_{g_o} are known.

7.5.3 - Heat transfer coefficient.

The area and volumetric heat transfer coefficients h and h_v do not include the effect of evaporation as explained on page 37 Chapter 2 . The modified area heat transfer coefficient h^o given on page 24 includes the effect of evaporation, but has not been used instead of h, because the modification is small enough to be neglected as shown by the calculation below :-

The modified heat transfer coefficient

$$h^o = \frac{h\,\lambda \ln\left[1 + \frac{c_{p_w}}{\lambda} t_m\right]}{c_{p_w}\, t_m}$$

(data of Experiment No.4, given in Appendix 1 , is used in this calculation)

$$\lambda = 2440 \text{ KJ/Kg}$$

$$t_m = 44^oC$$

Mean C_{p_w} over the film at $20^oC + 44^oC = 64^oC$

i.e. $C_{p_w} = 1.89$ KJ/Kg ^oC (38)

$$h^o = \frac{h \times 2440 \ln\left[1 + \frac{1.89}{2440} 44\right]}{1.89 \times 44}$$

$$h^o = h \times 1.01$$

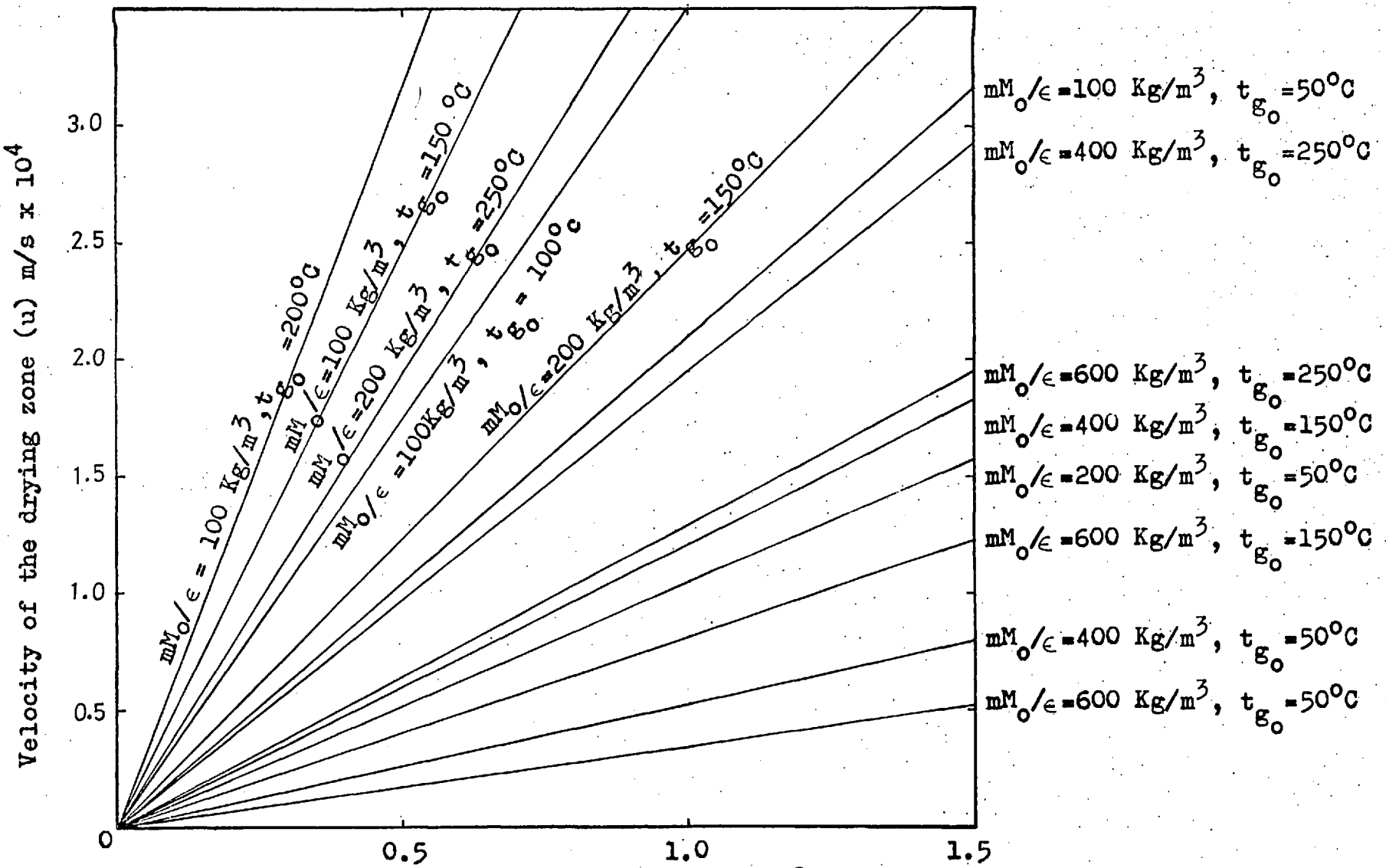

FIGURE 7.8 - Plot of velocity of the drying zone against specific mass flow rate.

7.5.4 - Assumptions of the model.

Assumption (iii) of the model that air leaving the drying zone is saturated is confirmed by Fig. 7.9 This shows a plot of moisture evaporated against time for Expt. No.4 (data in Appendix 1 , page 163). Also shown in Fig. 7.9 is a plot of moisture evaporated against time assuming that the air leaves the bed saturated at 32°C. This temperature of 32°C was the temperature of the air leaving the bed for Expt. No.4 (Fig. 7.1 , page 123). This line was obtained by plotting moisture evaporated ($g \times_2 T$) at any time T. It can be seen that agreement between this line and the moisture removed is good in the constant drying rate period. This shows that air leaving the bed was saturated at 32°C and therefore assumption (iii) is justified.

According to assumption (iv), there are no heat losses from the column. However heat loss calculations given in Section 7.1 (ii) of this chapter show that the mean heat loss from the column during a run is about 14% of the rate of heat input. The heat lost from that part of the column surrounding the bed is about 3%. However heat loss calculations given in Section 7.1 (ii) show that heat losses are not negligible. The main heat loss occurred below the bed and would have the effect of lowering the gas inlet temperature. The heat losses from the bed itself are unlikely to affect drying rates within experimental error.

According to assumption (v), no heat or mass transfer takes place in the wet zone. Data of Expt.No.4 (Appendix 1

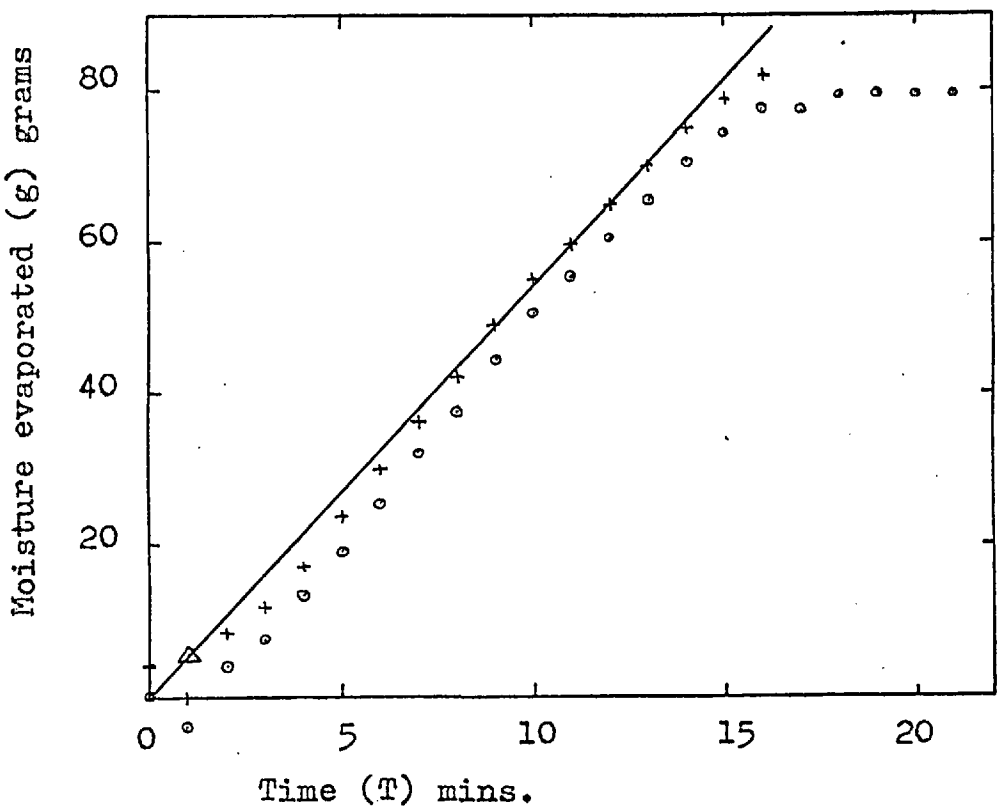

+ Corrected for moisture evaporated during the pre-heating of air.

⊙ Moisture evaporated.

△ Calculated value for saturated air at 32°C.

FIGURE 7.9 - Plot of moisture evaporated against time for Run No.4.

page 163) shows that the temperature of the air leaving the bed during the experiment at 32°C (page 123) was greater than the assumed temperature of the solid (20°C) and therefore heat transfer did take place in the wet zone. However this rate of heat transfer would be small compared to the rate of heat transfer during drying. If mass transfer took place in the wet zone, i.e. moisture evaporating from the drying zone condensed in the wet zone, then the total drying time should increase with bed height. But this does not happen to a noticeable extent because Fig. 7.4 shows that drying time is a linear function of bed height and therefore condensation in the upper parts of the bed is unlikely.

According to assumption (ix), gas velocity is not influenced by pressure drop. The maximum pressure drop in this work was obtained in Expt.No.32 (Appendix 1 , page 177), i.e. 38.6 mm. This is an approximately 1% change in atmospheric pressure and will have negligible effect on the velocity of the gas.

It has been shown in Section 7.3.5 of this chapter that the bed height does not have any effect on the rate of drying. This is in agreement with the model, because it is one of the assumptions of the model that drying takes place in the drying zone only and since the drying zone is assumed to be smaller than the total height of the bed, the bed height cannot affect the rate of drying.

It is not possible to justify assumptions (i), (ii), (vi), (vii) and (viii) because there is no relevant experimental data available.

7.6 - Comparison with the results of other workers.

(i) and (ii) - The experimental work of Marshall and Hougen [23], and Gamson et al [24] has been described in Chapter 2, Section 2.5. Their work was on low temperatures and they did not envisage the concept of a drying zone in packed bed drying. They found that a long constant drying rate period existed, during which gas phase only contributed resistance to the transfer of heat and mass. The constant drying rate period was attributed to the complete coverage of the individual particles with water. This is a condition for tray or slab drying as explained in Chapter 2, Section 2.2 and does not necessarily apply to packed beds. In a packed bed, whether there is any surface moisture present or not, there would be a constant drying rate period, as long as the drying zone is within the bed.

They also assumed that the change in temperature in the bed is proportional to the change in humidity over the bed. This may be true over the range of temperatures at which they worked, but is not true when applied to temperatures up to 200°C, as shown in Fig. 7.10(*). Therefore equation 2.45 cannot be applied to this work.

(*) which was plotted by using the data of experiments nos: 16, 17, 4, and 19, given on page 96.

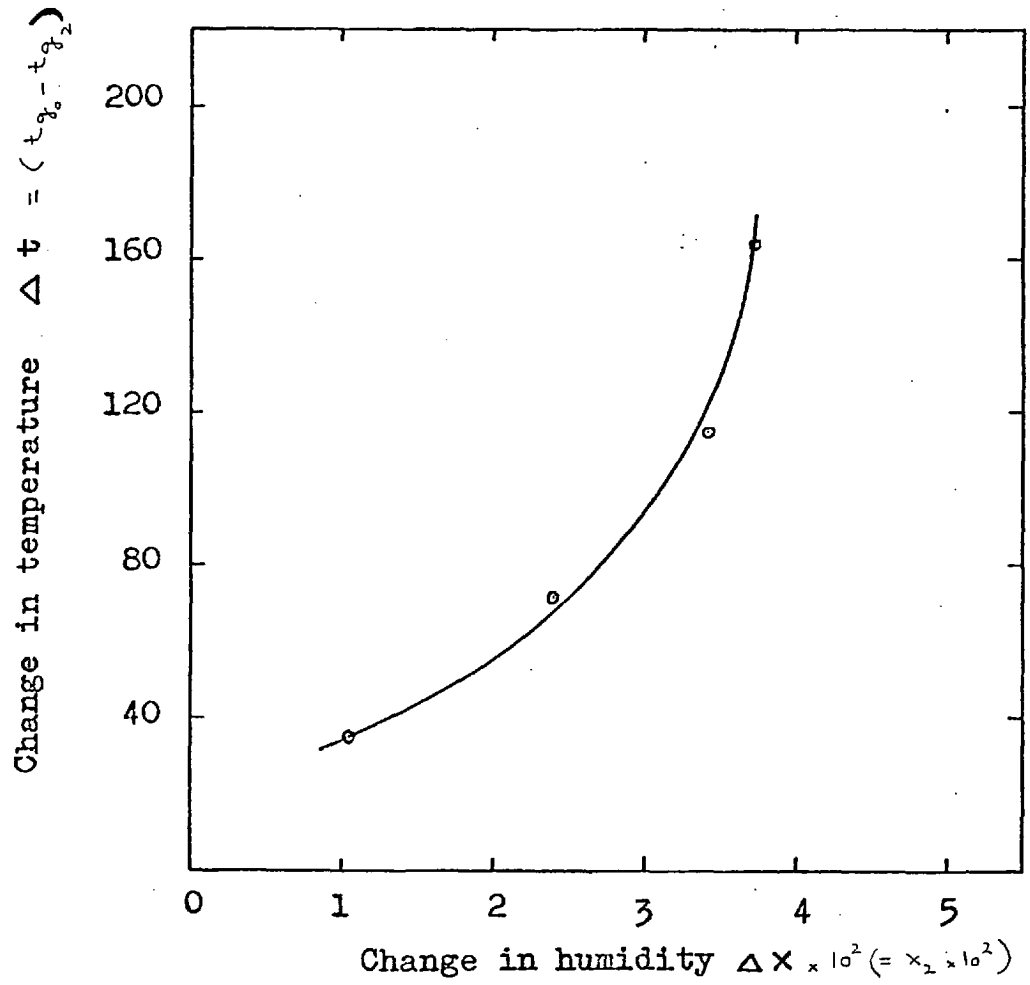

FIGURE 7.10 - Change in humidity against change in temperature.

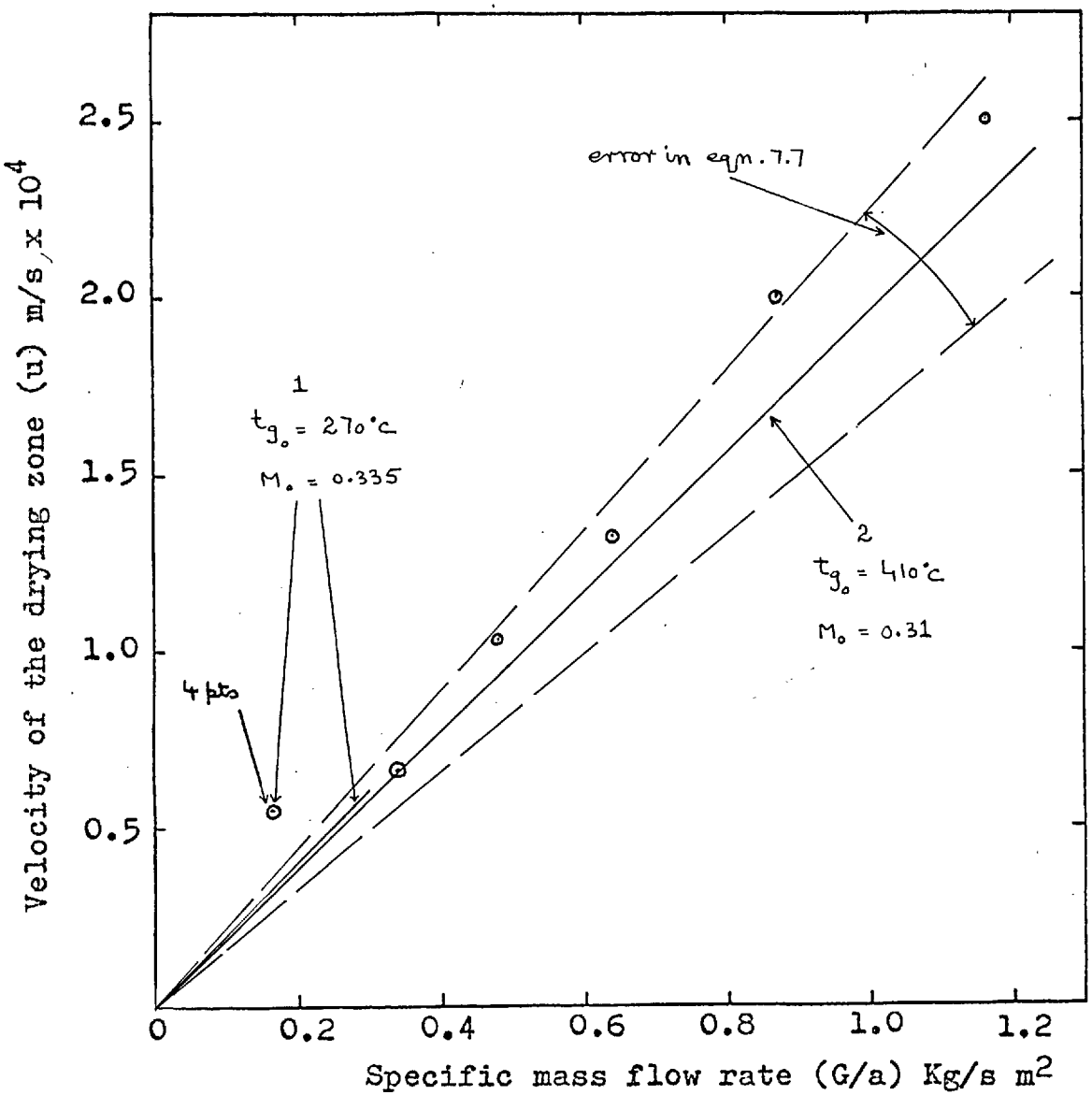

⊙ Beveridge's experimental data.

—— Predicted.

FIGURE 7.11 – Data of other workers fitted to the model.

Allerton[34] formulated an expression for calculating the efficiency of drying in packed beds which is given by Eqn.2.a.on page 46 . The value of j_D which is required to calculate the efficiency can be obtained from Eqn.2.53 on page 44 . This relationship for j_D includes the effect of axial mixing. A typical efficiency value can be calculated from this relation using the data of Run No.4 given on page 163.

For Re = 260, $\epsilon = 0.4$,

$j_D = 0.12$ from Eqn.2.53 on page 44

In order to calculate $(Sc)_f$, the film temperature t_f must be found and

$$t_f = \frac{t_m}{2} + t_s$$

$$= \frac{44}{2} + 20 = 42^{\circ}C$$

where t_m is given on page 96 and t_s, according to an assumption of the model, is equal to the room temperature.

The diffusivity of water vapour in air at $25^{\circ}C$ is given as

$$D_{V\ 25^{\circ}C} = 0.256 \times 10^{-4}\ m^2/s$$

But $$D_V \propto (273 + t_g)^{1.5}$$

$$D_{V\ 42^{\circ}C} = 0.256 \times 10^{-4} \left(\frac{273 + 42}{273 + 25}\right)^{1.5}$$

$$= 0.26 \times 10^{-4}\ m^2/s.$$

From appendix 4.2,

$$\mu_{42^{\circ}C} = 1.85 \times 10^{-5}\ Kg/m\ s$$

and $$\rho_{42^{\circ}C} = 1.1\ Kg/m^3$$

Hence $$Sc_{42^{\circ}C} = \left(\frac{\mu}{\rho D_V}\right)_{42^{\circ}C} = 0.78$$

and $$Sc^{\frac{2}{3}}_{42^{\circ}C} = 0.85$$

Allerton's term for the area of the air-liquid interface can be expressed as

$$\frac{s}{a} = (1 - \epsilon)\ \mathcal{Z}\ S$$

assuming that the area of the air-liquid interface is equal to the surface area of the solid.

Hence $\frac{s}{a} = (1 - 0.4)\ 0.03\ \frac{6}{0.007}$

$= 15.$

Therefore, the efficiency

$$\frac{p_2 - p_1}{p_s - p_1} = 1 - e^{-2.1}$$

$$= 0.88$$

Alternatively, the efficiency of drying can be obtained as follows :

$j_D = j_h$ on page 44 of Chapter 2

$$j_h = \frac{h}{c_p\ G/a}\ Pr_f^{\frac{2}{3}}$$

Therefore the exponent of Allerton's relation becomes

$$\frac{\frac{h}{c_p\ G/a}\ \left[Pr\right]_f^{\frac{2}{3}}}{\left[Sc\right]_f^{\frac{2}{3}}}\ \frac{S}{A}$$

$$= \frac{h}{c_p\ G/a}\ Le_f^{\frac{2}{3}}\ (1 - \epsilon)\ Z\ S = \frac{h_V}{c_p\ G/a}\ Le_f^{\frac{2}{3}}\ Z$$

But Le $\simeq$ 1.0 for an air-water system (see page 21).

Therefore exponent = $\frac{h_V\ Z}{c_p\ G/a} = \frac{80 \times .03}{1 \times 0.72} = 3.3$

Therefore $\frac{p_2 - p_1}{p_s - p_1} = 1 - e^{-3.3} = 1 - \frac{1}{27} = 1.0$

It can be seen from the above two calculations that the efficiency of drying of a packed bed is greatly dependent

on the exponent and a small change makes a large difference in the efficiency. Therefore the efficiency of drying of the packed beds used in this work can be assumed to be very high, and hence the assumption of the model that the air leaves the bed saturated during the process of drying is valid.

(iv) - Beveridge's [35] experimental data was fitted to the model and is shown in Fig.7.11. Line 1 is for kieselguhr spheres and line 2 is for zinc sulphide particles. Beveridge has neither given the voidage nor the weight of his packed beds. The voidage for zinc sulphide particles was taken to be 0.32 because it had a particle distribution similar to the sinter feed used in this work. The voidage of the bed of kieselguhr spheres was taken to be 0.4, as for the bed of green pellets. In order to calculate the value of m, the mass of solid per unit volume of bed, which is required to compare Beveridge's results with the model, the densities of kieselguhr and of zinc sulphide are required. These are given as $2 g/cm^3$ and $4.1 g/cm^3$ respectively, and can be used to obtain the values of m for kieselguhr spheres and zinc sulphide particles as follows

$$m_{\text{kieselguhr}} = m_{\text{green pellets}} \frac{\rho_{\text{kieselguhr}}}{\rho_{\text{green pellets}}} \qquad 7.9$$

$$m_{\text{zinc sulphide}} = m_{\text{sinter feed}} \frac{\rho_{\text{zinc sulphide}}}{\rho_{\text{sinter feed}}} \qquad 7.10$$

These equations are only true if the voidages of the beds are given by

$$\epsilon_{\text{kieselguhr}} = \epsilon_{\text{green pellets}}$$

and

$$\epsilon_{\text{sinter feed}} = \epsilon_{\text{zinc sulphide}}.$$

Beveridge's data is expressed as velocity of the drying zone u plotted against mass flow rate per unit area $\frac{G}{a}$ in Fig.7 on page 101 of his paper [35]. His experimental points at $M_o = 0.33 - 0.34$ and $t_{g_o} = 260 - 280^oC$ for kieselguhr and at $M_o = 0.30 - 0.32$ and $t_{g_o} = 410^oC$ for zinc sulphide have been plotted in Fig.7.11. Equation 7.7 on page 138 has been plotted as u against $\frac{G}{a}$ for these two sets of results, and the relevent data for M_o and t_{g_o} given above. It can be seen that the experimental data agrees reasonably with the model, considering the estimates that have been made to obtain values of ϵ and m for the packed beds used by Beveridge and the standard error in u given on page 138.

7.7 - Axial mixing.

Epstein's axial mixing factor F given in Chapter 2 page 44 will be calculated for both, green pellets and sinter feed.

Green Pellets

If we consider temperature differences to be the driving forces, then

$$R = \frac{t_{g_1} - t_r}{t_{g_2} - t_r} = \frac{122 - 20}{34 - 20} = 7.3$$

where 122^oC and 34^oC are the inlet and outlet temperatures

of the drying zone for a typical drying experiment (Expt. No.4, data on page 163).

$$n = \frac{L}{D_p} \frac{Pe}{2}$$

Since Peclet number is approximately equal to $2^{(33)}$,

$$n = \frac{Z}{D_p} = \frac{26}{6.8} = 3.8$$

where $L = Z$ in this case because heat transfer is assumed to occur over the length of the drying zone only.

$$\text{Therefore} \quad F = \frac{\ln R}{n\left[R^{\frac{1}{n}} - 1\right]} = 0.77$$

Sinter Feed

A similar calculation based on the data of Run No.31 for sinter feed gives (data on page 177)

$$R = \frac{91 - 20}{28 - 20} = 8.9$$

$$\text{and} \quad n = \frac{4.5}{3.1} = 1.45$$

Therefore $F = 0.57$.

It can be seen from the calculations for Run Nos.4 and 31 that axial mixing is significant for both green pellets and sinter feed, particularly so for sinter feed where the factor F drops to 0.57. The greatest influence on F is that of n, taken here to be given by $\frac{Z}{D_p}$. The height of the drying zone therefore affects the axial mixing more than any other factor in these calculations;

as ℵ decreases, so F decreases. Axial mixing will however not affect the semi-empirical relation given by Eqn. 7.8 because axial mixing effects will be included.

Values of n were calculated for the experiments of Marshall and Hougen[23] and Allerton [34]. In the case of Marshall and Hougen, the data used was from Curve 1 of Fig.10 in his paper. The height of the drying zone was obtained using the relationship given by Allerton (see page 45). The value of n was found to be 2.5. The data available was insufficient to calculate the value of R and hence the value of F. The value of n indicates that correction must be made for axial mixing.

Data of Run No. 207 of Allerton given in his paper was used for calculating n. Because of lack of data, values of R and hence F could not be obtained. The value of n was found to be 3, indicating that correction was needed for axial mixing.

It should be noted that the heights of the drying zones calculated by using Allerton's relationship do not agree with the heights calculated by using Eq.(3.13) of the model.

7.8 - Applications of the model.

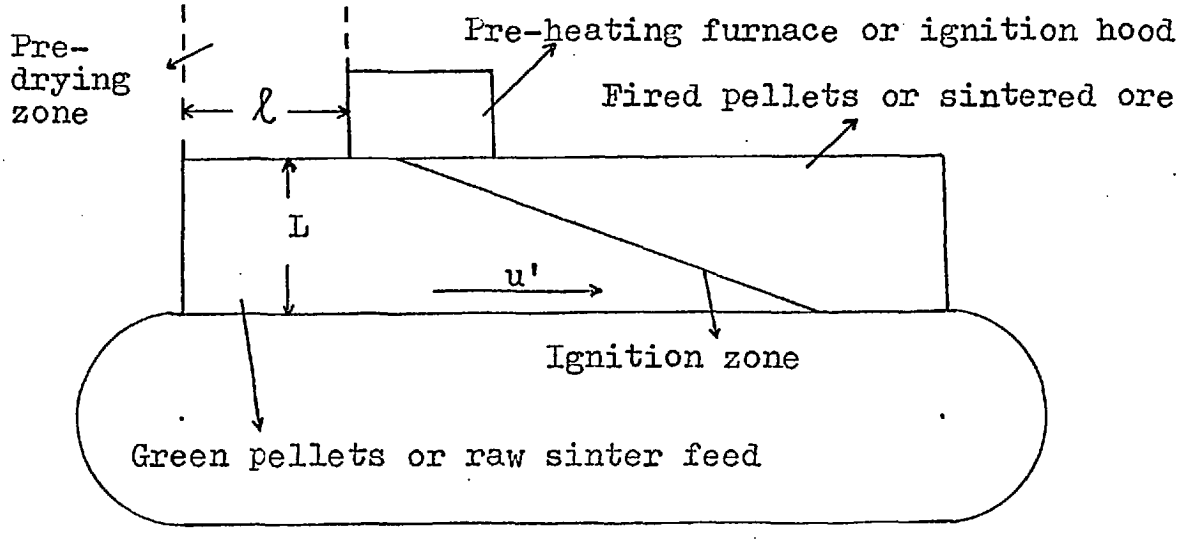

FIG.7.12 - A pellet firing machine or sinter strand.

Detailed diagrams of a sinter strand and a pellet firing machine have been given in Fig.1.1 and 1.3 respectively in Chapter 1. As explained in Chapter 1, in a pellet firing machine the green pellets are dried before they reach the furnace, but the sinter feed goes directly under the ignition hood without any pre-drying.

a) Pellet hardening machine.

The following equation will be used in order to calculate the length of the strand ℓ, required to dry the green pellets before the pre-heating furnace is reached,

$$u = \frac{2.8 \times 10^{-4}(1-\epsilon)(t_{g_o}+24)}{m\, M_o} \frac{G}{a} \qquad 7.7$$

It is assumed that updraught drying is used and that a constant drying rate exists throughout the bed depth L, then

$$u = \frac{L}{T'} \qquad 7.11$$

where T' is the time for complete drying. But the strand speed u' is given by

$$u' = \frac{\ell}{T'} \qquad 7.12$$

assuming that drying is completed when the material reaches the pre-heating furnace. Equations 7.7, 7.11 and 7.12 give

$$\ell = \frac{m\, M_o\, u'\, L}{2.8 \times 10^{-4}(1-\epsilon)(t_{g_o}+24)\, \frac{G}{a}} \qquad 7.13$$

The length of the pellet hardening strand required for drying the pellets will now be calculated using industrial

data. This data is given in a paper [40] which describes the operation of a horizontal grate pellet hardening machine using magnetite pellets. This material is dried from 10% initial moisture to 2% on a length of the grate ℓ = 12.8 m. Other details given are :-

height of the bed, L = 0.33 m

speed of strand, u' = 0.03 m/s

temperature of drying air, t_{g_o} = 425°C

specific mass flow rate of drying air, $\frac{G}{a}$ = 2.21 kg/s. m^2

The values of m and ϵ for the bed are not known but the data of Expt.No.4 (data on page 163) which was carried out on green pellets can be used. For this experiment, m = 1777 kg/m^3. As in all the pellet work, the voidage is assumed to be 0.4.

Using eqn.7.13, and the errors in the numerical constants given in eqn. 7.6 complete drying is obtained when ℓ = 10.4 ± 1.5 m. This value of ℓ has been calculated using an initial moisture content of material to be 10% instead of 7.9% used in Expt.No.4. This value of ℓ would be higher than it should be because this is based on the fact that the material is dried from 10% to 0% instead of 10% to 2%, as in the industrial process. The length of strand used for drying of 12.8 m is higher than the 10.4 m predicted by the model. The predicted value is likely to be lower because of leakage of air between the grate and the windbox. Also the humidity of the inlet drying air is not known because in the process some of the waste gas from the

pellet firing process is used for drying together with hot air from cooling the pellets. Under these circumstances agreement between the calculated and actual values of ℓ is reasonable.

b) Sinter strand.

On sinter strands there is no provision for drying of sinter feed prior to hood and therefore only about 3.3 m^2 of bed area is available between the feeder and the ignition hood, assuming a strand width of 1.8 m (6 ft).

Equation 7.13 can be used to find the depth of the bed L, which is completely dried for a given value of ℓ, in this case 1.8 m (6 ft). Note that here L is not the total bed height. Fig.7.13 shows a plot of L against flow rate $\frac{G}{a}$ at inlet air temperatures of 100°C, 200°C and 400°C. A reasonable value for the air flow rate through this part of the bed can be calculated using the data of Expt.No.31 in the Ergun equation (2.25) given on page 31. A value of 0.5 kg/s m^2 was obtained assuming a typical pressure of 0.76 m w.g. and that the bed has a permeability similar to that of Expt.No.31 (data on page 177). If the air for drying is at 400°C, then Fig.7.13 shows that L = 26 mm. Above L = 26 mm there will be a partially dry zone corresponding to the drying zone. For sinter feed, $\bar{z}$ = 4 mm (see Table 6.4) and the existance of the drying zone can be ignored for the purpose of estimating L. This value of L may well be sufficiently large to prevent the bottom of the bed during sintering from becoming impermeable due to condensation effects.

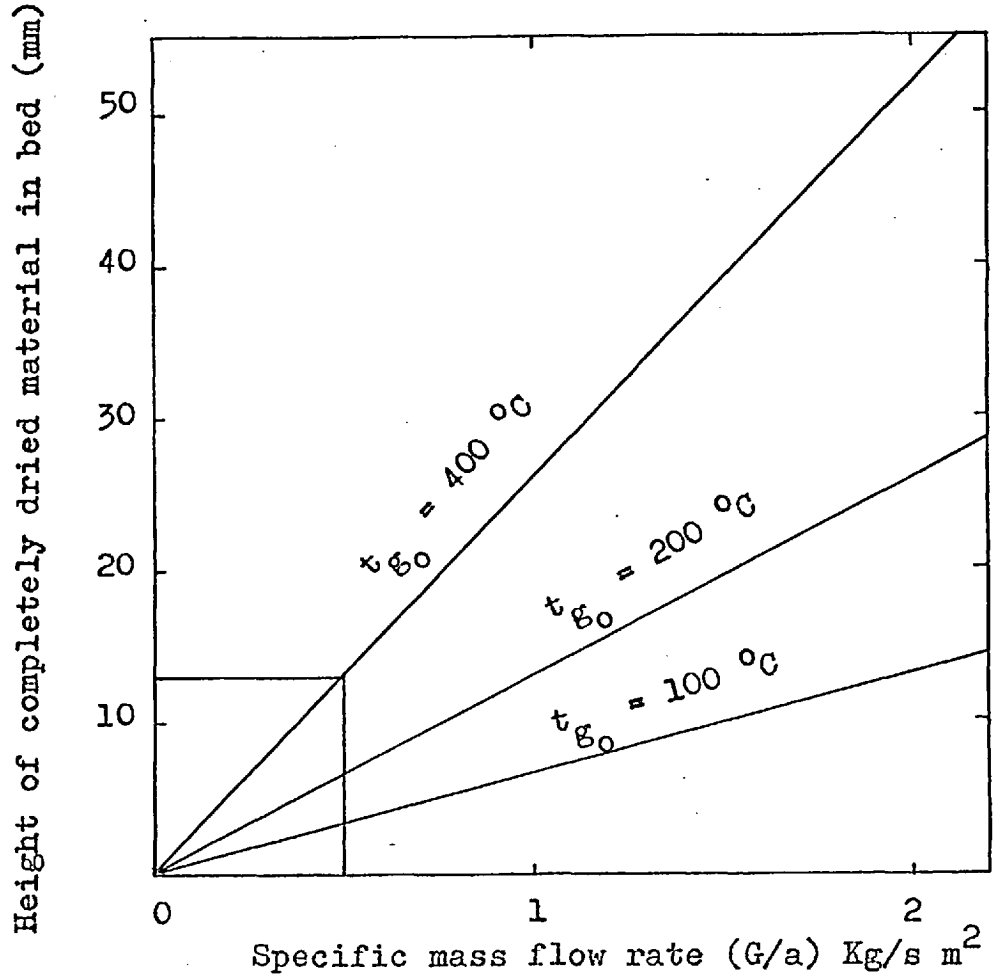

FIGURE 7.13 - Depth of bed dried after travelling 2m at 0.04m/s.

CHAPTER 8

CONCLUSIONS

CHAPTER 8 CONCLUSIONS

The drying experiments on green pellets, sinter feed, fired pellets and silica gel have shown (e.g. Expt.No.4, Fig. 6.9), that a constant drying rate is obtained over a significant period of the total drying time.

The experiments have also shown the following :-

1) In the constant rate period, the drying rate of these materials, except for silica gel, is a linear function of air flow rate in the range 0.4 $m^3/s\ m^2$ to 1.4 $m^3/s\ m^2$, and the humidity of the outlet air is independent of air flow rate.

2) The drying rate of these materials, except for silica gel, is a linear function of the inlet air temperature in the range 50°C to 200°C.

3) The initial moisture content has no significant effect on the rate of drying of these materials used except for silica gel.

4) The drying rate of all materials under the same conditions of inlet air temperature and flow rate, except silica gel, was the same within experimental error.

5) Variation in the size of green pellets in the range -5.6 + 4 mm to -9.5 + 8 mm has no effect on the rate of drying.

6) The rate of drying is independent of bed height in the range of 7.6×10^{-2} m to 30.5×10^{-2} m.

7) A constant drying rate does not occur when drying peas and conclusions 3 to 6 do not hold for peas.

The existence of the constant drying rate found experimentally is in agreement with the proposed model. The model is justified further by visual observations, which confirm the existence of a drying zone moving up the bed. Equation (3.9)

$$\frac{G\,x_2}{a} = \frac{\Sigma h_v (1-\epsilon)\, t_m}{\lambda}$$

which describes the rate of drying according to the model cannot be used to predict the rate of drying directly. However Eqn.(7.6)

$$\frac{G\,x_2}{a} = 2.8 \times 10^{-4} (1-\epsilon)(t_{g_o}+24)\frac{G}{a}$$

which has been obtained by determining Σh_v and t_m in terms of $\frac{G}{a}$ and t_{g_o} by experiment can be used to predict the rate of drying of any of the materials, except for silica gel and peas, within the range of the experimental conditions used for this work. Fig. 7.8 based on Eqn.(7.6) can be used to predict the velocity of the drying zone and the rate of drying directly.

Agreement between Equation (7.7)

$$u = \frac{2.8 \times 10^{-4}\ \frac{G}{a}(1-\epsilon)(t_{g_o}+24)}{m\,M_o}$$

(which is a modified form of Equation (7.6)), and drying rate data obtained by other workers is satisfactory within the errors involved in making the comparisons.

The model can be used to predict the length of the grate required for drying pellets on a pellet firing machine. The prediction will under-estimate actual lengths for reasons given on page 155 . The depth of sinter feed which is completely dried by up-draught drying for a given time can also be estimated from the model.

APPENDIX 1 - Data of drying experiments.

Experiment No.1

Weight of wet solid = 611 g.
Weight of dry solid = 569 g.
Weight of moisture = 42 g.
Percentage moisture = 7.4
1 mm of water in manometer 7.6 g.

Time (min)	Manometer reading (mm)	Load Cell reading (mV)
0	0	0
1	0.76	0.16
2	0.84	0.26
3	0.89	0.37
4	0.96	0.47
5	1.02	0.59
7	1.78	0.83
9	2.54	1.04
10	2.79	1.10

Experiment No.2

Weight of wet solid = 1202 g.
Weight of dry solid = 1118 g.
Weight of moisture = 84 g.
Percentage moisture = 7.5
1 mm of water in manometer 8.1 g.

Time (min)	Manometer reading (mm)	Load Cell reading (mV)
0	0	0
1	1.02	0.10
2	1.68	0.22
3	1.78	0.27
4	1.55	0.32
5	1.52	0.35
9	1.63	0.68
11	1.78	0.86
14	2.08	1.13
17	2.49	1.38
20	2.79	1.62
22	3.10	1.80
24	3.45	1.95
26	3.56	2.02

Experiment No.3

Weight of wet solid = 1187 g.
Weight of dry solid = 1107 g.
Weight of moisture = 80 g.
Percentage moisture = 7.2
1 mm of water in manometer 8.1 g.

Time (min)	Manometer reading (mm)	Load Cell reading (mV)
0	0	0
1	0.81	0.08
2	1.63	0.18
3	1.88	0.24
4	1.78	0.27
5	1.68	0.34
7	1.85	0.50
9	2.01	0.68
12	2.39	0.92
15	2.59	1.22
20	3.25	1.65
23	3.56	1.85
25	3.81	1.95
27	3.96	2.00
29	4.04	2.00
31	4.04	2.01
35	4.06	2.02

Experiment No.4

Weight of wet solid = 1204 g.
Weight of dry solid = 1116 g.
Weight of moisture = 88 g.
Percentage moisture = 7.9
1 mm of water in manometer 7.9 g.

Time (min)	Manometer reading (mm)	Load Cell reading (mV)
0	0	0
1	3.07	0.40
3	4.17	0.80
6	4.17	1.16
8	4.67	1.47
11	5.64	1.97
13	6.55	2.31
15	7.37	2.61
16	7.72	2.73
18	8.23	2.84
21	8.28	2.86

Experiment No.5

Weight of wet solid = 1172 g.
Weight of dry solid = 1092 g.
Weight of moisture = 80 g.
Percentage moisture = 7.3
1 mm of water in manometer 7.9 g.

Time (min)	Manometer reading (mm)	Load Cell reading (mV)
0	0	0
1	3.05	0.41
2	4.01	0.64
4	4.06	0.78
6	4.37	1.04
8	5.03	1.34
10	5.64	1.69
12	6.15	2.00
14	7.11	2.30
16	7.72	2.49
18	7.92	2.53
21	7.98	2.54

Experiment No.6

Weight of wet solid = 1162 g.
Weight of dry solid = 1082 g.
Weight of moisture = 80 g.
Percentage moisture = 7.4
1 mm of water in manometer 7.9 g

Time (min)	Manometer reading (mm)	Load Cell reading (mV)
0	0	0
1	3.15	0.45
2	3.96	0.60
3	4.17	0.70
4	4.37	0.83
5	4.88	1.04
6	5.44	1.02
7	5.89	1.40
8	6.35	1.60
9	6.76	1.78
10	7.11	1.94
11	7.62	2.15
12	8.13	2.34
13	8.48	2.51
14	9.04	2.66
15	9.40	2.78
16	9.91	2.90
17	9.91	2.90
18	9.91	2.92
19	9.91	2.93
20	9.91	2.95
25	9.91	2.95

Experiment No.7

Weight of wet solid = 1189 g.
Weight of dry solid = 1104 g.
Weight of moisture = 85 g.
Percentage moisture = 7.7
1 mm of water in manometer 8.7 g.

Time (min)	Manometer reading (mm)	Load Cell reading (mV)
0	0	0
1	2.03	0.30
2	2.79	0.47
3	2.79	0.55
4	2.79	0.65
6	2.92	0.90
8	3.40	1.20
10	4.06	1.47
12	4.62	1.77
14	5.08	2.05
15	5.59	2.15
16	5.84	2.25
17	6.10	2.32
18	6.35	2.40
19	6.40	2.40
21	6.45	2.40
23	6.45	2.40

Experiment No.8

Weight of wet solid = 1153 g.
Weight of dry solid = 1072 g.
Weight of moisture = 85 g.
Percentage moisture = 7.6
1 mm of water in manometer 8.5 g.

Time (min)	Manometer reading (mm)	Load Cell reading (mV)
0	0	0
1	4.06	0.70
3	4.06	1.00
5	5.08	1.44
9	8.13	2.52
10	9.14	2.80
11	9.91	3.00

Experiment No.9

Weight of wet solid = 1182 g.
Weight of dry solid = 1097 g.
Weight of moisture = 85 g.
Percentage moisture = 7.7
1 mm of water in manometer 8.7 g.

Time (min)	Manometer reading (mm)	Load Cell reading (mV)
0	0	0
1	5.59	0.81
2	5.84	1.01
3	6.10	1.16
4	6.60	1.41
5	7.37	1.68
6	8.13	1.96
7	8.89	2.26
8	9.40	2.56
9	10.92	2.90
10	11.94	3.20
11	12.95	3.46
12	13.72	3.60
13	13.97	3.62
14	14.22	3.62
15	13.97	3.61

Experiment No.10

Weight of wet solid = 1209 g
Weight of dry solid = 1126 g.
Weight of moisture = 83 g.
Percentage moisture = 7.4
1 mm of water in manometer 7.9 g.

Time (min)	Manometer reading (mm)	Load Cell reading (mV)
0	0	0
1	7.87	1.53
2	7.87	1.72
3	8.64	2.08
4	10.67	2.55
5	12.57	3.00
6	14.73	3.53
7	16.51	3.97

Experiment No. 11

Weight of wet solid = 1173 g.
Weight of dry solig = 1089 g.
Weight of moisture = 84 g.
Percentage moisture = 7.7
1 mm of water in manometer 7.4 g.

Time (min)	Manometer reading (mm)	Load Cell reading (mV)
0	0	0
1	6.98	1.19
2	7.80	1.46
3	8.89	1.81
4	10.03	2.20
5	11.43	2.64
6	13.72	3.11
7	15.24	3.52
8	16.89	3.86
9	17.91	4.02
10	18.54	4.07
11	18.41	4.05
13	18.54	4.02
15	18.67	4.01

Experiment No.12

Weight of wet solid = 1198 g.
Weight of dry solid = 1112 g.
Weight of moisture = 86 g.
Percentage moisture = 7.7
1 mm of water in manometer 7.4 g.

Time (min)	Manometer reading (mm)	Load Cell reading (mV)
0	0	0
2/3	7.11	1.15
1	8.51	1.30
2	8.91	1.60
3	10.16	2.02
4	12.06	2.45
5	13.59	2.95
6	15.24	3.40
7	17.40	3.75
8	18.41	4.10
9	20.32	4.45
10	20.95	4.60
11	21.08	4.65

Experiment No.13

Weight of wet solid = 1182 g.
Weight of dry solid = 1098 g.
Weight of moisture = 84 g.
Percentage moisture = 7.65
1 mm of water in manometer 7.9 g.

Time (min)	Manometer reading (mm)	Load Cell reading (mV)
0	0	0
1	7.37	1.20
2	7.62	1.50
3	9.40	2.02
5	14.99	3.24
6	17.78	3.97
7	21.08	4.54
8	23.88	5

Experiment No.14

Weight of wet solid = 1123 g.
Weight of dry solid = 1044 g.
Weight of moisture = 79 g.
Percentage moisture = 7.6
1 mm of water in manometer 8.1 g

Time (min)	Manometer reading (mm)	Load Cell reading (mV)
0	0	0
1	8.38	1.40
2	7.62	1.65
3	9.91	2.15
4	12.70	2.80
5	16.00	3.52
6	20.07	4.25
7	23.11	4.84

Experiment No.15

Weight of wet solid = 1185 g.
Weight of dry solid = 1102 g.
Weight of moisture = 83 g.
Percentage moisture = 7.5
1 mm of water in manometer 7.4 g.

Time (min)	Manometer reading (mm)	Load Cell reading (mV)
0	0	0
1	10.16	1.70
2	10.16	1.90
3	11.43	2.35
4	13.72	2.85
6	18.80	4.06
7	21.34	4.56
8	23.11	4.86
9	23.88	4.92
11	24.13	4.92
13	24.13	4.92
15	24.13	4.92

Experiment No.16

Weight of wet solid = 1197 g.
Weight of dry solid = 1116 g.
Weight of moisture = 81 g.
Percentage moisture = 7.3
1 mm of water in manometer 8.7 g

Time (min)	Manometer reading (mm)	Load Cell reading (mV)
0	0	0
1	0.76	0.10
3	1.27	0.20
7	0.91	0.30
13	0.81	0.50
21	0.81	0.80
28	0.81	1.04
35	0.81	1.30
39	1.02	1.42
42	1.02	1.50
48	1.07	1.55

Experiment No.17

Weight of wet solid = 1211 g
Weight of dry solid = 1126 g
Weight of moisture = 85 g
Percentage moisture = 7.5
1 mm of water in manometer 8.0 g

Time (min)	Manometer reading (mm)	Load Cell reading (mV)
0	0	0
1	1.47	0.25
2	2.29	0.41
4	2.21	0.53
7	2.31	0.80
12	2.90	1.33
16	3.66	1.73
18	3.86	1.93
20	4.22	2.09
22	4.37	2.15

Experiment No.18

Weight of wet solid = 1196 g
Weight of dry solid = 1110 g
Weight of moisture = 86 g
Percentage moisture = 7.7
1 mm of water in manometer 7.9 g

Time (min)	Manometer reading (mm)	Load Cell reading (mV)
0	0	0
1	1.42	0.22
2	2.44	0.42
3	2.64	0.51
4	2.49	0.55
5	2.59	0.62
7	2.64	0.77
9	2.79	0.95
11	3.10	1.17
13	3.33	1.35
15	3.66	1.55
17	4.06	1.78
19	4.27	1.94
21	4.42	2.07
24	4.83	2.17

Experiment No.19

Weight of wet solid = 1203 g
Weight of dry solid = 1120 g
Weight of moisture = 83 g
Percentage moisture = 7.4
1 mm of water in manometer 7.5 g

Time (min)	Manometer reading (mm)	Load Cell reading (mV)
0	0	0
1	4.44	0.44
2	5.21	0.70
3	5.21	0.81
4	5.59	1.00
6	6.60	1.35
8	7.49	1.77
10	8.64	2.17
11	9.27	2.35
12	9.65	2.51
13	10.16	2.65
14	10.79	2.75
16	10.97	2.81
18	11.00	2.82
20	11.00	2.82
22	11.05	2.83

Experiment No.20

Weight of wet solid = 1185 g
Weight of dry solid = 1100 g
Weight of moisture = 85 g
Percentage moisture = 7.7
1 mm of water in manometer 7.9 g

Time (min)	Manometer reading (mm)	Load Cell reading (mV)
0	0	0
0.5	13.97	2.30
1	12.70	2.21
2	11.68	2.32
3	13.21	2.80
4	14.99	3.37
5	18.29	4.02
6	21.59	4.62
7	24.13	5.10
8	25.91	5.25
9	26.42	5.26
11	26.69	5.30
13	27.43	5.32
15	27.69	5.38
17	28.19	5.40

Experiment No.21

Weight of wet solid = 1190 g

Weight of dry solid = 1102 g

Weight of moisture = 88 g

Percentage moisture = 8.0

1 mm of water in manometer 7.1 g

Time (min)	Manometer reading (mm)	Load Cell reading (mV)
0	0	0
2	5.08	0.83
5	6.10	1.18
7	7.37	1.54
10	9.14	2.05
14	11.94	2.82
15	12.57	3.00
17	13.97	3.30

Experiment No.22

Weight of wet solid = 1148 g

Weight of dry solid = 1066 g

Weight of moisture = 82 g

Percentage moisture = 7.7

1 mm of water in manometer 8.6 g

Time (min)	Manometer reading (mm)	Load Cell reading (mV)
0	0	0
1	4.57	0.75
2	6.60	1.05
3	6.60	1.10
4	6.65	1.25
5	7.11	1.40
6	7.62	1.60
7	8.13	1.80
9	9.40	2.15
11	10.41	2.50
13	11.43	2.85
15	12.45	3.25
16	13.21	3.45
17	13.82	3.65
18	14.22	3.70
19	14.22	3.70
20	14.22	3.70
21	14.73	3.65
24	14.22	3.65
26	14.22	3.6
28	14.22	3.6

Experiment No.23

Weight of wet solid = 1226 g

Weight of dry solid = 1143 g

Weight of moisture = 83 g

Percentage moisture = 7.3

1 mm of water in manometer 7.4 g

Time (min)	Manometer reading (mm)	Load Cell reading (mV)
0	0	0
1	5.08	0.63
2	6.10	0.82
3	5.97	0.88
4	6.60	1.06
5	7.37	1.23
6	8.51	1.43
7	9.40	1.62
8	10.16	1.78
10	11.43	2.17
12	12.70	2.54
14	13.46	2.93
16	14.73	3.33
18	16.13	3.56

Experiment No.24

Weight of wet solid = 1133 g

Weight of dry solid = 1052 g

Weight of moisture = 81 g

Percentage moisture = 7.7

1 mm of water in manometer 8.8 g

Time (min)	Manometer reading (mm)	Load Cell reading (mV)
0	0	0
1	1.52	0.25
2	2.13	0.40
4	2.03	0.60
6	2.03	0.85
9	2.64	1.25
11	3.1	1.52
14	3.96	1.90
15	4.06	2.00
17	4.57	2.12
19	4.67	2.15

Experiment No.25

Weight of wet solid = 1186 g
Weight of dry solid = 1105 g
Weight of moisture = 81 g
Percentage moisture = 7.3
1 mm of water in manometer 8.2 g

Time (min)	Manometer reading (mm)	Load Cell reading (mV)
0	0	0
1	1.27	0.13
2	1.90	0.26
3	1.90	0.34
4	1.96	0.44
5	1.96	0.53
6	1.96	0.66
7	1.98	0.76
8	2.54	0.91
10	2.54	1.19
12	2.54	1.36
14	3.05	1.56
16	3.56	1.71
18	3.81	1.76
21	3.81	1.79

Experiment No.26

Weight of wet solid = 1183 g
Weight of dry solid = 1104 g
Weight of moisture = 79 g
Percentage moisture = 7.2
1 mm of water in manometer 7.8 g

Time (min)	Manometer reading (mm)	Load Cell reading (mV)
0	0	0
1	1.65	0.29
2	3.94	0.55
5	4.44	0.97
7	4.95	1.24
11	6.22	1.82
16	7.62	2.55
18	7.87	2.84
19	8.51	2.97
21	9.02	3.24
22	9.02	3.35
24	9.78	3.50

Experiment No.27

Weight of wet solid = 1716 g
Weight of dry solid = 1592 g
Weight of moisture = 124 g
Percentage moisture = 7.8
1 mm of water in manometer 8.5 g

Time (min)	Manometer reading (mm)	Load Cell reading (mV)
0	0	0
1	2.79	0.51
2	5.59	0.98
3	5.84	1.08
5	5.59	1.28
6	5.84	1.48
8	6.35	1.66
10	6.60	1.88
12	6.86	2.21
14	7.37	2.48
15	7.62	2.60
17	8.13	2.88
19	8.64	3.18
21	9.14	3.46
22	9.40	3.63
23	9.65	3.73
24	9.91	3.83
25	10.16	3.93
26	10.41	3.98
27	10.41	4.01

Experiment No.28

Weight of wet solid = 2483 g
Weight of dry solid = 2307 g
Weight of moisture = 176 g
Percentage moisture = 7.6
1 mm of water in manometer 6.3 g

Time (min)	Manometer reading (mm)	Load Cell reading (mV)
0	0	0
2	6.35	0.95
5	7.37	1.32
7	7.37	1.52
10	7.87	1.90
15	8.64	2.60
19	9.52	3.15
23	10.29	3.70
29	12.06	4.48
32	12.70	4.82
35	13.46	5.10
37	13.59	5.20

Experiment No.29

Weight of wet solid = 2487 g
Weight of dry solid = 2316 g
Weight of moisture = 171 g
Percentage moisture = 7.4
1 mm of water in manometer 8.1 g

Time (min)	Manometer reading (mm)	Load Cell reading (mV)
0	0	0
1	3.30	0.34
2	5.84	0.88
3	7.37	1.10
4	6.98	1.22
5	7.11	1.31
6	7.62	1.44
8	8.13	1.69
11	8.64	2.14
12	9.14	2.27
13	9.40	2.40
14	9.65	2.57
16	9.91	2.84
18	10.67	3.12
20	10.92	3.42
22	11.94	3.72
24	12.19	4.02
26	13.08	4.33
28	13.46	4.66
30	14.48	4.96
32	14.73	5.27
34	15.75	5.42
36	15.87	5.46
39	15.24	5.41

Experiment No.30

Weight of wet solid = 494 g
Weight of dry solid = 434.5 g
Weight of moisture = 59.5 g
Percentage moisture = 13.7
1 mm of water in manometer 8.7 g

Time (min)	Manometer reading (mm)	Load Cell reading (mV)
0	0	0
1	2.29	15.80
2	2.79	23.20
3	2.79	26.30
5	2.67	33.70
7	2.67	42.20
9	2.79	51.10
11	3.30	60.10
13	3.35	66.10
15	3.38	70.90
17	3.56	74.30
19	3.73	78.50
21	3.76	80.60
23	3.81	82.20

Experiment No.31

Weight of wet solid = 476 g

Weight of dry solid = 424 g

Weight of moisture = 52 g

Percentage moisture = 12.3

1 mm of water in manometer 7.8 g

Time (min)	Manometer reading (mm)	Load Cell reading (mV)
0	0	0
1	6.35	0.95
2	7.62	1.26
4	10.16	1.85
6	13.59	2.52
8	16.38	3.11
10	18.16	3.54
12	19.05	3.69

Experiment No.32

Weight of wet solid = 483 g

Weight of dry solid = 434 g

Weight of moisture = 49 g

Percentage moisture = 11.3

1 mm of water in manometer 7.8 g

Time (min)	Manometer reading (mm)	Load Cell reading (mV)
0	0	0
1	11.43	1.66
2	16.38	2.50
3	21.72	3.44
5	28.45	4.70
7	36.16	5.80
9	38.61	6.54

Experiment No.33

Weight of wet solid = 516 g
Weight of dry solid = 451.5 g
Weight of moisture = 64.5 g
Percentage moisture = 14.3
1 mm of water in manometer 7.9 g

Time (min)	Manometer reading (mm)	Load Cell reading (mV)
0	0	0
1	2.16	0.32
2	3.68	0.57
3	3.94	0.67
4	3.68	0.72
8	3.56	1.00
10	3.94	1.18
12	4.06	1.36
14	4.57	1.51
16	4.95	1.66
18	5.14	1.76
20	5.27	1.83
22	5.46	1.89
24	5.59	1.92
26	5.59	1.94

Experiment No.34

Weight of wet solid = 489 g
Weight of dry solid = 434.5 g
Weight of moisture = 54.5 g
Percentage moisture = 12.5
1 mm of water in manometer 7.9 g

Time (min)	Manometer reading (mm)	Load Cell reading (mV)
0	0	0
1	2.67	0.39
2	3.56	0.57
3	4.44	0.75
5	5.08	0.99
7	5.97	1.27
9	6.98	1.56
11	7.62	1.81
13	8.38	1.99
15	8.89	2.16
17	9.40	2.27
19	9.52	2.28
20	9.52	2.28

Experiment No.35

Weight of wet solid = 547 g
Weight of dry solid = 476 g
Weight of moisture = 71 g
Percentage moisture = 14.9
1 mm of water in manometer 7.9 g

Time (min)	Manometer reading (mm)	Load Cell reading (mV)
0	0	0
1	2.03	0.30
2	3.81	0.59
3	4.19	0.75
4	4.06	0.80
6	3.30	0.78
8	2.67	0.80
10	2.48	0.91
12	2.35	1.04
14	2.41	1.11
16	2.41	1.21
18	2.54	1.28
20	2.67	1.35
22	2.67	1.41
24	2.67	1.47
26	2.79	1.51
28	2.92	1.55
30	3.30	1.59
32	3.68	1.62
34	3.68	1.63
36	3.81	1.65
38	3.81	1.65

Experiment No.36

Weight of wet solid = 500 g
Weight of dry solid = 443 g
Weight of moisture = 57 g
Percentage moisture = 12.9
1 mm of water in manometer 7.8 g

Time (min)	Manometer reading (mm)	Load Cell reading (mV)
0	0	0
1	9.02	1.34
2	11.30	1.80
4	14.35	2.50
6	16.64	3.03
8	18.67	3.60
9	19.56	3.80
11	20.70	4.00

Experiment No.37

Weight of wet solid = 1022 g
Weight of dry solid = 908 g
Weight of moisture = 114 g
Percentage moisture = 12.5
1 mm of water in manometer 7.8 g

Time (min)	Manometer reading (mm)	Load Cell reading (mV)
0	0	0
1	3.81	0.55
2	8.00	1.17
3	9.91	1.54
5	10.03	1.66
7	10.16	1.81
9	10.67	2.01
11	11.18	2.24
13	11.30	2.41
15	11.56	2.60
17	11.56	2.75
19	11.56	2.88
21	11.56	3.00
23	11.56	3.15
25	11.81	3.30
27	11.94	3.44
29	12.19	3.55
31	12.32	3.67
33	12.45	3.74
35	12.57	3.78
37	12.70	3.81

Experiment No.38

Weight of wet solid = 190 g
Weight of dry solid = 44 g
Weight of moisture = 146 g
Percentage moisture = 331.8
1 mm of water in manometer 6.6 g

Time (min)	Manometer reading (mm)	Load Cell reading (mV)
0	0	0
1	0.38	0.08
2	0.02	0.12
3	0	0.13
4	- 0.51	0.19
6	- 0.76	0.33
8	- 1.27	0.51
10	- 1.40	0.71
12	- 1.78	0.86
14	- 1.97	1.03
16	- 1.97	1.21
19	- 1.97	1.43
22	- 1.97	1.61
25	- 1.97	1.75
28	- 1.97	1.91
33	- 1.97	2.10
39	- 1.97	2.24
43	- 1.97	2.31
45	- 1.9	2.33

Experiment No.39

Weight of wet solid = 377 g
Weight of dry solid = 74 g
Weight of moisture = 303 g
Percentage moisture = 409.5
1 mm of water in manometer 8.9 g

Time (min)	Manometer reading (mm)	Load Cell reading (mV)
0	0	0
1	2.29	0.28
2	4.44	0.65
3	5.21	0.77
4	4.70	0.80
6	2.41	0.66
8	0.13	0.65
10	- 1.14	0.72
12	- 2.54	0.79
14	- 3.68	0.92
17	- 5.08	1.10
20	- 6.48	1.32
25	- 8.64	1.65
30	- 9.65	2.10
35	- 10.16	2.53
40	- 10.16	2.95
45	- 10.29	3.24
50	- 10.29	3.52
55	- 10.29	3.71
60	- 10.29	3.87
65	- 10.29	3.95
70	- 10.29	4.01
75	- 10.29	4.04
80	- 10.29	4.04
85	- 10.29	4.07

Experiment No.40

Weight of wet solid = 390 g
Weight of dry solid = 81 g
Weight of moisture = 309 g
Percentage moisture = 381.5
1 mm of water in manometer 8.6 g

Time (min)	Manometer reading (mm)	Load Cell reading (mV)
0	0	0
1	1.02	0.20
2	1.65	0.30
4	0.25	0.30
6	- 1.27	0.31
8	- 2.41	0.40
11	- 3.68	0.62
15	- 5.59	0.89
20	- 7.49	1.32
25	- 8.51	1.83
30	- 9.78	2.28
35	- 10.16	2.74
40	- 10.16	3.16
45	- 10.41	3.42
50	- 10.67	3.61
55	- 10.79	3.83
60	- 10.79	3.94
65	- 10.79	4.03
70	- 10.79	4.06

Experiment No.41 **

Weight of wet solid = 397.5 g
Weight of dry solid = 77 g
Weight of moisture = 320.5 g
Percentage moisture = 416.2
1 mm of water in manometer 8.7 g

Time (min)	Manometer reading (mm)	Load Cell reading (mV)
0	0	0
1	1.78	0.28
2	2.29	0.40
4	2.35	0.66
6	1.27	0.87
8	0	1.05
10	- 1.27	1.23
12	- 2.79	1.42
14	- 4.7	1.56
16	- 5.46	1.87
18	- 6.48	2.06
20	- 7.37	2.45
21	- 7.62	2.60
23	- 8.38	2.90
24	- 8.89	2.98
26	- 8.89	3.45
28	- 9.14	3.76
29	- 9.21	3.97
30	- 9.21	4.25
31	- 9.52	4.44
32	- 9.52	4.15
33	- 9.52	3.87
34	- 9.52	3.96
40	- 9.52	4.27
45	- 9.52	4.29
50	- 9.52	4.26
55	- 9.52	4.25
60	- 9.52	4.24

Experiment No.42

Weight of wet solid = 251 g
Weight of dry solid = 217 g
Weight of moisture = 34 g
Percentage moisture = 15.7
1 mm of water in manometer 7.8 g

Time (min)	Manometer reading (mm)	Load Cell reading (mV)
0	0	0
1	3.05	0.51
2	4.38	0.75
4	6.22	1.15
6	7.37	1.41
8	8.13	1.61
10	8.51	1.70
12	8.89	1.78

** Experiment No.41 is unreliable because near the end of the run, peas were burnt, and the bed reduced to half its original size.

Experiment No.43

Weight of wet solid = 248 g

Weight of dry solid = 218 g

Weight of moisture = 30 g

Percentage moisture = 13.8

1 mm of water in manometer 8.1 g

Time (min)	Manometer reading (mm)	Load Cell reading (mV)
0	0	0
1	3.05	0.43
2	4.3	0.64
4	6.10	1.04
6	6.86	1.32
8	7.37	1.43
10	8.00	1.53
12	8.13	1.58
14	8.25	1.64

Experiment No.44

Weight of wet solid = 1296 g

Weight of dry solid = 1222 g

Weight of moisture = 74 g

Percentage moisture = 6.1

1 mm of water in manometer 7.6 g

Time (min)	Manometer reading (mm)	Load Cell reading (mV)
0	0	0
1	1.02	0.08
2	1.40	0.33
4	1.40	0.55
6	1.52	0.77
8	1.78	1.00
10	2.22	1.22
12	2.29	1.42
14	2.48	1.60
16	2.67	1.70
18	3.17	1.76
20	3.17	1.77
22	3.30	1.77
25	3.30	1.77

APPENDIX 2

Data of Dry Pellet Experiment

Weight of solid = 1102 g

1 mm of water in manometer = 8.2 g

Time (min)	Manometer Reading (mm)	Load Cell Reading (mV)
0	0.0	0.00
2	4.4	0.60
4	6.9	0.94
8	8.9	1.20
11	9.1	1.26
15	9.3	1.30

APPENDIX 3

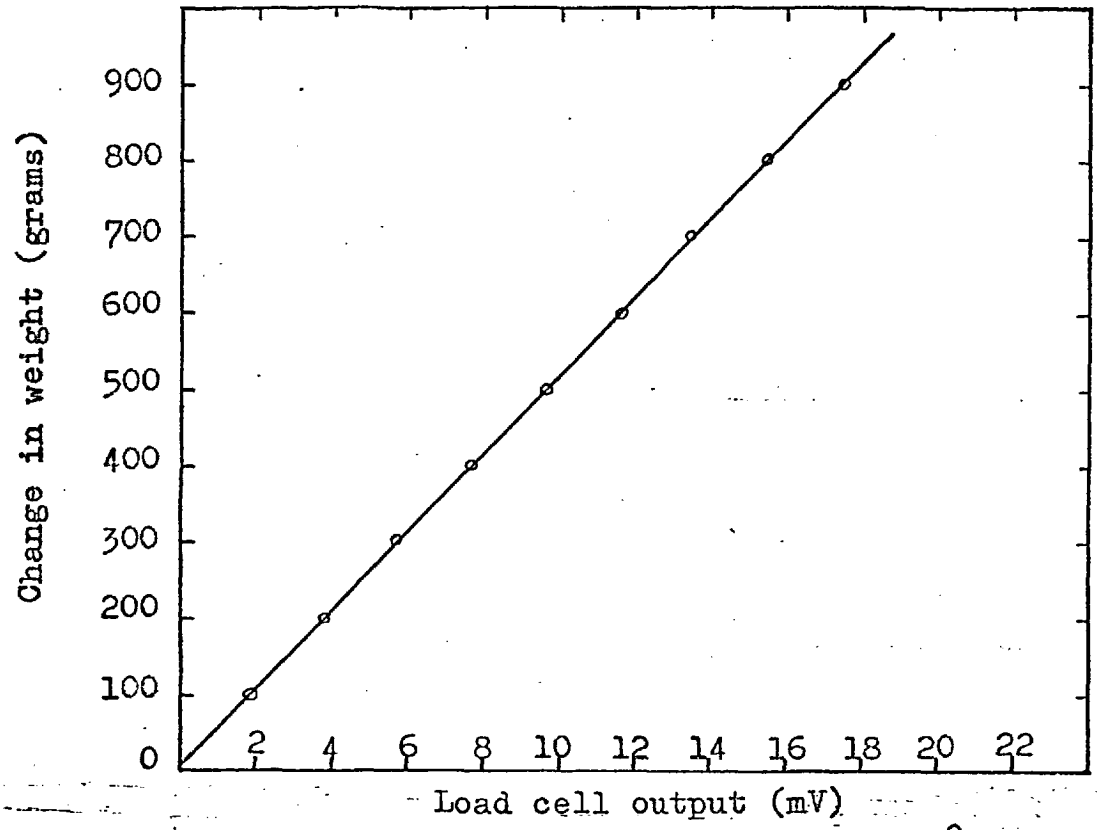

FIGURE 6.2 - Load cell calibration carried out at 75°C, 15.2 cm bed height, and 0.4 $m^3/s\ m^2$.

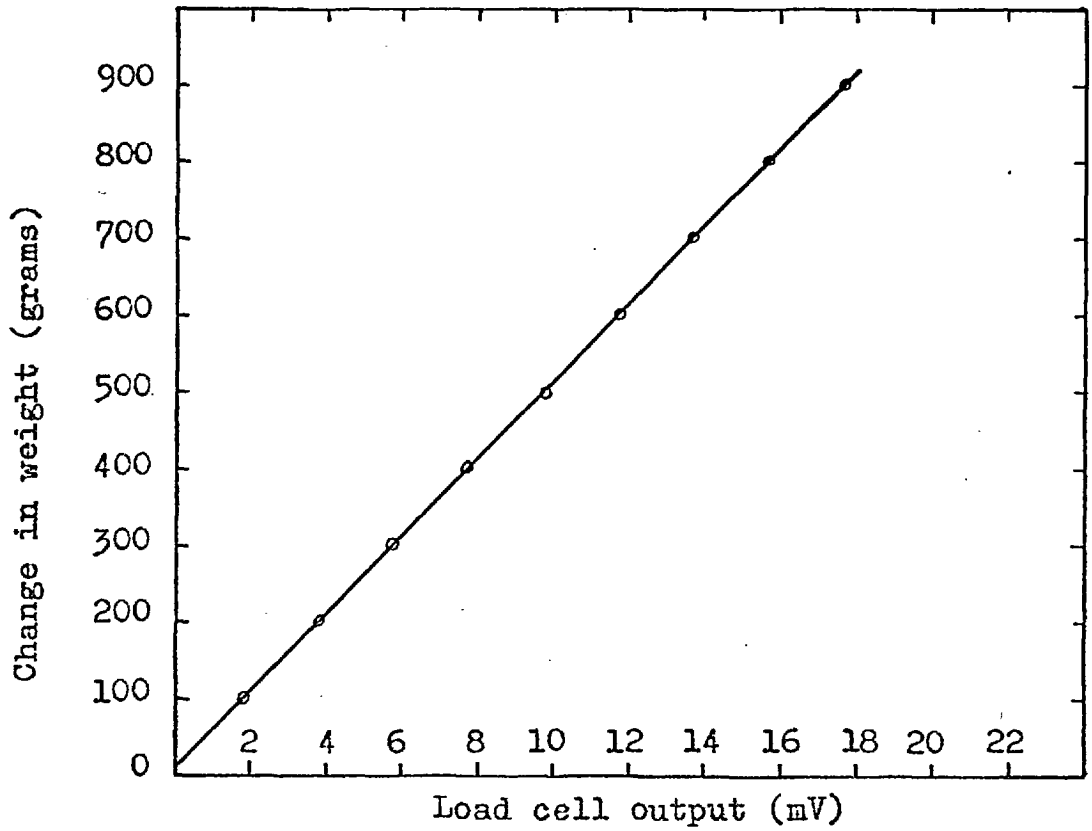

FIGURE 6.3 - Load cell calibration carried out at 75°C, 15.2 cm bed height, and 0.6 $m^3/s\ m^2$.

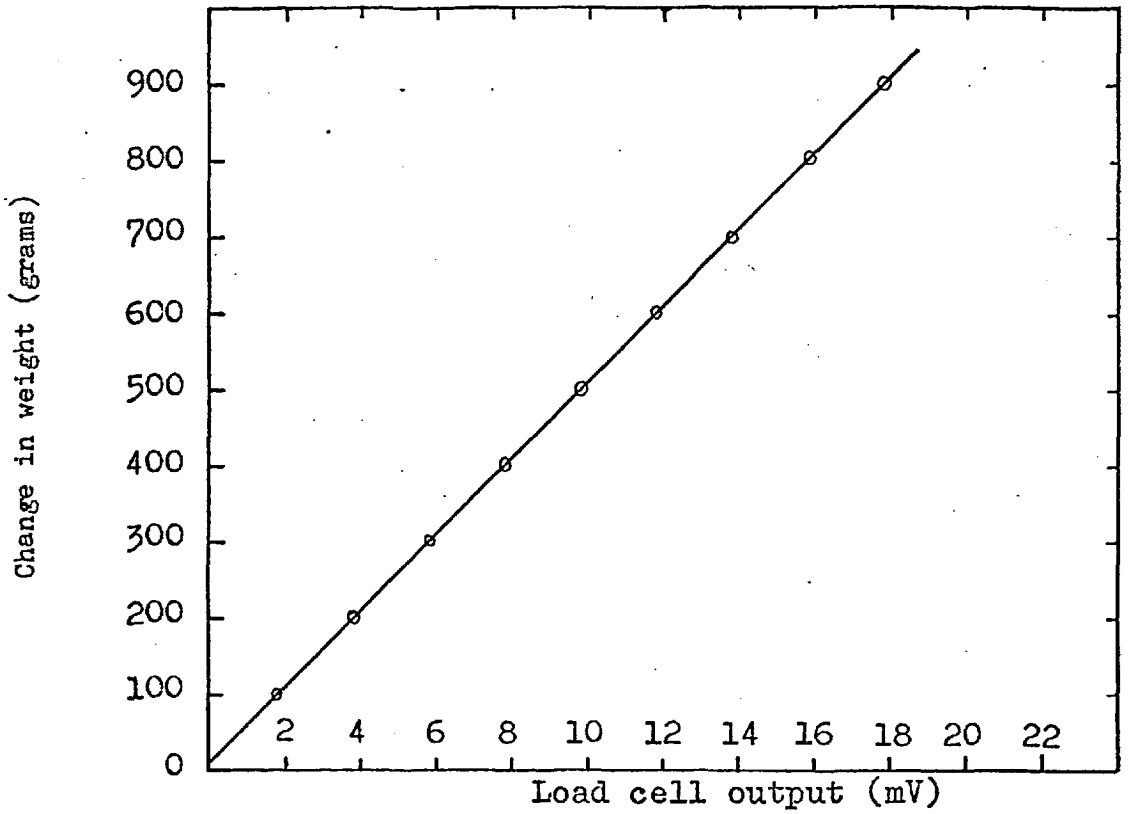

FIGURE 6.4 - Load cell calibration carried out at 100°C, 15.2 cm bed height, and 0.4 $m^3/s\ m^2$.

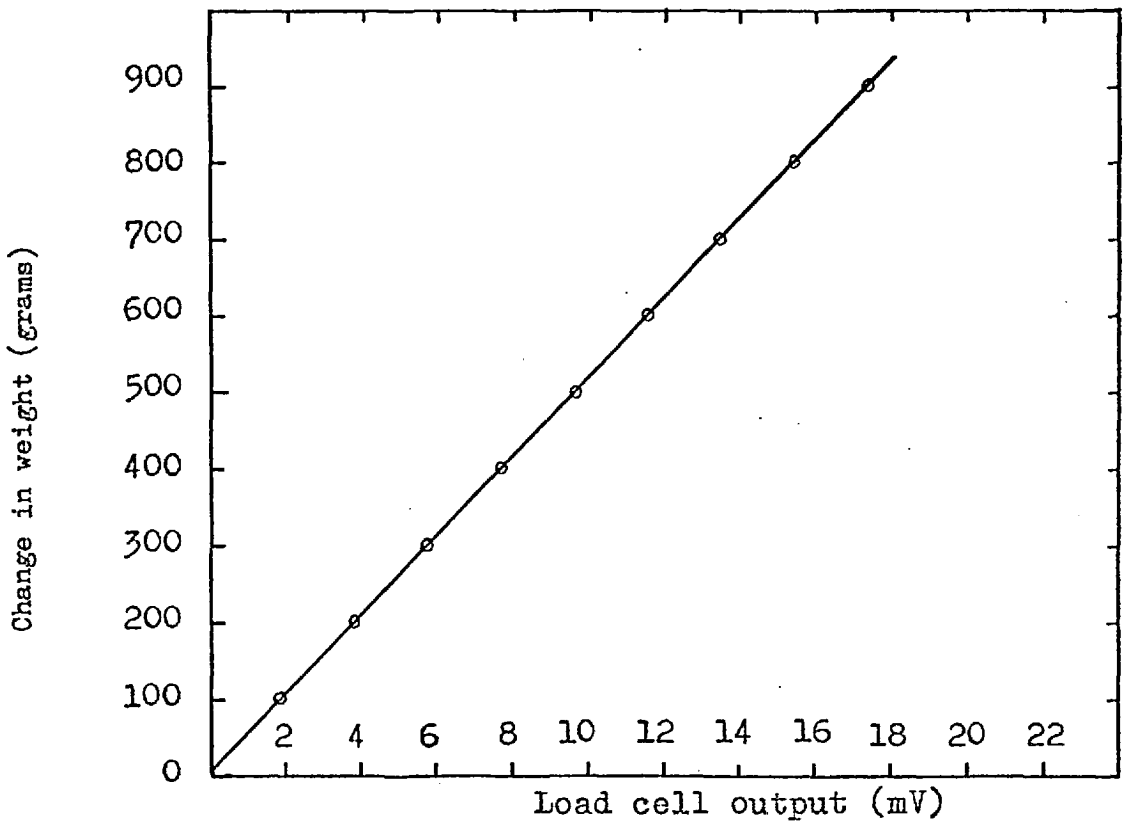

FIGURE 6.5 - Load cell calibration carried out at 75°C, 30.5 cm bed height, and 0.4 $m^3/s\ m^2$.

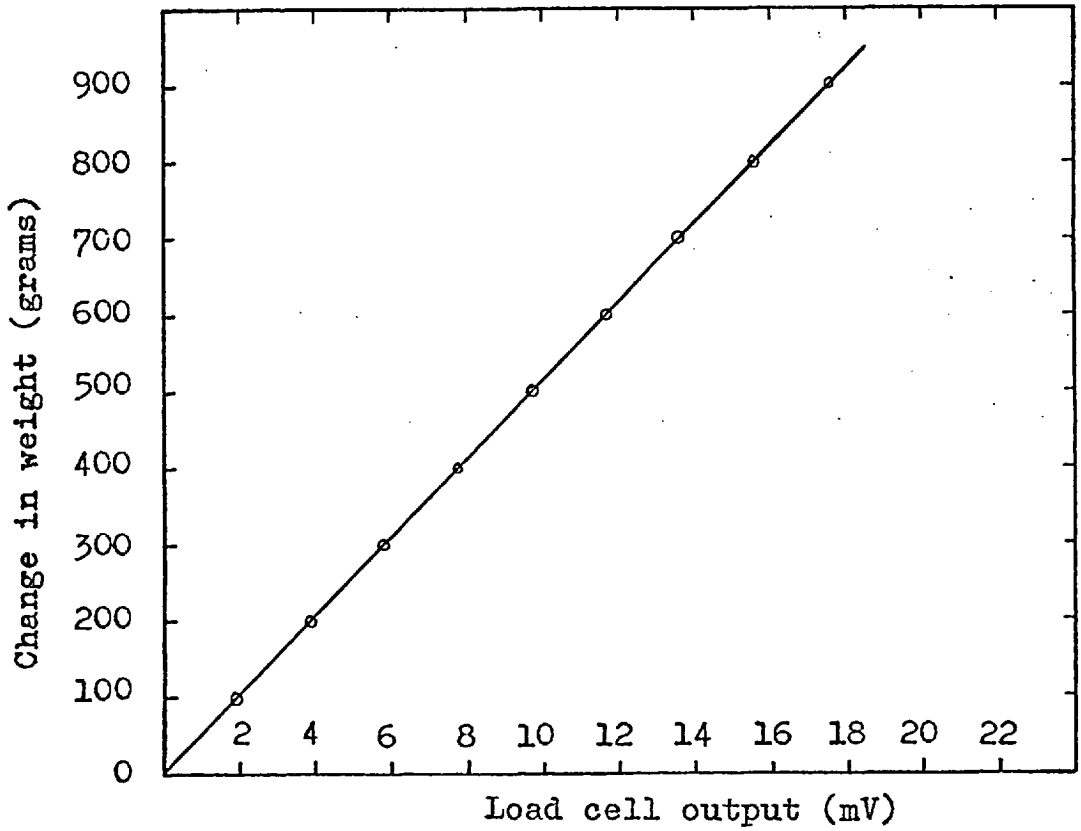

FIGURE 6.6 - Load cell calibration carried out at room temperature with 15.2 cm bed height without any air passing through the bed.

APPENDIX 4.1

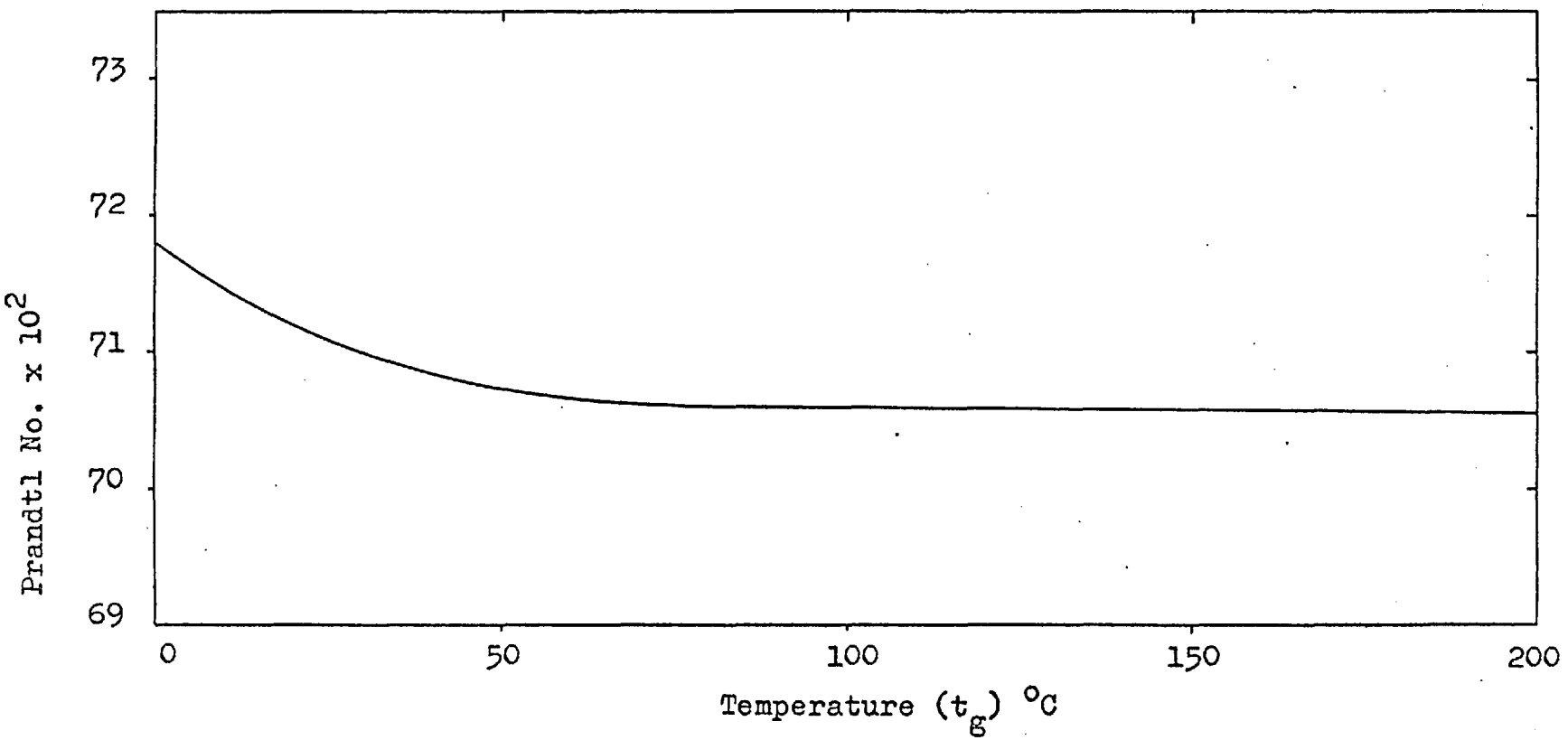

Effect of temperature on the Prandtl number of dry air.

APPENDIX 4.2

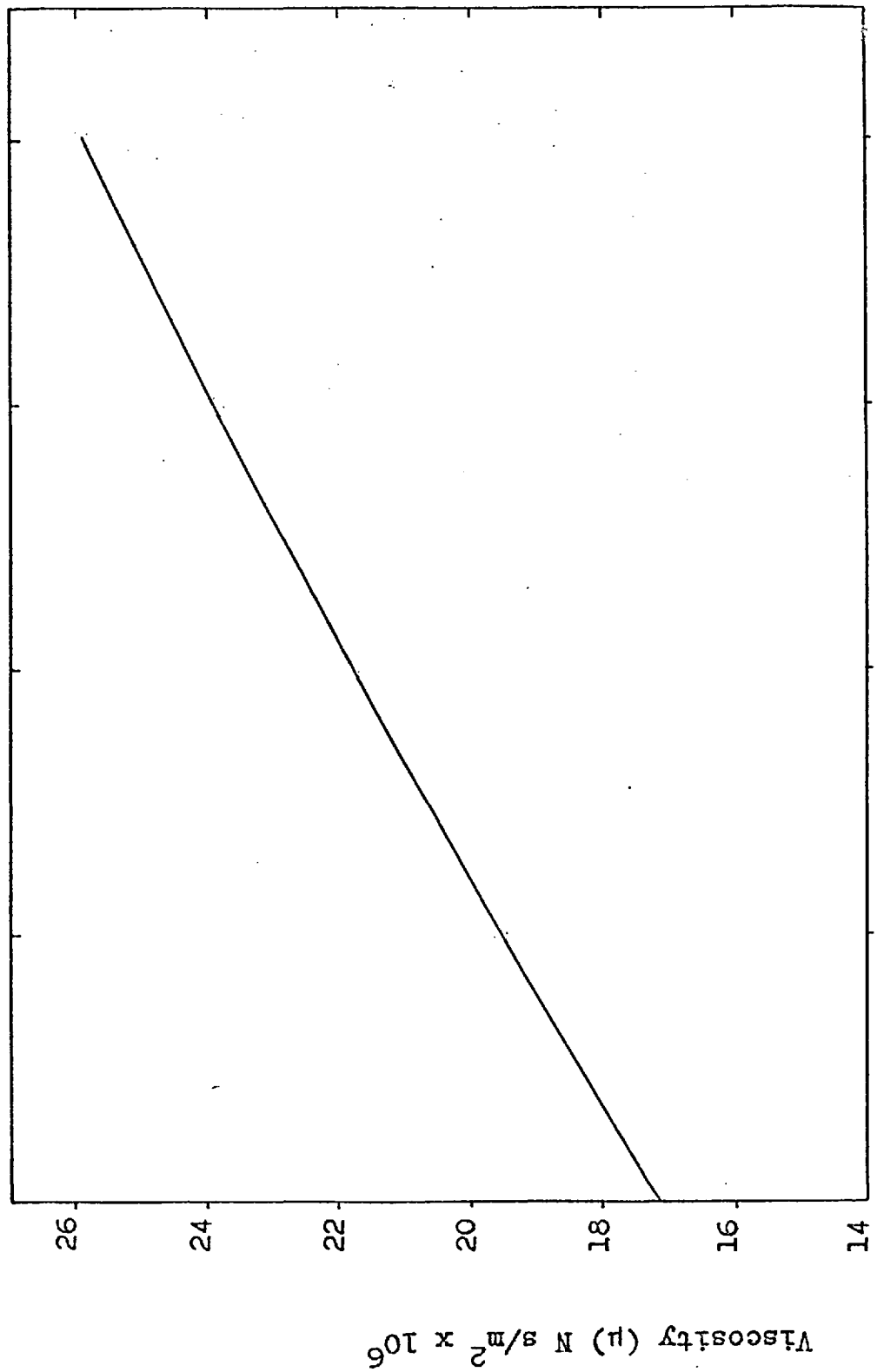

Effect of temperature on the viscosity of dry air.

APPENDIX 4.3

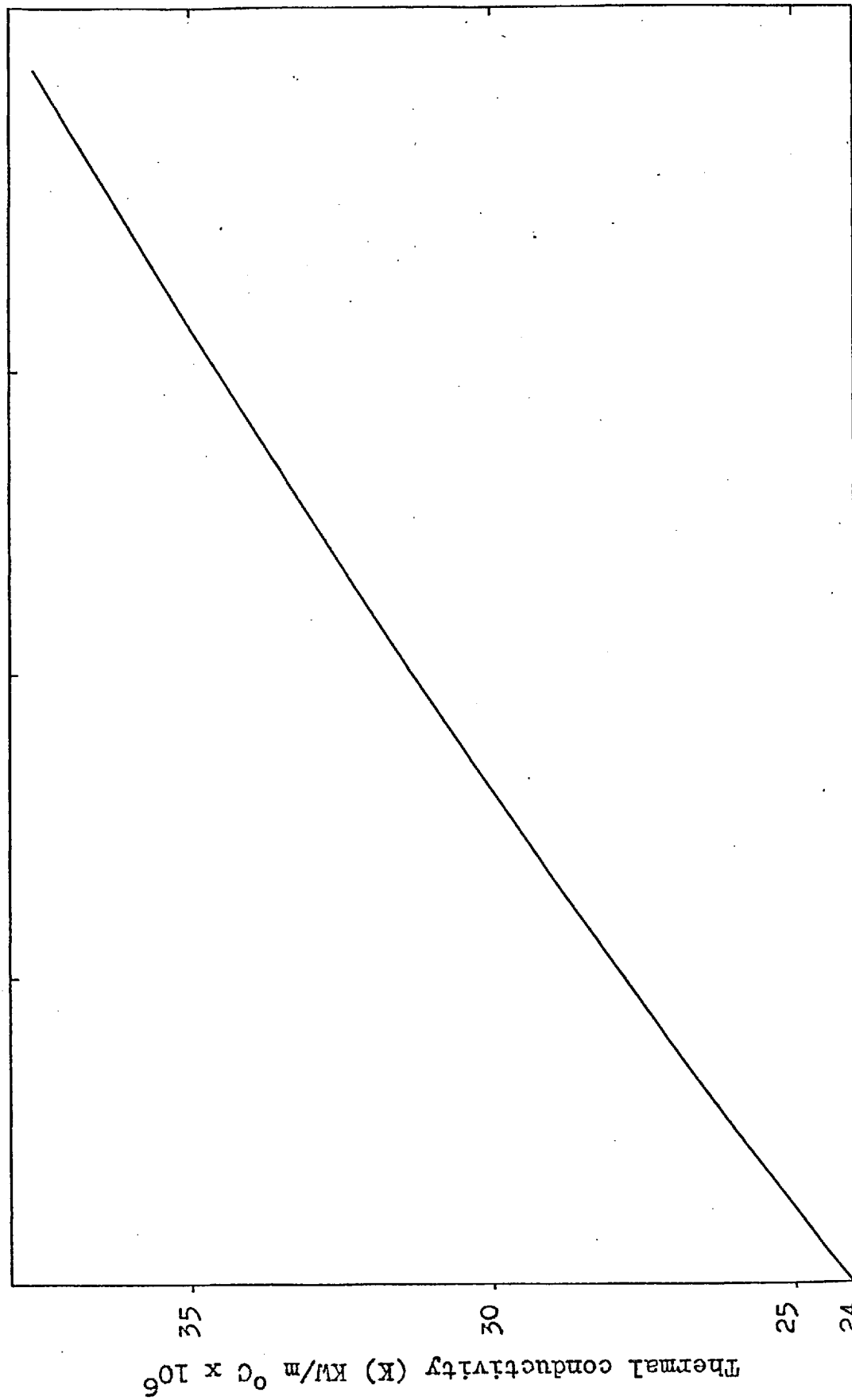

Effect of temperature on the thermal conductivity of dry air.

APPENDIX 4.4

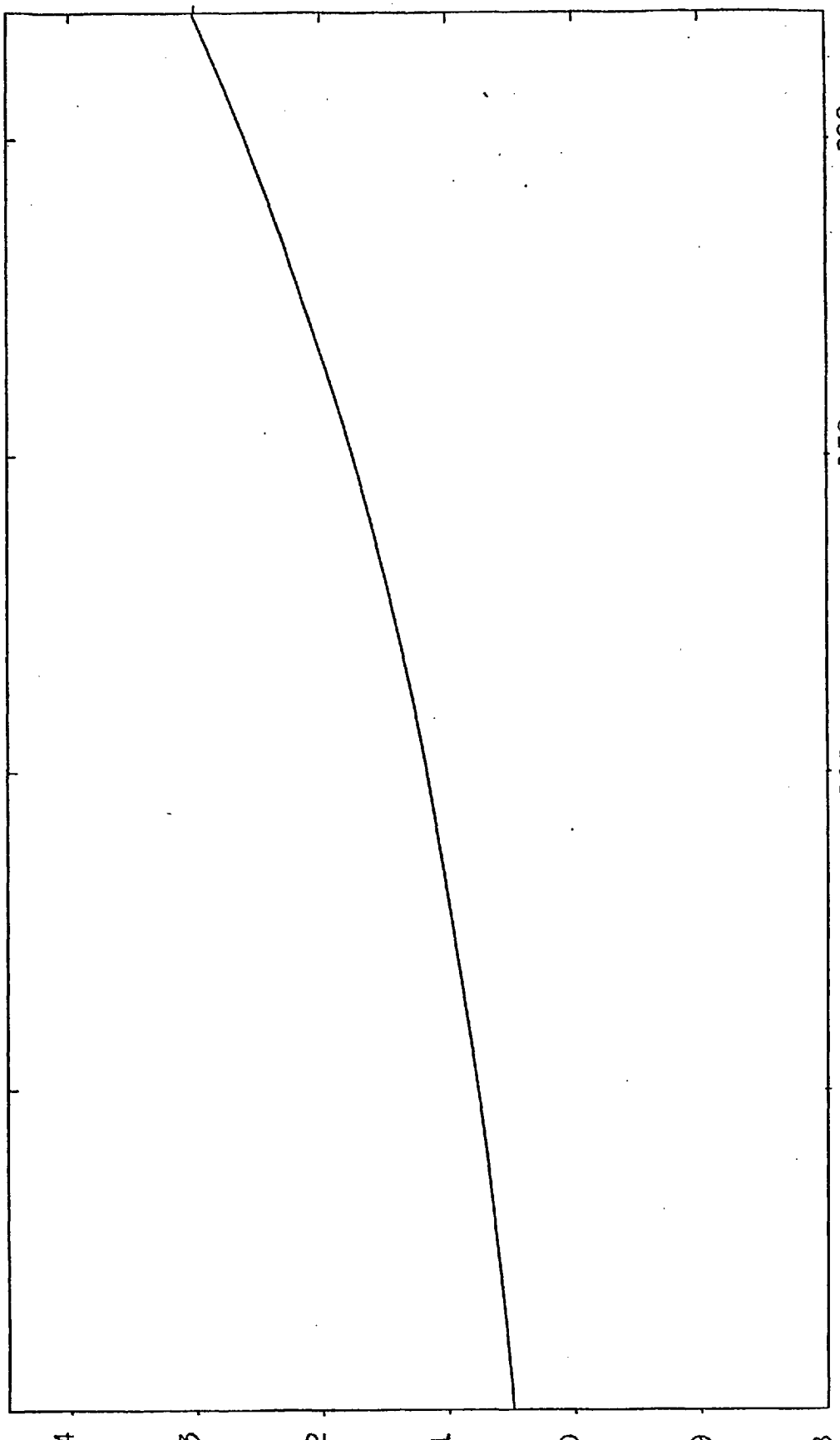

Effect of temperature on the specific heat of dry air.

APPENDIX 5

a) Data of sinter feed

The sinter feed consisted of the following ore mix kindly supplied by the British Steel Corporation.

Ore	Percentage
Frodingham	46.5*
Bomi	10.7
Lac Jeannine	10.7
Sierra Leone	10.7
Itabira	10.7
Tazadit	10.7

*combined water approximately 4% included in this figure.

Sieve Analysis

Sieve size (mm)	Weight (g)	Mass fraction
-9.5 + 8.0	71.0	0.022
-8.0 + 6.7	92.0	0.028
-6.7 + 5.6	107.0	0.033
-5.6 + 4.75	73.0	0.023
-4.75+ 4.0	119.0	0.037
-4.0 + 2.8	87.0	0.027
-2.8 + 2.0	114.0	0.035
-2.0 + 1.0	266.0	0.083
-1.0 + 0.5	390.0	0.121
-0.5 + 0.25	581.0	0.180
-0.25	1319.0	0.410

b) The iron ore used for rolling green pellets was a magnetite concentrate (Sydvaranger) also supplied by the British Steel Corporation. The approximate cumulative size distribution of the concentrate was:

87%	-100 mesh
53%	-200 mesh
30%	-300 mesh

c) The fired pellets used were made of Carol Lake concentrate.

LIST OF SYMBOLS

Symbol	Explanation	Units
A, A', A'', A'''	Constants	
A_s	Coefficient characteristic of material.	
a	Area of cross-section.	m^2
a*	Surface area of column.	m^2
a', b	Factors which are function of the system.	
a", b"	Constants of proportionality.	
C_p	Specific heat of gas.	KJ/Kg ^oC
C_{p_w}	" " " water vapour.	"
C	Specific heat per unit volume of bed.	KJ/Kg m^3 ^oC
C'	Specific heat per unit volume of gas at constant pressure.	"
D	Column diameter.	m
D_p	Particle diameter.	m
D_V	Diffusivity of gas.	m^2/s
E	Rate of evaporation per unit area.	Kg/s m^2
E'	Axial dispersion coefficient.	m^2/s
e	Emissivity.	
F	Axial mixing factor.	
f'	Coefficient depending on bed voidage.	
f	At the film.	
G	Mass flow rate.	Kg/s
g	Gravitational constant.	m/s^2
g_c	Constant.	

Symbol	Explanation	Units
H_g	Heat capacity of gas per unit volume of bed.	KJ/Kg m^2 ^oC
H_s	Heat capacity of solid per unit volume of bed.	"
h	Heat transfer coefficient.	KW/m^2 ^oC
h_1, h_2	Modified heat transfer coefficient.	"
h_E	Effective heat transfer coefficient.	"
h_c	Convective heat transfer coefficient.	"
h^o	h including the influence of mass transfer.	"
h_V	Volumetric heat transfer coefficient.	KW/m^3 ^oC
h_D	Mass transfer coefficient.	m/s
h'_D	Mass transfer coefficient.	K moles/s m^2 atm
J_D	Mass transfer factor.	
K	Thermal conductivity.	KW/m ^oC
K_s	Thermal conductivity of solid.	"
K_g	Thermal conductivity of gas.	"
k_{gl}	" " " glass.	"
K_{tr}	Turbulent thermal conductivity.	KW/m ^oC
k_1, k_2	Coefficients of viscous and kinetic energies; $k_1 = 72\alpha = 150$ and $k_2 = 0.75\beta = 1.75$.	
L	Total height of the bed.	m
ℓ	Length of grate required for drying.	m

Symbol	Explanation	Units
M'	Molecular weight.	Kg
M_o	Initial mass of water per unit mass of solid.	Kg/m^2 s
m	Mass of solid per unit volume of bed.	Kg/m^3
N_A	Flux of A.	Kg/m^2 s
n	Number of perfect mixers.	
P	Total pressure.	KN/m^2
P_L	Vapour pressure of liquid.	"
P_A	Mean partial pressure of vapour in gas.	"
$\triangle P^*$	Pressure drop across the bed.	"
P'	Impact pressure	mm
p_a	Partial pressure of water vapour in air.	KN/m^2
p_s	Partial pressure of water vapour at the surface of the solid.	"
$p_{m\ air}$	Log mean partial pressure difference of air in the boundary layer.	"
Q	Heat transferred.	KW
Q'	per unit area	KW/m^2
R	Ratio of inlet and outlet driving forces for mass transfer.	
R'	Rate of adsorption.	$moles/m^3$ s
S	Specific surface.	m^{-1}
S'	Area of liquid surface.	m^2
S_c	Surface of column per unit volume of bed.	m^{-1}

$^*\triangle P$ (in fig 2.a) mm

Symbol	Explanation	Units
Δ	Humid heat.	KJ/Kg °C
Δ_m	Mean humid heat.	"
T	Time.	s
T'	Time for complete drying.	s
T_{suc}	Suction temperature.	°C
$T_{n.suc}$	Non-suction temperature.	°C
T_t	True temperature.	°C
t_1, t_2	temperature difference	°C
t'	Thickness of column wall.	m
t_r	Room temperature.	°C
t_{gl}	Glass temperature.	°C
t_g	Gas temperature.	°C
t_{g_o}	Initial gas temperature.	°C
$t_{g_{as}}$	Adiabatic saturation temperature of gas.	°C
$t_{g_{av}}$	Average gas temperature.	°C
$t_{g'}$	Exit gas temperature.	°C
t_m	log mean temperature difference	°C
t_s	Temperature of the solids.	°C
t_{s_o}	Initial temperature of the solids.	°C
t_w	Wall temperature	°C
u	Velocity of the drying zone.	m/s
u'	Speed of strand.	m/s
V	Velocity of fluid based on empty cross-section.	m/s

Symbol	Explanation	Units
V_m	Velocity of fluid measured at average pressure.	m/s
V_o	Velocity of gas at 0^oC.	m/s
V'	Velocity of gas.	m/s
V_i	Intersticial gas velocity.	m/s
V'_b	Volume of bed.	m^3
V'_s	Volume of solids.	m^3
v_B	Volume of bed.	m^3
v_s	Volume of spheres.	m^3
w	Amount of adsorbate on bed.	moles/m^3
x	Humidity of gas.	
x_{as}	Humidity of gas at adiabatic saturation temperature.	
$x_{w.B.t.}$	Humidity of gas at wet bulb temperature.	
x'_i	Initial absolute humidity.	
x'_{as}	Absolute humidity at adiabatic saturation temperature.	
x	Distance along the axis of bed.	m
Y, Y''	Drying rate.	Kg/s m^2
Y'	Drying rate in constant rate period.	Kg/Kg of solid s.
y	Distance from surface.	m
Z	Distance up the bed after time T.	m
$\mathcal{Z}$	Height of drying zone.	m
Φ	Enthalpy.	KJ/Kg

Symbol	Explanation	Units
ϵ	Function of.	
η	Concentration.	Moles/m^3
λ	Latent heat.	KJ/Kg
ϵ	Voidage.	
μ	Viscosity.	Ns/m^2
α, β	Statistical coefficients of viscous and kinetic energies.	
Ψ	Friction factor.	s^2/m
Θ	$\rho_f^2 \beta'_f g C_p/\mu_f K_f$	$m^2 {}^oC/Kg\ s^2$
β'	Coefficient of volumetric expansion.	$^oC^{-1}$
σ	Stefan-Boltzmann constant.	$W/m^2 {}^oK^4$
ρ	Density.	Kg/m^3
ρ_m	Molar density.	Kg/m^3
ρ_g	Gas density.	Kg/m^3
ρ_b	Bulk density.	Kg/m^3
ρ_t	True density.	Kg/m^3
Pe	Peclet number.	
Re	Reynolds number	
Nu	Nusselt number.	
Sh	Sherwood number.	
Pr	Prandtl number.	
Sc	Schmidt number.	

REFERENCES

1. Bennet, R.L. and Lopez, R.D. Chem.Eng.Progress Symposium Series, 1963, 59, 41.
2. Bennet, C.O. and Myers, J.E. "Momentum, Heat and Mass Transfer", McGraw Hill, 1962, 543.
3. Hougen, O.A. and McCauley, H.J. Trans.Am.Inst.Chem. Engrs., 1940, 36, 183.
4. Ceaglske, N.H. and Hougen, O.A. Trans.Am.Inst.Chem. Engrs., 1937, 33, 283.
5. Comings, E.W. and Sherwood, T.K. Ind.Eng.Chem., 1934, 26, 1096.
6. Pearse, J.F., Oliver, T.R. and Newitt, D.M. Trans.Inst. Chem.Engrs.(London)., 1949, 27, 1,9.
7. Collins, R.E. "Flow of fluids through porous materials" Reinhold. Publish.Corp., 1961, 47.
8. Ergun, S. Chem.Eng.Prog., 1952, 48, 89.
9. Carman, P.C. Trans.Inst.Chem.Engrs.(London)., 1937, 15, 150.
10. Blake, F.E. Trans.Am.Inst.Chem.Engrs., 1922, 14, 415.
11. Kozeny, J. Sitzber.Akad.Wiss.Wien, Math-Naturiu. Klasse., 1927, 136, 271.
12. Burke, S.P. and Plummer, W.B. Ind.Eng.Chem., 1928, 20, 1196.
13. Ergun, S. and Orning, A.A. Ind.Eng.Chem., 1949, 41, 1179.
14. Coulson, J.M. Trans.Inst.Chem.Engrs., 1949, 27, 237.
15. Schumann, T.E.W. J. Franklin Inst., 1929, 208, 405.
16. Furnas, C.C. Ind.Eng.Chem., 1930, 22, 721; 1931, 23, 534.

17. Saunders, O.A. and Ford, H. J.Iron and Steel Inst., 1940, 1, 291.

18. Kitaev, B.I., Yaroshenko, YU. G., Suchkov, V.D. "Heat Exchange in Shaft Furnaces", Pergamon Press, 1967, 64.

19. Rowe, P.N. and Claxton, K.T. Trans.Inst.Chem.Engrs., 1965, 43, 321.

20. Amundson, N.R. Ind.Eng.Chem., 1956, 48, 35.

21. Bradshaw, A.V., Johnson, A., McLachlan, N.H. and Chiu, Y-T. Trans.Inst.Chem.Engrs., 1970, 48, 77.

22. Acrivos, A. Ind.Eng.Chem., 1956, 48, 703.

23. Marshall, Jr. W.R. and Hougen, O.A. Trans.Am.Inst.Chem. Engrs., 1942, 38, 91.

24. Gamson, B.W., Thodos, G. and Hougen, O.A. Am. Inst. Chem. Engrs., 1943, 39, 1.

25. DeAcetis, J. and Thodos, G. Ind.Eng.Chem., 1960, 52, 1003.

26. Evnochides, S. and Thodos, G. Am.Inst.Chem.Eng.J., 1961, 7, 78.

27. Sen Gupta, A. and Thodos, G. Chem.Eng.Prog., 1962, 58, 58.

28. McConnachie, J.T. and Thodos, G. Am.Inst.Chem.Eng.J., 1963, 9, 60.

29. Malling, G.F. and Thodos, G. Int.J.Heat and Mass Transfer., 1967, 10, 489.

30. Petrovic, L.J. and Thodos, G. Ind.Eng.Chem. Fundamentals, 1968, 7, 274.

31. Epstein, N. Can.J.Chem.Eng., 1958, 36, 210.

32. Carberry, J.J. Am.Inst.Chem.Eng.J., 1960, 6, 460.

33. Colquhoun-Lee, I. and Stepanek, J. The Chem.Eng., 1974, No.282, 108.

34. Allerton, J., Brownell, L.E. and Donald, L.K. Chem.Eng.Prog., 1949, 45, 619.

35. Beveridge, G.S.G. / Symp.Chem.Eng. in Metall. Industries., Inst.Chem.Engrs., 1963, 87.

36. Myklestad, O. Int.J.Heat and Mass Transfer., 1968, 11, 675.

37. Sarkar, K.M. "Heat and Mass Transfer between Gases and Solids in a Moving Bed" - Ph.D. Thesis, London University, 1971.

38. Spiers, H.M. "Technical Data on Fuel", The British National Committee., 1950.

39. McAdams,W.H.- "Heat Transmission" , McGraw Hill., 1954, 172.

40. Haley, K.M. and Apuli, W.E. in "Agglomeration", edited by Knepper, W.A.,Interscience Publishers., 1962, 931.

41. Perry, J.H. (Editor-in-Chief) - "Chem. Engrs. Handbook", Mcgraw Hill., 1949.

ACKNOWLEDGEMENTS

I wish to express my sincere gratitude and appreciation to Dr. R.J. Tait for his supervision and continuous encouragement during the course of this work.

I also wish to express my sincere gratitude to my parents without whose financial and moral support this work would not have been possible.

The help of the technicians and my colleagues in the John Percy Group, and the technicians in the Metallurgy Department Workshop is gratefully acknowledged.

Finally I would like to thank Mrs. T. Wright for typing this thesis.